UNIVERSITÀ
DEGLI STUDI
DI PADOVA

DIPARTIMENTO
DI INGEGNERIA

DIPARTIMENTO DI INGEGNERIA DELL'INFORMAZIONE

CORSO DI LAUREA MAGISTRALE IN BIOINGEGNERIA PER LE NEUROSCIENZE

"3D Bioprinted cancer microenvironments"

Relatore: Prof. Alessandro Gandin

Laureanda: Nadine La Salvia

ANNO ACCADEMICO 2023 – 2024

Data di laurea 16 Ottobre 2024

Abstract

Tumour development induces a major modification of the surrounding microenvironment through the remodelling of its architecture and composition, in turn stimulating tumour cells proliferation and healthy cell differentiation. The investigation of this complex scenario of interactions and extra cellular matrix rearrangements is often hindered with the overly simplified 2D cells culture or in-vivo studies which don't allow to dissect key aspects of the cell-cell and cell-ECM interplay. This study aims to exploit 3D bioprinting to recreate it through a simplified, yet representative model.

We exploited 3D bioprinting to create spatial compartmentalization of different components of the tumour microenvironment and specific architectures, in terms of morphology, of the extracellular matrix. For this, both natural and natural modified polymers were used: pure collagen, Matrigel and methacrylate gelatin.

Specifically, we used Matrigel embedding tumour cells to simulate the tumour compartment and methacrylate gelatin or collagen mixed with fibroblasts to mimick the surrounding stromal tissue. We investigated the mechanical properties of each gel, and we explored different printing strategies to optimize the fabrication of this multimaterial and multicellular structure. Moreover, we studied how collagen morphology can be controlled tuning the bioprinting parameters.

Summary

Introduction

Cancer is one of the leading causes of death worldwide. Despite the progress achieved in oncological field, a deep understanding of the biological mechanisms behind its behaviour is still a challenge. Indeed, cancer is a complex disease, characterized by changes in its surrounding extracellular matrix which helps it to create an environment suitable for its growth and proliferation. This changes made by cancer cells create the tumour microenvironment (TME), [1] in which malignant cells rearrange the components of the ECM, such as collagen fibers, and intensely communicate with the native cells, including the stromal cells, the immune cells and the endothelial cells. Moreover, cancers present a high level of heterogeneity, not only between individuals, but also between cells within the tumour.

It's therefore mandatory to develop clinically relevant models to study cancer's biology and test drugs response. Traditionally, cancer' studies were conducted using animal models or two-dimensional (2D) in vitro models. Animal models, although physiologically significant, fail to reflect human responses to drug treatment: they lack human cells and often animals with compromised immune system are used which, overall, results in failure. Furthermore, they're expensive, laborious, time-consuming, and usually surrounded by ethical concerns. On the other hand, 2D monolayer environments don't resemble the TME present *in vivo* as three-dimensionality is highly involved in cells behaviours and overall ECM remodelling. Three-dimensional (3D) models on the other hand, better recapitulate the TME, enabling a more accurate model of the disease development. [2] Principal strategies in 3D modelling include organ-on-a-chip, organoids cell culture and 3D bioprinting. In this work of thesis, we will focus on 3D bioprinting to recreate a simple model of TME, carefully optimizing both the materials and the techniques to increase the resemblance to the conditions observable in vivo. We wanted to recreate a complex multilayered structure using multiple materials to represent different compartments of the tumour niche, such as healthy stromal tissue and cancerous basement membrane, to study their interactions between each other's as well as their intertwined remodelling of the surrounding ECM. We used extrusion bioprinting, as it allows both high spatial control and high cellular concentration, improving the

resemblance to the physiology presents *in vivo.* Moreover, we implemented the more recently FRESH technique, which allow to increased control on soft hydrogel printability, which may result fundamental for improving resemblance to the *in vivo* model.

In this work of thesis, we aimed to develop a complex structure, in which stromal tissue and cancerous cells are well compartmentalized, to better recapitulate the TME. Gelatin methacrylate (GelMA) was implemented with fibroblasts to resemble the stromal tissue, along with Matrigel embedded with cancerous cells representing the cancerous basement membrane. Furthermore, we explored collagen printability, to control the fibrillar structure presents in TME, as considered fundamental in oncological field for both cancer diagnostics and development. We tried to recreate similarly the stromal tissue – cancerous basement membrane interactions, using collagen and Matrigel. Finally, to improve collagen's printability we explored FRESH bioprinting.

The proposed work starts with an introductory section (Chapter I) in which we briefly give a background to the TME, explaining its consequences and development in vivo, along with the current strategies to contrast it. Consequently (Chapter II), we will explain 3D bioprinting current implemented techniques and materials, focusing on extrusion bioprinting. Later, (Chapter III) we will explain the materials and methods implemented in our experiments, to finally show the achieved results (Chapter IV), which are divided into two sub-chapters, one related to GelMA bioprinting and the other one to collagen bioprinting.

Chapter I
Cancerous microenvironments

Cancer is one of the leading causes of death throughout the world. Cancer treatments present many limitations, due to the required long times and high costs to produce novel drugs, the requirement for more selective drugs, personalized medicine development. For these reasons is cancer research one of the main goals in biomedical field. Traditional methods comprised monolayer cell culture and animal models, which resulted inadequate. Indeed, 2D cell cultures can't completely recapitulate the complexity of the disease, and although animal models are physiologically suitable, they present limitations in replicating human responses. The tumour microenvironments present high complexity and high variance in terms of components and behaviours among different cancer types. However, they all share the presence of a dynamic network, constituted by the extracellular matrix, cancer cells and stromal tissue. [3]

1.1 Extracellular Matrix (ECM)

The ECM is the essential non-cellular component present within all tissues and organs constituting not only the physical scaffold for all cellular constituents but has also an important role for biochemical and biomechanical cues initiations. Therefore, it controls a wide range of cells functions, such as differentiation, homeostasis and morphogenesis. The ECM is composed of water, polysaccharides and proteins and it differs in composition and topology depending on the tissue considered. It allows a dynamic tissue-specific environment, that is constantly remodelled either enzymatically or non-enzymatically, to generate the required biochemical and mechanical properties of each organ, such as elasticity, protection, tensile and compressive strength. Furthermore, the ECM also directs fundamental morphological organization and the interactions with cell-surface receptors through the growth factors (GFs), allowing cells signalling and gene transcription regulation. These properties vary tremendously from one tissue to another and even within one tissue. Furthermore, it varies between physiological and pathological state and may differ depending on the age of the subject considered. For these

reasons there are a lot of studies regarding the extracellular matrix, particularly with respect to its effects on cell behaviours. [4]

Principal components

The ECM is an intricate network, formed by a variety of macromolecules organized in a cell/tissue-dependent manner. Its components are linked together and harmonized to explicit fundamental cells behaviours like adhesion, migration, apoptosis, differentiation and proliferation. Proteins are a fundamental component of the ECM and each of them is specialized with distinct biochemical properties. [5] In **Table 1** are summarized the principal protein components of the ECM.

Table 1: ECM components and principal functions [5], [6]

ECM Component	**Structure**	**Function**
Collagens	It's a family of proteins composed of 3 polypeptide alpha-chains forming a triple helix. Could be either fibrillar (like Collagen I), or non-fibrillar (like Collagen IV)	- Influence cell processes like migration and adhesion - Provide tensile strength
Proteoglycans	They consist of a core protein to which side chains of glycosaminoglycans (GAG) are attached. Four groups of GAGs are present, which are hyaluronic acid, keratan sulfate, chondroitin sulfate and heparan sulfate	- Structural basis for different biological functions
Fibronectin	It's a protein secreted as dimers linked by disulfide bonds, showing binding sites for other fibronectin dimers as well as collagen, heparin and cell surface receptors	- Promotes cell adhesion - It's involved in the wound healing process

Laminins	It's a family of glycoproteins assembled into a cross-linked web, interwoven with Collagen IV.	- Allow close interaction with cells - Essential role in organogenesis and embryonic development
Elastin	It's a protein secreted as a tropoelastin monomer, which with fibulins associate with microfibrils forming elastic fibers.	- Allows elasticity to tissue subjected to repeated stetches

The ECM is furthermore composed by other molecules including growth factors and matrix metalloproteinases (MMPs). Growth factors are cytokines which regulate tissue development and other cells behaviour including migration and survival in all body tissues. [7] Other fundamental components are represented by the MMPs. Exploiting collagens and other ECM elements as substrates, MMPs ensure the ECM to be continuously remodelled, through deposition, degradation and modification of its components.[5]

ECM structure

The ECM is a complex and well-organized network of proteins, GAGs and proteoglycans, which together support cells, tissues and organs. These components interact with each other's and play a role also in the regulation of cell proliferation. The ECM is a dynamic structure which includes two distinct entities, the interstitial matrix (IM) and the basement membrane (BM) which are highly interconnected. These two sub-units differ in terms of composition, function and location. [8] The basement membrane is enriched with laminins, fibronectin and collagen type IV, conferring tensile strength to the overlying tissue, resulting in a denser and "less porous" matrix compared to IM. Perlecans, which are involved in angiogenic processes, are also largely present in the basement membrane. Furthermore, due to its integrins, BM is able to direct cells shape and motility. Interstitial matrix, on the other hand, is located beneath the BM or between connective tissue cells [6]. In IM,

collagens are present mainly in fibrillar forms, like Collagen I and III, and provide tensile strength to tissue. Furthermore, collagens interact with MMPs, surface receptors, fibronectin, proteoglycans and other ECM molecules. [8]

1.2 Tumour microenvironment (TME)

Cancer is a multifactorial disease caused by uncontrolled cellular division, due to genetic mutations. Tumour cells rearrange the surrounding microenvironment, by recruiting the cells populations that promote cancer progression and invasion, creating a 3D tumour niche, defined as the tumour microenvironment, reported in Figure 1.

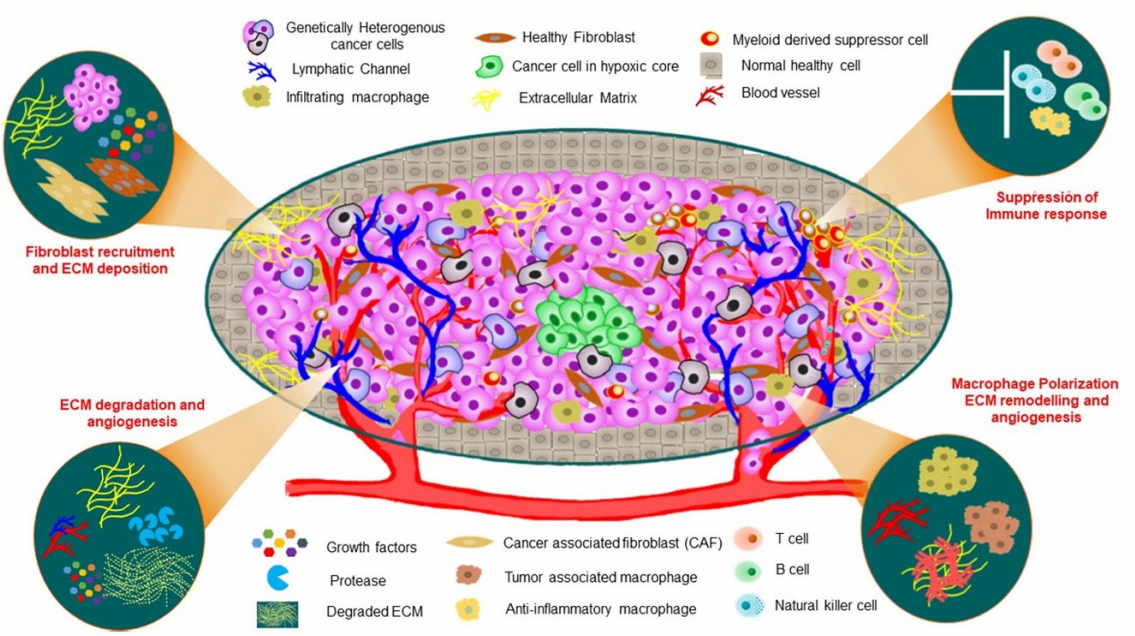

Figure 1: TME structure and components [9]

The TME is a dynamic environment consisting of cancer cells, tumour vasculature, host immune cells, stromal components like fibroblasts, as well as ECM proteins such as collagens, glycoproteins, proteoglycans, and other components which are highly involved in tumorigenesis. [9] Indeed increased ECM proteins production and crosslink, furnish biochemical and biophysical cues, which help cancer cells to proliferate and invade the surrounding tissues. [10] As its components continuously interact between each other's to promote the tumour progression, TME constantly changes and evolves through time by remodelling and reorganizing itself. [10] Stromal cells like fibroblasts, which are normally involved in structural integrity,

healing and regeneration of the ECM, [8] secrete their own ECM proteins which conjugated with cancer cells, form a tumour-supporting microenvironment, improving cancerous stability and signalling between cancer cells and its components. Cancer cells could also recruit normal fibroblasts to transform them into cancer-associated fibroblast (CAFs), which, by secreting specific signalling molecules, control tumour cell migration, epithelial-to-mesenchymal transition (EMT) and invasion processes. Tumours can also change the vascular network through angiogenesis to improve their nutrients supply and overall proliferation. Furthermore, cancer cells can influence the immune system helping cancer progression and cancerous cells survival. [9] In Figure 2, is reported an example of the TME progression and remodelling, focusing on breast cancer. Here is highlighted the role of stromal ECM components surrounding, with fibroblasts, the cancerous core, to guide the tumour's growth.

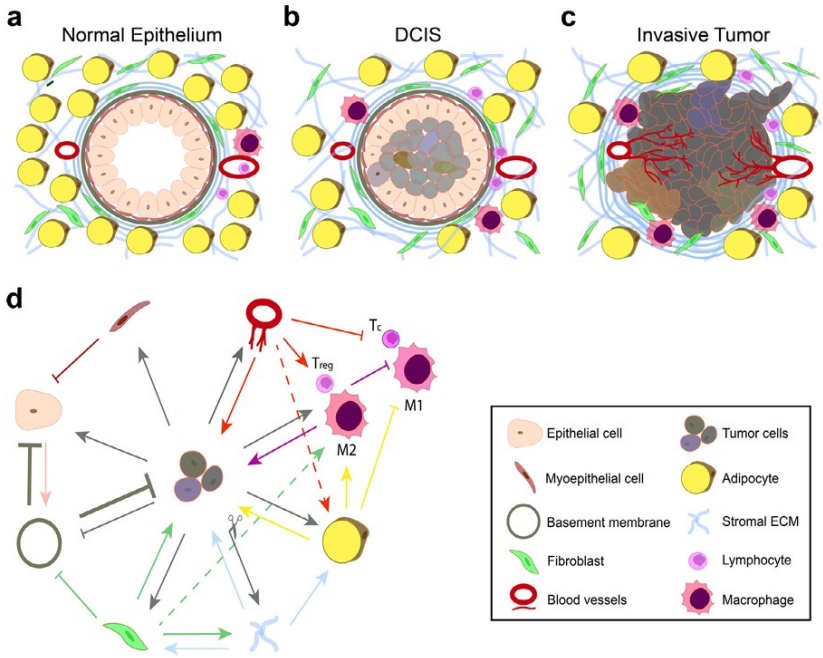

Figure 2: Simplified representation of a 3D breast cancer model. In (a) is reported the normal epithelium; in (b) ductal carcinoma in situ (DCIS) formation and in (c) an invasive tumour. In (d) is reported a simplification of the interactions between cells and the ECM. The communication occurs between the cancer cells, stromal cells (fibroblasts and adipocytes), immune cells (T_{reg}, regulatory cells, T_c cytotoxic T cells, and type 1 (M1) and type 2 (M2) macrophages), the endothelial cells changing the surrounding microenvironment. [2]

In our experiments we aimed to reproduce the 3D TME, compartmentalizing tumour cells and stromal tissue cells, to study the interactions between them. To

give a general idea of our aim, we reported the experiment conducted by Puls et al ([11]), replacing their customized dispensing method, with extrusion 3D bioprinting method. In Figure 3 is reported their proposed model of TME replicated *in vitro*.

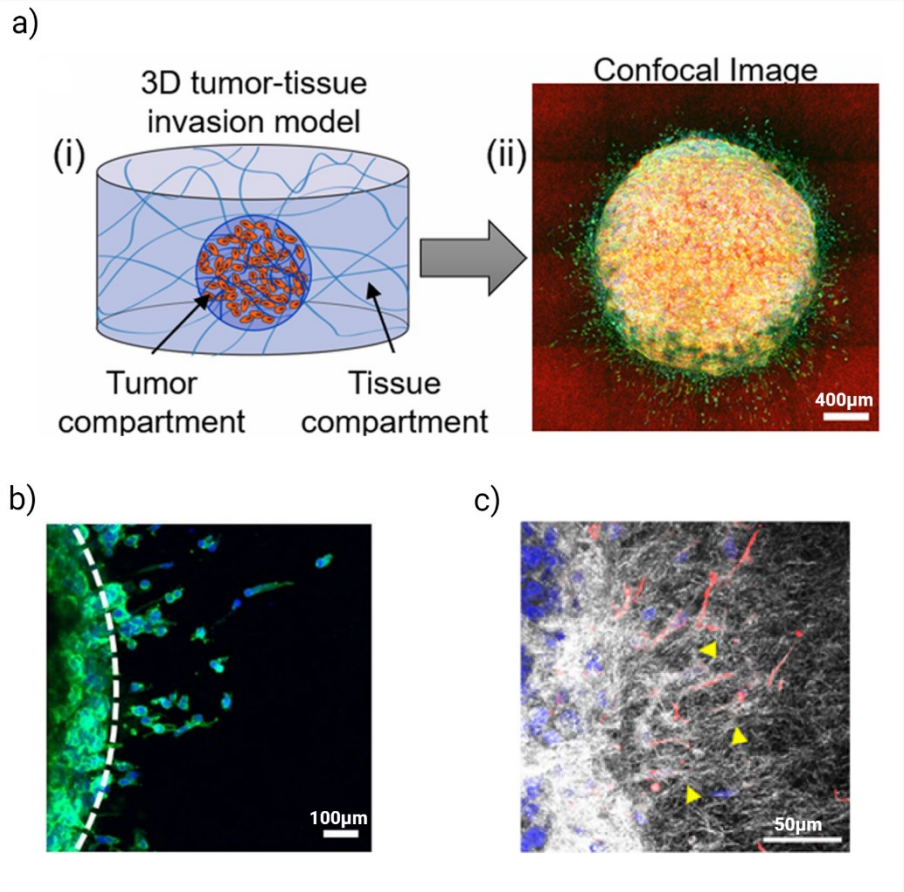

Figure 3: Example of an in vitro model of TME. In this experiment both compartments are composed of collagen's oligomers, differed by the presence of pancreatic cancer cells (Panc-1) in the tumour compartment. Results are reported after 5 days of observation. In (a) is reported the designed model to evaluate the invasiveness of tumoral cells. The model (i) is shown under confocal imaging in (ii), reporting in green the actin, in blue the nuclei, and in red fibrillar collagen. In (b) is reported the invasiveness of cancer cells, with green actin and blue nuclei. In (c) are reported collagen fibers under confocal reflectance, with yellow arrowheads denoting collagen's remodelling and alignment. Vimentin is reported in red, along with stained blue nuclei. Both vimentin and integrin are proteins involved in cellular adhesion. The images were adapted from Puls et al. ([11]).

1.2.1 Collagen's role in TME remodelling

Collagens are the major component in both IM and BM, creating specific ECM compositions in a variety of tissues. Therefore, it should be not surprising that collagens play a fundamental role in multiple stages of cancer progression as well

as precancerous lesion, highlighting their importance in terms of diagnosis and prognosis for cancer treatment. Collagens are mainly divided into fibrillar and non-fibrillar collagens. Fibrillar collagens, like Collagen I, make up the 90% of the totality, and provide mechanical support and dimensional stability. Non-fibrillar collagen like type IV Collagen, on the other hand, are not only essential to maintain tissue structure, but they also work as key regulators to organize and anchor the ECM meshwork. Collagens' shape alterations are present in many diseases, especially fibrosis and precancerosis. Different imaging modalities exist to detect these changes, including immunostaining, second-harmonic generation (SHG), confocal microscopy under reflective mode and electron microscopy, like scanning electron microscope (SEM) and transmission electron microscope (TEM). [12]

Pre-cancerous lesions

Fibrosis is commonly representing an excessive deposition of ECM components, within and surrounding a constantly damaged tissue, usually representing the outcome of a severe tissue injury or chronic inflammatory diseases (CID). The presence of fibrosis and alterations in membrane physiology are mainly due to changes related to collagens, like an abnormal ratio of collagen types, abnormal molecular structure and new collagen types' secretion. [13] Fibrosis is correlated to a higher risk of many cancerous types, such as the hepatocellular carcinoma, lung cancer and oral malignant tumour. Taking the liver as an example, in physiological condition, the ECM is constituted predominantly of non-fibrillar collagens such as type IV and VI, while in a fibrotic liver a great accumulation of fibrillar collagens, like type I and III occurs. Also, the ratio of the collagens' sub-chains could be an indicator of fibrosis. Indeed, oral submucous fibrosis is characterized by an increased collagen synthesis and an abnormal ratio of α1(I) to α2(I) chains in Collagen type I. These results highlight the importance of collagen fibers analysis in predicting cancer. [12] An interesting study conducted by Despotović et al ([14]), showed the alteration in morphology of a colorectal malignant tumour. Particularly, there is an increased alignment and thickness in the collagen fibers closer to the tumour's site as can be seen in Figure 4.

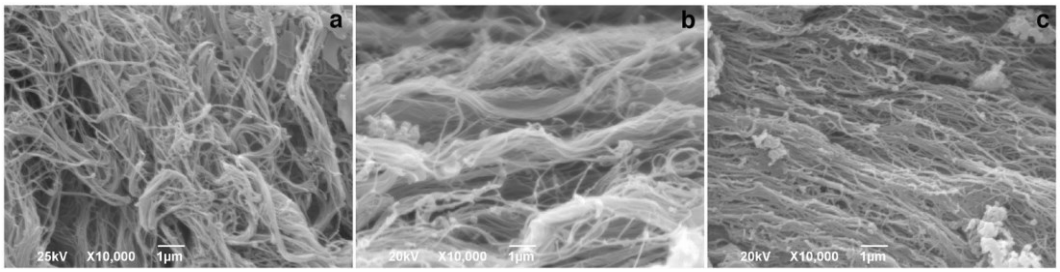

Figure 4: Representative SEM images of collagen fibers alterations. They represent in (a) a healthy patient's tissue, in (b) 10cm and in (c) 20cm away from the malignant tumour. [14]

Cancerous lesions

Initially the base membrane act like a barrier between tumour cells and physiological tissue. However, at the early stages of carcinogenesis, it is usually breached, mainly due to degradation of collagen IV, the major component of the base membrane, caused by tumour cells. Degrading collagens is an effective strategy used by the tumour to invade and migrate in tissues. Another factor improving tumour cell migration and invasion is the ECM stiffness as it is determined by fibrillar and non-fibrillar collagen. There is a tumour rise as age increases, and it has been proven that older tissues are stiffer than young ones, due to an increased presence of aberrant crosslinked collagens. However, a clear correlation between collagen density and cancer progression is still not completely disclosed. Collagen fibers orientation is another phenomenon related to ECM cancer remodelling. Tumour growth apply stresses to the collagen fibers, which are induced to align radially from the tumour core towards the tumour periphery. These newly oriented fibers contribute to tumour invasion and proliferation creating a pathway for cancerous cells, as reported in Figure 5. Tumour fibers realignment is involved in angiogenesis (Figure 5a), to enable nutrients supplies to tumour cells to promote cancerous growth, as well as invasion towards the surrounding tissues (in Figure 5b-d). The tensions so generated, increase furthermore the ECM stiffness. Cancers could also exploit these collagen fibers orientation to form new leaky vasculature network in the process known as angiogenesis, to enhance the supply of oxygen and nutrients to improve their progression. [12]

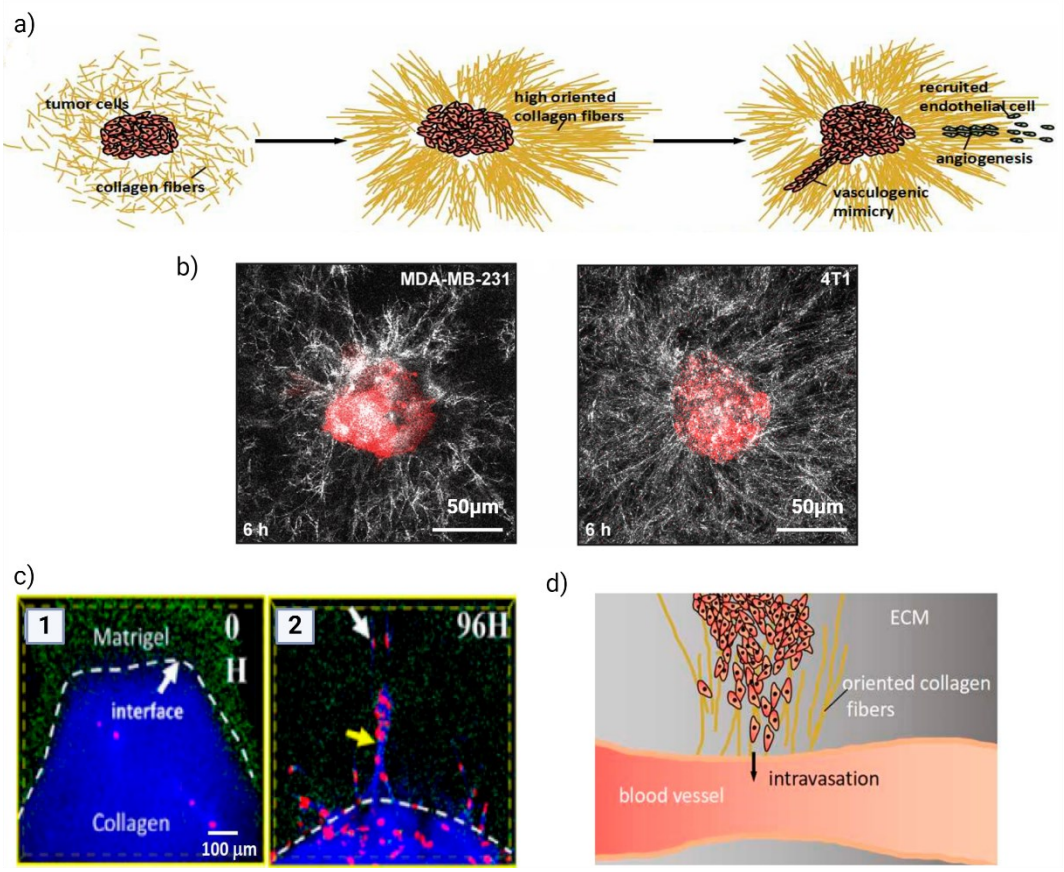

Figure 5: Tumour's rearrangement of collagen's fibrillar structure. In (a) is reported schematically the realignment of collagen fibers around the cancerous core, ultimately representing, among its role in angiogenesis process.[12] In (b) are reported cancer mammary cells, of both human (MDA-MB-231) and murine (4T1) origin, after 6 hours of sedimentation, showing the high fibers organization surrounding them. Images were readapted from Piotrowski-Daspit et al. ([15]). In (c) they showed how cancer cells (red) can infiltrate in the basement membrane (green) exploiting collagen fibers (blue). In (d) another example of collagen's rearrangement, in which fibers lead cancer's invasion towards blood vessels.[12]

1.2.2 3D Cancer modelling strategies

The complexity of cancer significantly hinders the understanding of the underlines mechanisms that lead to the malignancy onset and limits the development of new life-saving treatments. This situation is also exacerbated due to cancer heterogeneity: differences exist not only between different patients, but also between cells within the tumour. Traditionally, the efficiency of drugs treatments has been studied using 2D *in vitro* cytotoxicity, however these methods are not fully representative of the complex 3D TME, thus giving an incomplete analysis on drugs efficiency. 2D models are less complex and useful to investigate singularly the effects of each parameter tested and enable cell-cell interactions studies as well as

cell-material ones. However, cells tend to adapt to the 2D monolayer environment, not recapitulating the original phenotype. Furthermore, cells exhibit random morphology, altered shape and absence in orientation-related signalling. Cancer cells when cultured in 2D, exhibit non-native signal response, altering their biological functions like growth, metabolism, differentiation and ultimately, their shape. Recently, there is an increasing interest in 3D cell culture techniques, as they more closely mimic the *in vivo* cell environment, in terms of gene expression, cell migration, morphology, heterogeneity and proliferation. [2] There is a variety of cancer models, with their advantages and disadvantages. The choice of which model depends on the intended application. Here, we will present a short description of the main approaches, which are organ-on-a-chip devices, spheroids/organoids and bioprinting.

Organ-on-a-chip is an innovative 3D culture system, which exploit the principle of microfluidics to create miniature devices able to process or manipulate small amounts of fluids. They use micro-channels, which thanks to their reduced size (from ten to hundreds of micrometres) can create chambers and fluids passaging, to simulate biological models with reduced quantities and cost. However, they have many drawbacks, including difficulties to maintain cell viability and functionality, as well as structural integrity of the models.

Spheroids or organoids are one of many scaffold-free methods to 3D model tumours. Organoids are a self-aggregation of cells and share lots of similarities with *in vivo* tumours, like volume growth kinetics, cell secretions and cellular heterogeneities. They could be derived directly form the patient, enabling patient-specific testing and drug development. The hanging drop method is a common technique to grow tumour spheroids, it uses specialized plate which allow the formation of drops of media with encapsulated cells, which self-aggregate due to the absence of adhesion force. The formation of tumour-like structures require several days. Also, cells directly seeded within hydrogels like collagen and Matrigel can also lead to tumours structure. A big limitation remains the lack of vasculature, which causes a gradient in spheroids' supplies, as the inner cells are not able to get their nutrients and oxygen, which can result in cell death in the organoid's core. Conversely, the outer cells receive sufficient nutrients and oxygen exchange.

Another drawback is that only tumour cells secrete the ECM, which is not representative of the native environment's behaviour. However, they mimic the cancerous structure present *in vivo.* [16]

Bioprinting shows promising results not only for oncological research, due to the possibility of highly spatially controlled complex models' creation simulating TME's microarchitecture, but also for regenerative medicine. Generally bioprinting allows a predetermined spatial deposition of a biomaterial, through different technologies each with its weaknesses and strengthens, [1] which will be discussed in detail in the following chapter.

Chapter II
Bioprinting and biomaterials

As cancer is the second leading cause worldwide, different strategies have been studied to recreate and model TME, to improve our understanding in diagnostics and treatments. 3D bioprinting seems to be efficient in recapitulating the complex behaviour encountered in healthy tissues as well as pathological ones. [17],[1] Indeed, it offers great versatility and precise control on composition, configuration and overall architecture of the construct, to recapitulate the complex structure of the desired organ, and generally the microenvironment. [18] There exist several bioprinting modalities, which will be explored in this chapter, used for this purpose. Bioprinting materials mainly divide into two categories: biomaterial ink, which are acellular and are used to create 3D scaffolds, subsequently seeded with cells [19]; bioinks composed by a mixture of cells and biological materials, [17] which are typically hydrogels, as they ensure more resemblance to the natural ECM, creating a cellular-friendly environment and retain a high water content. [19] There is a focus on hydrogel-based bioinks, where collagen and gelatin-based formulations are commonly used which, due to their psychochemical properties, enable a bioprinted tissue similar to the original one. [17] The ideal characteristics of 3D printing biomaterials are biocompatibility, printability with tuneable parameters and similarity with the living tissues in terms of morphology and mimicry. In Figure 6, are reported the principal applications of bioprinting in disease modelling. We will focus on tumour microenvironment recapitulation, using both stromal cells (fibroblasts) and cancerous cells.

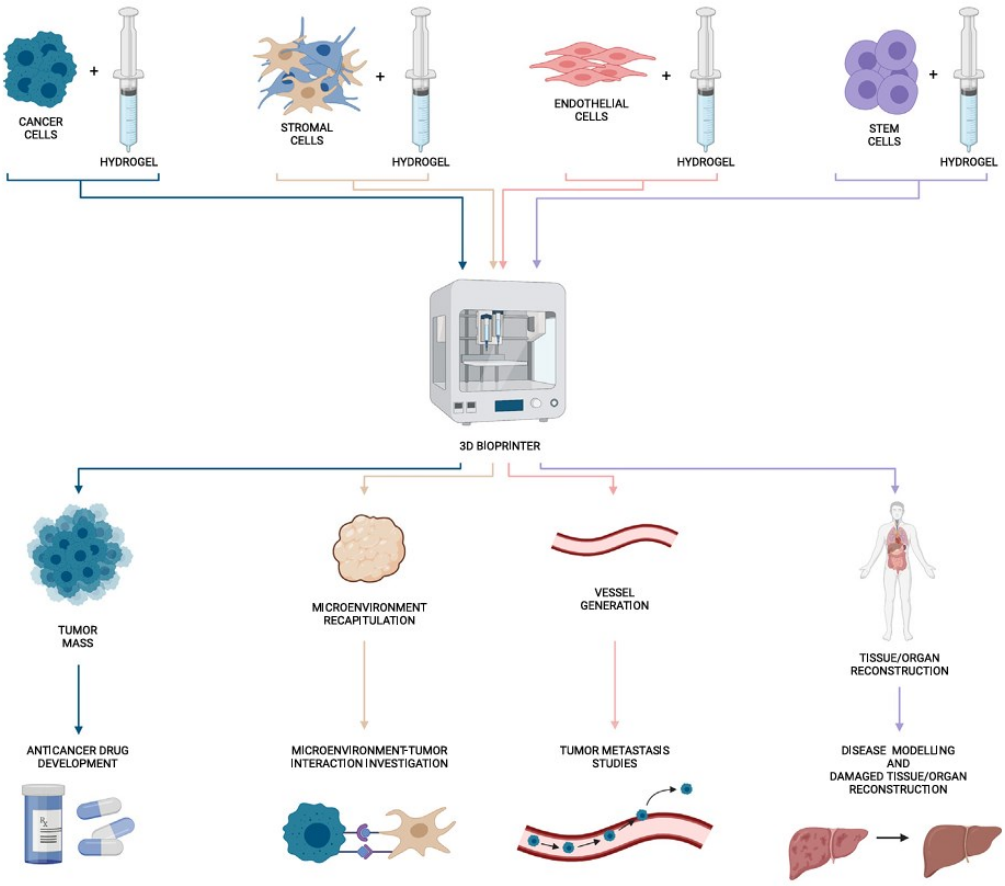

Figure 6: Disease modelling in bioprinting. [18]

2.1 The bioprinting process

3D bioprinting follows the workflow reported in Figure 7.

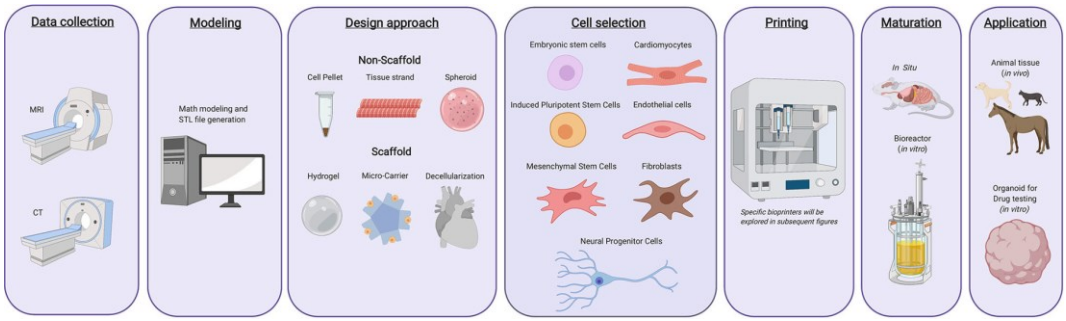

Figure 7: Bioprinting workflow.[20]

The first step is computational modelling, which could either be designed manually or derived from data collection. It is followed by the bioink preparation, which should be suitable for both the intended design approach and cell selection (consisting of both cellular type and concentration target) and printing approach.

Then, the bioink is deposited. Finally, the printed construct is implemented in its desired application. [20]

[20]Bioprinting is part of the macro-category of 3D printing, which comprises a wider range of techniques and materials, as well as application fields, including biomedical field. [21]Although we will focus on bioprinting, here briefly is reported the 3D printing approach, which helps to better understand the whole bioprinting process. First, the digital 3D object is realized through a computer aided design (CAD) software or digital scanning data. The designed object is later converted into a 3D printer-readable file format, like STL (standard tessellation language). STL file, allows the object to be represented in a three-dimensional cartesian coordinate system, storing further information, like surface's geometry, while excluding details like colour and texture. [21], [22] The object is then processed through *slicing*, resulting in a machine-readable file (.gcode), in which the 3D model is virtually cut into 2D slices of equal thickness, which are later consecutively sent to the 3D printer, to deposit the corresponding layer. [23],[21] The .gcode file could then be modified to control more precisely the movements of the nozzle/nozzles, specifically for each application. In Figure 8 is reported an example of the 3D printing of a human ear procedure.

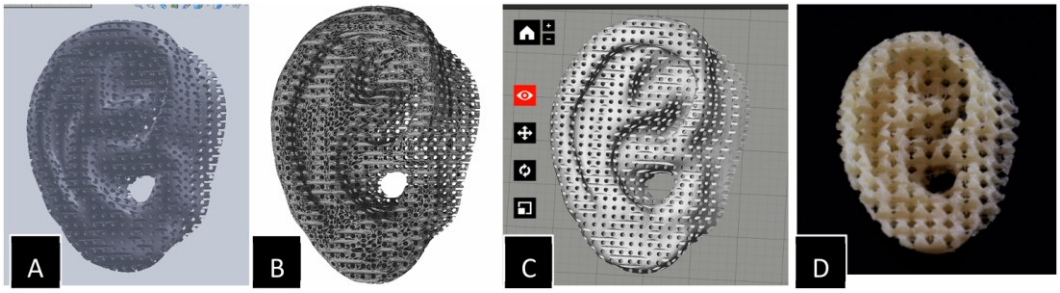

Figure 8: Bioprinting of a human ear. The construct is firstly designed using a computer aided design software (A), it's converted into a STL file (B), sliced through a 3D printing software (C), creating a .gcode and finally the object is printed (D) . [22]

Along with the printing procedure, there are other steps, which are principally related to bioprinting procedures. First, the design approach highly influences the bioprinting procedure. To generate tissue architecture, two methods exist, which are the scaffold-based bioprinting and the scaffold-free approach. Scaffold-based bioprinting use biomaterials to generate temporary structures to promote cell

adhesion, proliferation and tissue formation. These approaches are based on biomimicry and provide a higher resolution, and lower-costs compare to scaffold-free approaches. Usually, hydrogels are used for scaffold-based bioprinting. On the other hand, scaffold-free approaches are based on the concept of autonomous self-assembly of the tissue during its development. In other words, they rely on the innate tissular mechanisms of producing their surrounding architecture, without template or scaffold requirements. During scaffold-free bioprinting, cell pellets, spheroids or tissue strands are used as "building blocks", which are expected to fuse together, secreting the desired ECM components. However, they are usually printed at high cells concentrations, increasing the costs and limiting printer selection. [20] Cells is another important factor impacting on bioprinting procedure. The challenging aspect in 3D bioprinting is to produce minimal damage to cells throughout the printing process, ensuring good proliferation, and if requested, differentiation. Cells should be chosen depending on the specific intended application, to recapitulate correctly the target microenvironment. Therefore, their derived source is fundamental in bioprinting. Somatic cells like fibroblasts, chondrocytes and cardiac myocytes have been used in 3D bioprinting, however most applications focus on stem cells, to ease de novo tissue development, as the latter are able to self-renewal and differentiate. [18] Unfortunately, stem cells present many drawbacks, including ethical concerns, difficulty to achieve and maintain pluripotent state and invasiveness in extraction procedures. [20] Cells concentration significantly affects tissue formation and the printability of bioinks affecting their rheologic properties. Hence, it could constitute a limit for the choice of the appliable bioprinting technique. [24] Bioprinted construct are finally cultured under tightly regulated conditions usually in bioreactors. These systems enable precise control on parameters such as pH, temperature and CO_2 concentration, which highly influence tissues metabolism and growth. [20] In our experiments we cultured the bioprinted constructs in an incubator, at 37°C, in a humidified atmosphere 5% CO_2.

2.2 Principal techniques and materials in 3D bioprinting

The term bioprinting is generally used to indicate the processes regarding the materials transfer in a designed and controlled configuration, to enable the assemble

of molecules, cells and biodegradable tissues carrying one or more biological functions. It gives rise to a variety of techniques and biomaterials that could be used, offering more customizable and reliable manufacturing as well as an improved design complexity, compared to other biomedical methods. [21] The most popular techniques (Figure 9) include inkjet-based bioprinting, light-based methods (like laser-assisted bioprinting and stereolithography) and extrusion-based bioprinting. [1]

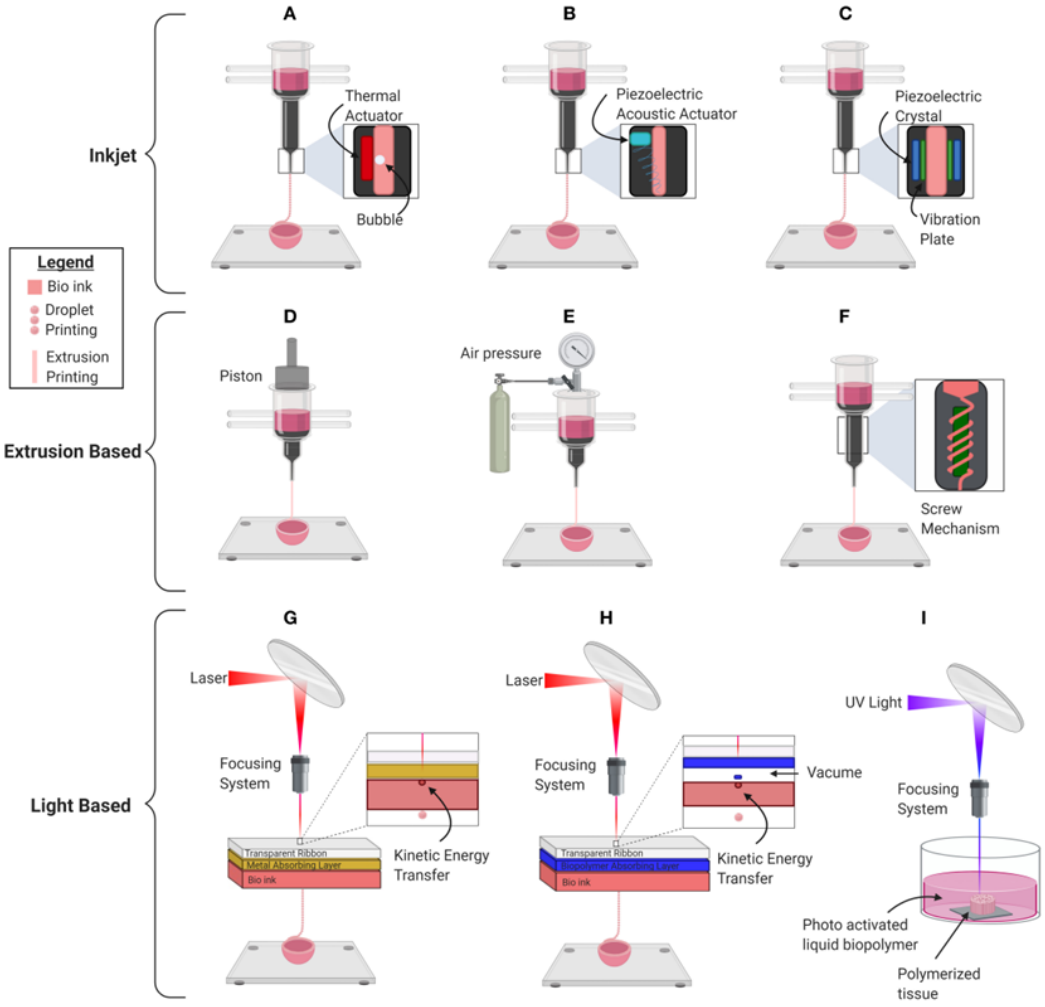

Figure 9: Principal bioprinting techniques. Precisely, there are three macro-categories reported: Inkjet bioprinting, represented by (A) thermal, (B) piezoelectric mechanical and (C) piezoelectric acoustic inkjet printer; Extrusion based bioprinting, represented by (D) piston-based extrusion, (E) pneumatic extrusion, (F) screw based extrusion printer; Light based bioprinting, represented by (G) Laser Induced Forward Transfer (LIFT), (H) Matrix-Assisted Pulsed Laser Evaporation (MAPLE) and (I) Stereolithography Bioprinter. [20]

Inkjet bioprinting

Inkjet-based bioprinting (Figure 9A-C) is based on the dispensing of the material in droplets of controlled dimensions. It is divided into thermal and piezoelectric techniques, depending on the dispensing method. In thermal inkjet bioprinting, the bioink is heated up to 200-300°C for a very short application time, ensuring an overall bioink increase in temperature of maximum 10°C. Acoustic piezoelectric inkjet works using sound waves which induce bioink's rupture and consequent drops extrusion, [1] while mechanical piezoelectric works by forcing a plate to vibrate, to apply pressure to the bioink, causing droplet extrusion. [20] Overall, inkjet techniques are fast, present high cell-viability, and good resolution (up to 30-50 μm), although droplets' size could vary during the printing process. However, they present many drawbacks, such as limited low-cell density, and low viscosity bioinks usage, required to prevent nozzle clogging.

Light-based bioprinting

Laser-assisted bioprinting techniques (Figure 9G-I) are nozzle-free, they work as noncontact methods, in which a laser beam is pulsed on a three-layer ribbon. In LIFT bioprinting, the three-layer ribbon consists of a laser-transparent glass, a laser-absorbing metal (like gold or titanium) and finally the bioink. The ribbon absorbs the beam, rapidly generates a local bubble on the opposite side, causing the ejection of the desired quantity of bioink on the receiving substrate. It can be used with high concentrations of cells (up to 10^7 cells/ml), ensuring also high viability, it's a fast method and allows good resolution (10-100 μm). However, it's an expensive technique, as high control is required throughout the procedure, as the intense energy absorption could generate contaminant fragments which could enter the bioink and damage the living cells. [1] In MAPLE the underlying principle is similar, but the metallic layer is replaced by a biopolymer matrix, which is able to transfer kinetic energy lowering toxic particles exposure. [20] In stereolithography, the light source consists of a focus laser beam. Typically, the process begins by immersing the printbed closely below the surface of the solution to be polymerized. The laser beam scans the first object's *slice* initiating the polymerization reaction. After the first layer has been processed, the printing bed is lowered and the next

layer is printed, repeating these steps till the 3D object results completed. Afterwards, the uncured resin is removed and postprocessing steps are usually applied to improve mechanical properties of the printed construct. [19] As it is a nozzle-free technique, it presents high cell viability, as no shear stress is applied during the process, reducing cellular damages. Furthermore, it's a fast-bioprinting method, presents high resolution control (up to 25 μm), and allows a good range of viscosities, although low viscosity bioinks are usually preferred. Its drawbacks regard cytotoxicity risks, caused by the used photoinitiators, low cell density to limit scattering and unreacted bioink's removal, and its high costs. [1]

Extrusion bioprinting

Extrusion-based 3D bioprinting techniques are now considered the most widely used in the production of 3D tissue constructs. [25] They derive from the Fused Deposition Modelling (FDM) technique, which is the most common material extrusion technique used in 3D printing. [21] In this technique a thermoplastic filament is inserted into a printhead, which heats it allowing its deposition on the build platform, till the object is formed. Although it's used in the biomedical field for prosthetics and drugs carriage, its required high temperatures, [22] present a limiting factor for the uses we intended. On the other hand, 3D extrusion bioprinting works similarly, but the materials are differently extruded. The process enables the embedding of cells and bioactive molecules, as it doesn't involve any high temperatures as well as minimal process-induced cell damage control. It's also cheaper and easier compared to other bioprinting technologies, and it's mainly divided into two sub-categories: pneumatic extrusion and mechanical extrusion, represented in Figure 9 (D-F). Pneumatic extrusion employs a compressed gas (like air or nitrogen) to move the bioink through a controlled pressure, while mechanical extrusion uses mechanical force which could be either applied by a piston or a screw, to move the bioink. [25] Although mechanical dispensing system might provide a better control over the material flow, compared to pneumatic systems, they are based on complex mechanisms, which hinder the maximum force capabilities. On the other hand, pneumatic systems are simpler and allows both good appliable force capabilities, as well as the use of high-viscosity materials (though, also screw-driven bioprinting is able to bare high viscosities materials).

Extrusion bioprinting can be performed also with high cellular concentration, useful to achieve physiological cell densities. However, due to high shear stress experienced during the process, cells viability is considerably reduced compared to other printing techniques, although it could be improved by using low pressures and large nozzle size, which unlucky reduce both printspeed [26] and resolution (lower than other techniques, up to 200-1000 μm [1]). Biomaterials used in extrusion bioprinting include natural polymers like collagen, gelatin, alginate and hyaluronic acid, as well as synthetic biomaterials such as PVA and PEG, that will be further discuss in the dedicated section. [25] Furthermore, the presence of multiple printheads, enable the serial dispensing of several materials, without retooling requirements. [26] 3D extrusion bioprinting allows also different methods, due to its versatility, like sacrificial and freeform embedded bioprinting, which allows bioprinting of aqueous materials and complex structures. [25]

Freeform Reversible Embedding of Suspended Hydrogels (FRESH) bioprinting

FRESH is an embedded approach which enables the development of complex 3D scaffold as well as soft biomaterials printing, which help in resembling the structure and functions present in human tissues and organs. The principal behind this approach lies behind the extrusion of bioinks within a yield-stress support bath, which holds in place the extruded material, till it's been cured. Soft and liquid-like bioinks, which are typically used for ECM recreation, suffer from loss of print fidelity, challenging further layer-by-layer construct development. [27] The presence of a fugitive ink, which can be washed away once printed, is fundamental to overcome these limitations. This ink, used as support bath, serves as support for the extruded bioink filaments, and it's characterized by a high plateau elastic modulus and low yield stress to facilitate nozzle translation. This support bath could either be prepared with macromolecules as well as microparticles, which permits a local fluidization with nozzle translation and subsequent solidification of the gel. [25] FRESH provide therefore support to the printed soft biomaterial, enabling it to reach its stability and print fidelity, although the bioinks' initial low rigidity and structure stability. FRESH bioprinting platform is highly customizable, and could be adapt to the specific application, as seen in Figure 10.

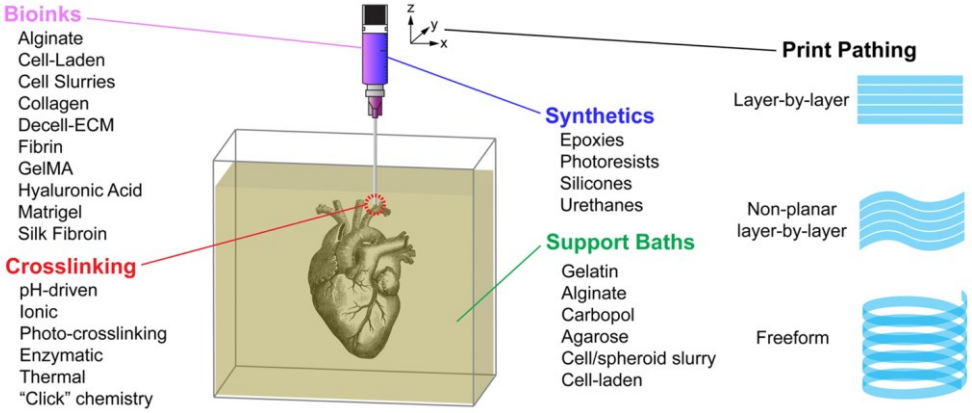

Figure 10: Highly customizable FRESH bioprinting platform. [27]

Although being a highly customizable technique, few aspects should be considered in the choice of FRESH bioprinting process. Firstly, the support bath should act as a viscoplastic material, with rheologic behaviour similar to Bingham plastic, where it acts as a solid till a certain shear stress is applied (denominated yield stress), and beyond this point, it acts as a liquid; secondly, the support bath's aqueous phase should be compatible with bioink's gelation dynamics; lastly, support bath's liquefaction should guarantee non-destructive print release under biologically compatible conditions. Most commonly used support baths are microparticles support gel (like gelatin and Carbopol), but also other strategies could be used, such as thermosensitive materials, used also for sacrificial bioprinting (like Pluronic F127). [27] Support baths removal occurs either via chemical or physical principles, although we will focus on the latter to ensure biomedical safety, with low cytotoxicity. Commonly used physical principles include water solubility (Carbopol) and temperature sensitivity (Pluronic F127, gelatin-based materials). [28]

2.3 Hydrogels as bioprinting materials

Biomaterials could be natural or synthetic substances, which when placed within biological systems, provide help to repair, replace or improve any tissue or organ. Hence, ideally biomaterials should be biocompatible, should provide good mimicry of living tissues and should be easily printable with tuneable parameters. [22] Naturally derived polymers can be either based on protein, like collagen and gelatin, or polysaccharide, like hyaluronic acid, both showing improved host-implant

integration and cytocompatibility compared to synthetic ones. Furthermore, they better recapitulate biophysical and biochemical microenvironment when their source is the ECM. On the other hand, synthetic biomaterials, like polyethylene glycol (PEG) and polycaprolactone (PCL), enable higher control on chemical composition and molecular weight, showing better qualities also in terms of mechanical strength. [29]

Among the most used polymers in 3D printing, there are the hydrogel-based polymers. Hydrogels are a 3D network of molecules, customizable in different shape and size, formed by cross-linking of polymer chains in a water-rich environment. Various cross-linking methods are used, mainly dividing into physical crosslinking, and chemical crosslinking. Physical crosslinked hydrogels generally present reversibility and easier synthesis process, although as their gelation mostly depend on their intrinsic properties, limited control could be exerted on their microenvironment. On the other hand, hydrogels formed through chemical approaches, allow the creation of more complex and accurate microenvironments, presenting however increased difficultness in their synthesis process. Among physical crosslinking's techniques, we encounter thermal condensation and ionic interaction. Thermal condensation, or gelation, regards the interaction between polymer and water in function of the temperature. Lower critical solution temperature (LCST) polymers, which are the most used, shows miscibility with water once they are below the critical value. As temperature increases, polymer-water interactions become unfavourable. In contrast, under critical solution temperature (UCST) polymers, show an opposite mechanism. One form of gelation process is the molecular self-assembly. Molecules tend to self-assembly as noncovalent, or weak bonds formation are present, usually related to protein-based hydrogels. These materials show viscous flow under shear stress, which can be consequently recovered once shear stress is removed, respectively shear-thinning and self-healing properties, key features for 3D bioprinting hydrogels. Ionic interaction's mechanism occurs when the hydrogel is formed due to electrostatic interaction or chelation, where the polymers are negatively (positively) charged, and the presence of a cation (anion) makes them binding creating a new configuration. Chemical crosslinking represents the most stable and tuneable

hydrogels synthesis technique, and includes methods as radical polymerization, enzyme-enabled crosslinking and high energy irradiation. Hydrogels in bioprinting should possess certain characteristics, trying to mimic the dynamicity of the ECM allowing also native cells' behaviours. However, it remains a challenge, due to ECM's high complexity microenvironment. The fundamental factors influencing bioprinting hydrogels are: biocompatibility, which is defined as the "ability of a material to perform with an appropriate host response in a specific situation" [30]; immunocompatibility, as the biomaterial should not induce a significant inflammatory response when applied *in vivo* microenvironments; Suitable mass transport, as cell encapsulated hydrogels should provide continuous exchanges of gases, nutrients, proteins and waste products to ensure cell viability and proliferation; biodegradation of the material, to enable both sufficient space for cellular proliferation and migration, and if required, blood vessels to infiltrate; low cytotoxicity, usually caused by byproducts or unreacted substances involved in hydrogels' synthesis as well as UV radiation, to avoid cellular damages; suitable viscosity, which is highly related to printability, indeed a too high viscosity requires higher extruding pressures (which could harm the cells), conversely, low viscosities of the bioink, although beneficial for the cells viability, may hinder the structural integrity of the printed structure. [30] Finally, as aforementioned in the previous paragraphs, biomaterials are divided into bioink and biomaterial ink, depending on the presence or absence of cells embedding, as reported in Figure 11.

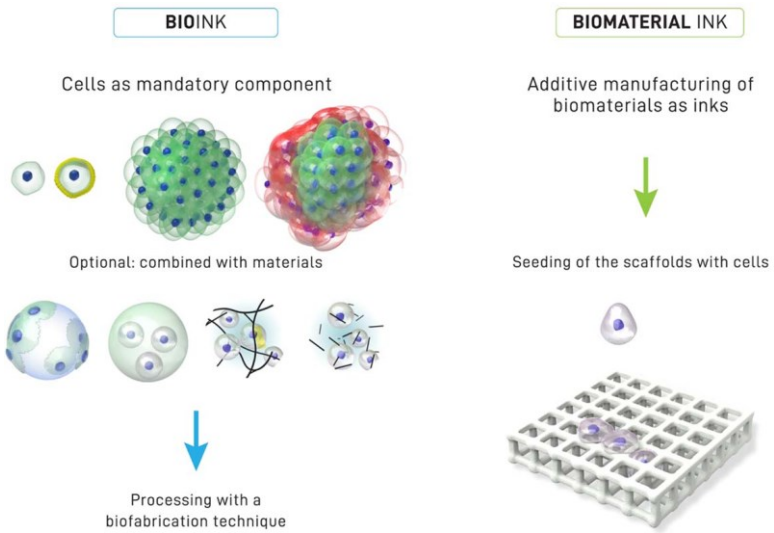

Figure 11: Inks used in 3D bioprinting. [31]

2.3.1 Gelatin Methacrylate (GelMA)

Gelatin is a partially hydrolyzed form of collagen. It's a water-soluble and biodegradable polypeptide and shows good biocompatibility. Due to its properties, is one of the most used natural derived polymers, generally used to form thermally driven hydrogels. Its properties change depending on the animal sources, usually gelatin is derived from mammalians, but also fish gelatin has been studied in literature. However, gelatin presents several drawbacks when applied in tissue engineering, like its poor mechanical stability, high enzymatic degradation rates along with high solubility in physiological environment. [30], [31], [32] To solve these limitations, functional groups can be added to the gelatin backbone creating gelatin methacrylate, or GelMA. [30] GelMA's synthesis and characterization is reported in Figure 12. Firstly, methacrylated groups are added to gelatin's backbone, and consequently, the so formed GelMA undergoes photoinitiated radical polymerization to form covalently crosslinked hydrogels. [33] GelMA possesses two solidification processes, due to its gelatin backbone and reactive lateral moieties. The reversible solidification is thermo-dependant and it's a solid-liquid transition due to the self-assembly of the gelatin chains. On the other hand, the irreversible process occurs when GelMA is crosslinked via radical polymerization, as covalent bonds are formed. Radical polymerization requires a photoinitiator to start the process, therefore it is usually added in GelMA hydrogel. Commonly, used photoinitiators are Irgacure 2959 or LAP (Lithium phenyl-2,4,6-trimethylbenzoylphosphinate), which differ on the radiation light matching absorption requirement, impacting therefore the crosslinking process. [34]

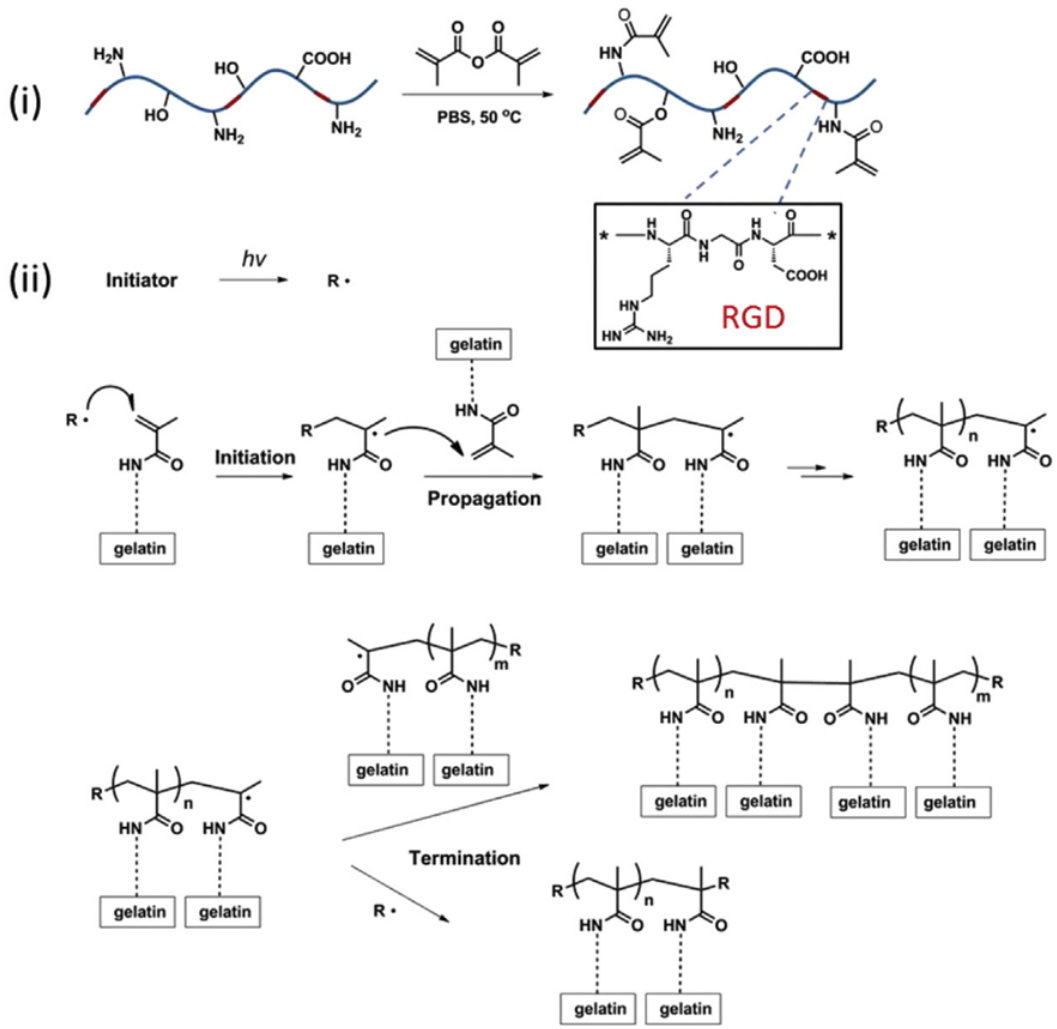

Figure 12: GelMA synthesis process. Firstly (i), gelatin reacts with methacrylic anhydride to graft methacryloyl substitution groups. RGD sequences, already present in gelatin, promote cell adhesion as well as MMPs for matrix remodelling and are highlighted from the inset. In (ii), is represented briefly its radical polymerization process, where the radical groups, generated from the reacted initiator, are involved with chain polymerization of the methacryloyl substitutions. Propagation proceeds between different chains, till either two propagating chains encounter each other or a reaction between one propagating chain and a free radical occurs. [33]

GelMA shows potential for its use as a bioink, due to its superior biocompatibility, on-demand photocrosslinkability and broadly tuneable properties. [35] Indeed, physical properties of GelMA such as the degree of substitution, GelMA's concentration, initiator concentration and UV exposure can influence GelMA's final characteristics. For instance, compressive modulus is directly proportional to the degree of substitution, but also to GelMA concentration. [33]. Another property that can be tuned is viscosity, allowing a great variety of applications. High concentrated GelMA hydrogels (> 30% w/v) presents a high viscosity and allow a higher

bioprinting fidelity, however, they could reduce cell viability as the polymer's network becomes too dense. [17] [33] Finally, GelMA can be combined with other materials as well as additives, which could enhance its mechanical properties and cells behavioural related properties. In Figure 13 are schematically reported the effects of the previously discussed factors on the properties of GelMA.

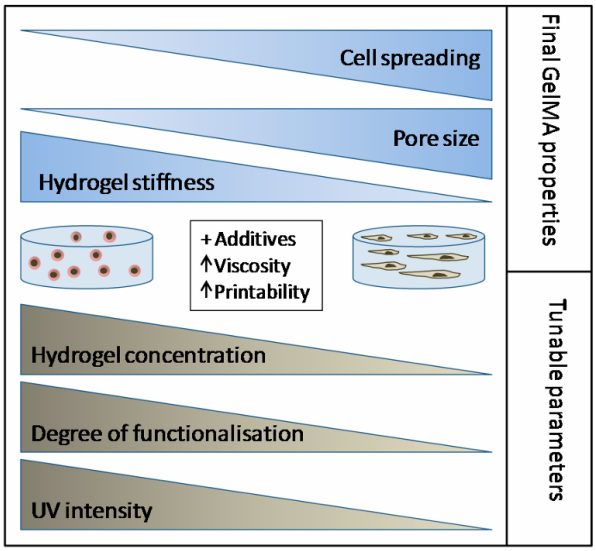

Figure 13: GelMA key features and influence on cell behaviours and gel's mechanical properties. [36]

GelMA is an optimal candidate for extrusion bioprinting, as it exhibits shear-thinning behaviour and it comes as an optimal candidate for cell culture. Indeed, it can be cheaply and easily synthesized, its transparency enables good monitoring on cells, allows cell attachment and it allows tuneable stiffness and pore size. [36]

In our experiments we used a commercially available CELLINK® bioink, named GelMA, porcine derived, with a degree of methacrylation considered to be low-medium (45-55%) which should enable a more permissive microenvironment, to help the spreading, organization and proliferation of cells. [37] The concentration lies between 15 and 10 % w/v, enabling good printability [31] and cell viability. [17]

2.3.1.1 GelMA with nanofibrillated cellulose

GelMA is an established bioink used in many fields but it is often used as a high-concentration material in bioprinting applications. Low-concentration GelMA (like less than 5 % w/v) would be an interesting bioink as its low-density polymer

network would allow cell-cell interactions, increase the efficiency of cellular metabolism and enable cellular migration. [38] However, low-concentration GelMA bioinks lead to poor processability during extrusion-based bioprinting, firstly due to the low-viscosity, which outcomes in irregular printed filaments; secondly its gelation rate from liquid to gel would not be fast enough to maintain structural integrity and post-printing shape fidelity; thirdly, its gel phase would not maintain the scaffold's initial geometry due to inadequate mechanical strength. [31] Different strategies exist to enhance viscosity and printability of low-concentrated GelMA, one emerging strategy is the addition of cellulose nanofibrils (CNFs). These are nanoscale cellulose fibrils, and their presence imparts excellent physical and mechanical properties to the material. [39] Their low-cytotoxicity, interesting rheological properties and structural similarity with the ECM are the key features which contribute to their use in 3D bioprinting. It's used in extrusion bioprinting as cellulose shows shear-thinning and thixotropic behaviours, as well as biocompatibility. [38] Nanocellulose could be used as a viscosity enhancer, allowing effective low-concentration GelMA's bioinks formulations. Although the addition of nanocellulose in gelatin-based bioinks proved to be effective in terms of mechanical properties, cells viability and proliferation, few studies were carried with GelMA and nanocellulose. [32] Shin et al [39] successfully managed to print simple and complex structures like a human ear model with GelMA 5% w/v and CNFs 2% w/v, while Xu et al [38] explored lower GelMA concentration (<1% w/v) and lower CNFs (<1% w/v) both showing good printability and low cytotoxicity. In Figure 14 is represented schematically the crosslinking of GelMA with nanofibrillated cellulose.

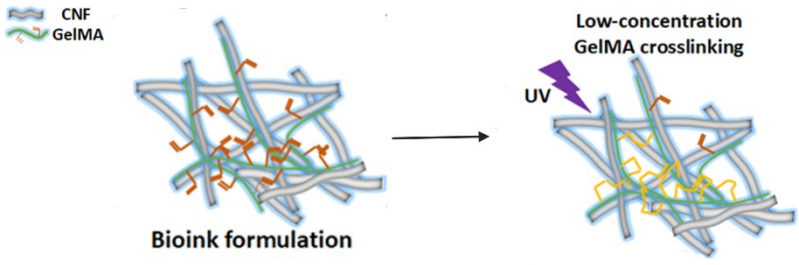

Figure 14: Crosslinking of GelMA with nanofibrillated cellulose. Image was readapted from Xu et al.. [38]

Successful applications of nanocellulose-based bioinks include tissue regeneration, like cartilage, human chondrocytes redifferentiation and adipose tissue engineering. [38]

In our experiments we used a commercial bioink sold by CELLINK®, named GelMA C, with a degree of methacrylation considered of (45-55%). Furthermore, from the collected information (both supplied by CELLINK and by our experiments) this GelMA C seems to be porcine derived, with a CNFs concentration <3% w/v and a GelMA concentration lying between 7 and 10.5 % w/v.

2.3.2 Collagen

Collagen is a protein present in 28 types, differing by the presence of the structural feature triple helix. Collagens account for 30% of the total protein content in humans resulting in the main protein content, therefore collagen is essential for the maintenance of structural and biological integrity in the ECM. Collagens is composed by two classes, namely fibrillar and non-fibrillar collagens. Fibrillar collagens represent more than 90% of human collagens and include types I, II, III, V, and XI providing stability of tissues and structural integrity. Collagen I is the most abundant type of collagen, present virtually in all the ECM and connective tissues, predominantly in skin and bone, while type II is mostly located in cartilage. Non-fibrillar collagens like type IV are involved in network structure's construction in basement membranes. Collagens allow constant remodelling of the ECM, aid cells behaviours like migration and adhesion, provide major tensile strength to the ECM and are involved in tissue repair. [40] Collagens play also a fundamental role in cancer progression, enlightening their opportunity to identify new therapeutic targets for cancer treatments, [12] as well as to become good candidates as bioinks in 3D bioprinting, for TME's modelling. Indeed, malignant tumours tend to secrete collagens altering the ECM by increasing their stiffness, EMT, migration of cancerous cells and metastasis. [9] For this reason, most of the used bioinks are made from type I collagen, considering it is the main component in the connective tissues of mammals. Although its good biocompatibility and low immunogenicity, collagen present lots of drawbacks such as low mechanical properties, difficult sterilization that can lead to degradation, heat sensitivity and contraction of collagen

scaffolds in response to cellular activity, that make it difficult to be bioprinted. [40], [41] To enhance its mechanical properties, different strategies have been pursued, like modification with photoactive methacrylate groups, combinations with other materials or increasing concentration. Low-concentration collagen bioinks enable better cell growth potentials compared to higher concentrated ones; however, they present weak mechanical strength and thermal instabilities. On the contrary, high-density collagen bioinks presents increased stiffness which limit cells bioactivity. [41] In our experiments we focused on low concentration collagen type I (at 3mg/ml), derived from rat tail, to obtain pure mechanical properties.

Collagen structure

Collagen is formed by two α1(I) chains and one α2(I) chain. The repetitive amino acid sequence consists of -[Gly (glycine)-X-Y]n, where usually X is proline and Y is hydroxyproline residues. These allow the individual left-handed α-chains to assemble into right-handed triple helical structure (tropocollagen) with a short non-helical telopeptide region. These triple helices are stabilized via intramolecular hydrogen bonding and van der Waals interactions, seen in Figure 15a. Collagen presents a hierarchical structure consisting initially of microfibrils, defined as small assembly of collagen molecules (usually around 5 units) arranged in parallel along their axial direction via covalent bonds, those further associate into fibrils and lastly into collagen fibers, as indicated in Figure 15b. The crosslinks can be both between and within microfibers [41].

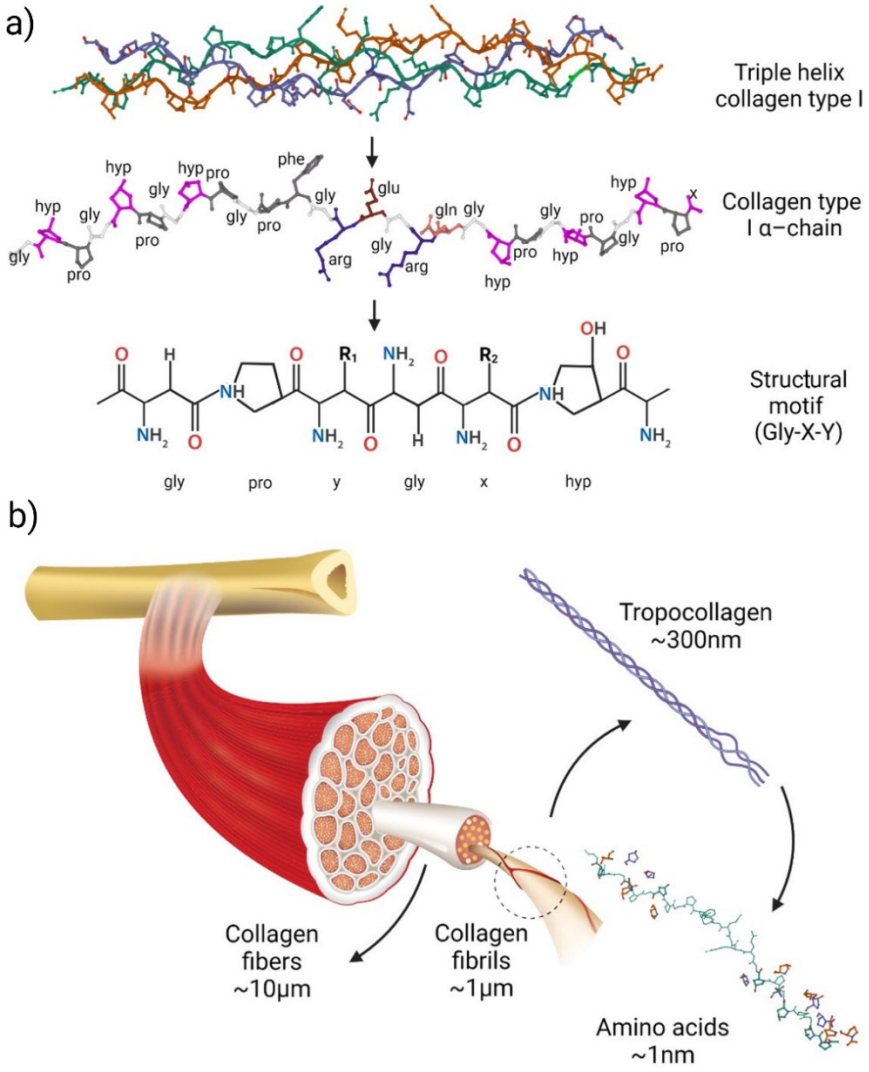

Figure 15: Collagen's hierarchical structure. Microscopical and macroscopical structural organization. Image adapted from Amirrah et al.. ([40])

2.3.3 Matrigel

Matrigel is a natural hydrogel ECM, commonly used in cancer research, purified from Engelbreth-Holm Swarm mouse sarcoma. It's mainly constituted by collagen type IV, laminin, perlecan and entactin. Although its composition reflects the one present in the basement membranes normally found in tissues, it shows many limitations. First of all, its exact composition is undefined and changes depending on the batch, moreover it cannot be clinically appliable as it derives from a mouse tumour. Nonetheless, its biologically active nature is of particular interest for 3D organoids' culture, as it's versatile for different types of cells culture, it's easy to use, highly available and it enables self-organization of cells into structure which

closely resemble the features of *in vivo* tissues. Application of this material in bioprinting is however shows several hurdles. Firstly, Matrigel shows poor mechanical properties and a complex rheology which highly hinder Matrigel's use as pure bioink. Therefore, it is often combined with other bioinks, which work as support material, however, this is not the optimal choice for 3D culture of organoids, as these additives carry also undesired biological variabilities. Furthermore, when using a pneumatic-driven dispensing system, like extrusion bioprinting, it shows similarities with the "spurt" effect. In other words, it's ejected uncontrollably out of the syringe as soon as pressure is applied. [42] Moreover, as Matrigel thermally cross-links at temperatures higher than 4°C, the dispensing system may easily occlude preventing further extrusion if not adequately controlled [43], which is difficult to achieve. In our experiments, we overcome these limitations following the strategy proposed by De Stefano et al ([42]), in which a pre gelling procedure is applied before printing: Matrigel is taken from its liquid phase at 4°C, transferred in a cartridge and gelled for 15 minutes at 37°C prior to bioprinting.

2.3.4 FRESH biomaterials

Bioinks with low viscosity, like collagen or low concentration GelMA, may result difficult to bioprint due to their inadequate mechanical properties. Embedded bioprinting overcome this limitation, as it's a gel-in-gel approach, where the bioink is deposited into a hydrogel/microgel support bath, which helps holding in place the extruded bioink in a pre-designed shape (Figure 16).

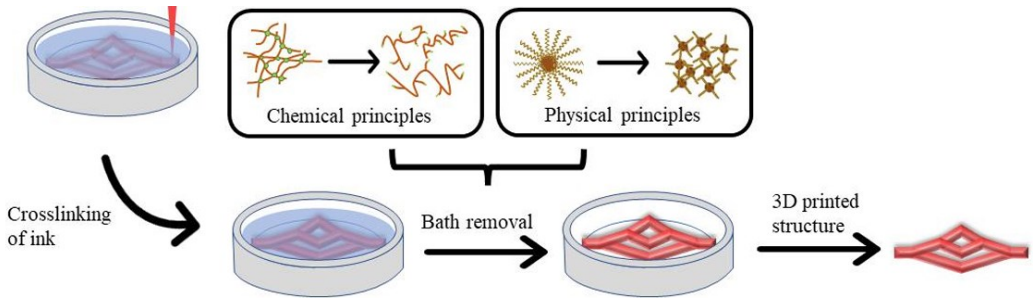

Figure 16: FRESH bioprinting simplified workflow. Image readapted from Liu et al.. ([28])

These support baths should also be biodegradable, non-immunogenic and easily removable. Granular or microgel support baths are available and show applications in modelling complex structures such as brain, kidney, vascular field, using weak

or low viscous bioinks. Common support baths materials include sacrificial bioinks, like Pluronic F127, Carbopol and gelatin-based hydrogels, like Lifesupport.[44] In our experiments we used these biocompatible supporting baths, which moreover, were easy to remove, since they are based on physical crosslinking. The mild retrieval of the printed structure from the supporting bath its of paramount importance when working with live cells. The absence of chemical crosslinking and the lack of organic solvents ensure a higher cell viability. [28]

Lifesupport

Lifesupport is the trade name of the support bath commercialized by Fluidform, consisting of gelatin microparticles, and it shows a Bingham plastic behaviour, [44] in which under low shear stress it behaves as a rigid body, counter wisely, under high shear stress it behaves like a viscous fluid. This property is fundamental in FRESH bioprinting, as when the extruding needle-shaped nozzle moves inside the gelatin bath it perceives very low mechanical resistance, allowing the bioink's deposition, which stays in position after being extruded. As stated before, gelatin is a derivative of collagen, it shows excellent biocompatibility properties, promotes cells bioactivity and comes at low-price. Furthermore, its thermoreversibility is of particular interest for sacrificial bioinks formulation, as it can be dissolved in water at temperatures higher than 37°C, forming an aqueous solution, and become a gel state at a temperature lower than 30°C. [28] Therefore it can be successfully removed at 37°C. However, gelatin-based support's baths show limitations, firstly gelatin could undesirably diffuse inside the bioink during the period required for polymerization, which is generally prolonged when using collagen as bioink, [45] and secondly its rapid dissolution at 37°C, could generate mechanical instabilities in the constructs.[46] In Figure 17, is reported its printing procedure along with its removal principle.

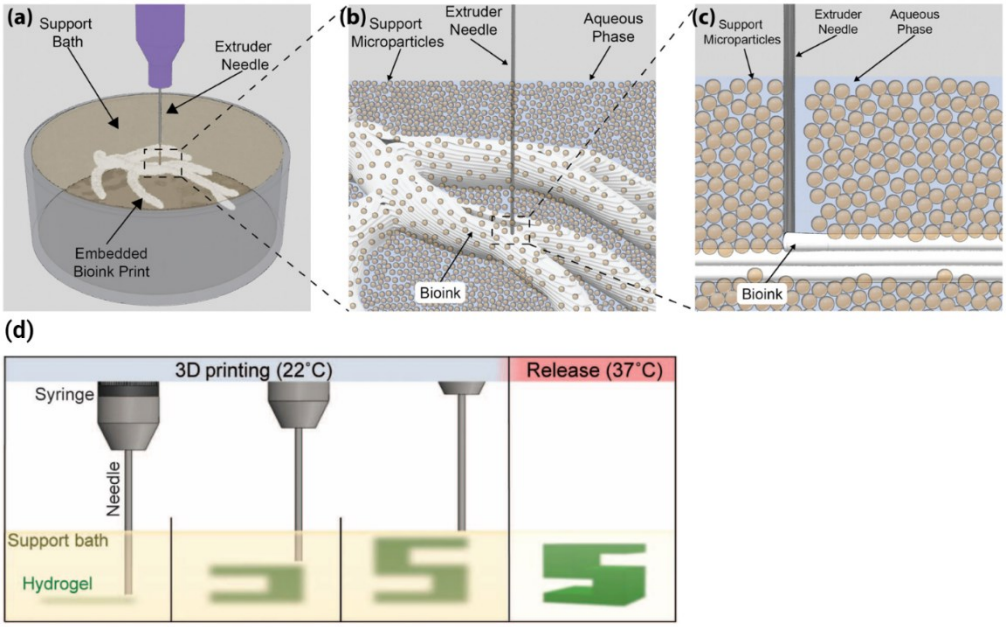

Figure 17: Gelatin FRESH bioprinting procedure. Upwards (a-c) is reported with more details the microparticle support bath, and the moving needle. As it moves through the support bath, the latter subsequently heal behind the needle, providing support to the extruded bioink. [27] In (d) is reported the printing process and the object's release after the support bath's removal. [47]

Carbopol 980NF

Carbopol is a soft granular microgels, composed of poly(acrylic acid) polymers, showing high molecular weight and low internal crosslinking density. It shows interesting properties, as it achieves maximum swelling in aqueous solution with physiological pH and no additional crosslinking is required, as it possesses reversible entanglements. It's considered a good support bath for its good printability and weak effects on cell viability, [48] hence, it could be considered a good solution for the limitations in 3D extrusion bioprinting of soft materials. It possesses a swelling property due to its electrostatic interactions, making it very sensitive to the ionic properties of the suspension medium. The ionic charge present in the initial suspension generates repulsion between the Carbopol microgels, resulting in an increased swell, changing its rheology. To remove the support bath after printing, its sufficient to exploit this principle. Subsequent addition of NaCl or DPBS (Dulbecco's PBS), can opposed to the electrostatic repulsion of Carbopol's microgels, causing them to shrink, fluidizing the suspension, reducing yield stress and viscosity. [28] Indeed, in our experiments, we used a physiological saline

solution, 0,9 % w/v sodium chloride solution, considered to be harmless to cells. Figure 18 summarizes its bioprinting procedure.

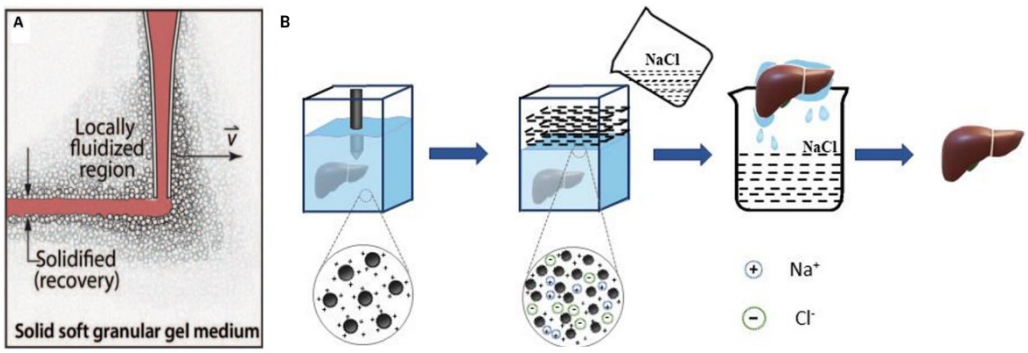

Figure 18: Carbopol FRESH bioprinting procedure. In (A) is reported the schematic representation of bioink extruded in the microgel support bath, [49] while (B) represents the removal of Carbopol to free the printed construct. [28]

Carbopol microgels comes in many types, though all of them are composed of acrylic acid, they differ from each other in terms of charge densities, crosslinking densities and functional groups. These properties influence swelling behaviour, printability and cells viability. Carbopol 980NF, differs from other commonly used materials in biomedical field, like ETD 2020, as it is a crosslinked polyacrylic acid polymer with no additional functional groups. However, 980-NF showed better results in terms of cells viability compared to others (including ETD2020, Ultrez and Pemulean). Chemical differences in carbopol microgels don't seem to alter qualitative rheological behaviour. [50]

For these reasons, we decided to use Carbopol 980NF, exploring its behaviour by varying its concentration, considered to be an influencing factor in Carbopol's rheology. [50]

Pluronic F127

Pluronic F127 is a synthetic non-ionic triblock copolymer, formed by poly(ethylene oxide) (PEO) and hydrophobic poly (propylene oxide) (PPO) blocks, together combined into PEO/PPO/PEO form. It's commonly studied in biomedical fields, due to its thermal sensitivity and crystalline structure. [28] Pluronic F127 is a thermoresponsive material, presenting a reversible sol-gel phase transition property, dependant on the surrounding temperature. This is caused by the formation of

micelle structures beyond the critical value (known as critical micelle temperature, CMC), which enable a solid phase, as reported in Figure 19B [51]. Its thermal sensitivity is hence related to its solution concentration and can be higher than its CMC at 4°C. At this temperature, the hydrophobic PPO blocks are entangled with each other's, present less solubility in water and starts to form micelles with dehydrated PPO cores and hydrated PEO shells. Therefore, at high Pluronic F127 concentrated solution is possible to form viscoelastic gels for temperatures higher than 10° C, which can present gel-to-sol transition by dropping the temperature lower than 4° C. Therefore, it's often used as a sacrificial template, as it can maintain the extruded bioink in place and subsequently be easily removed by decreasing the temperature. [28],[52] Pluronic F127 offers a wide range of viscosities, low stress to embedded cells when bioprinted, therefore establishing its role as sacrificial bioink for a variety of tissue engineering fields, including bone and articular cartilage regeneration and vascular template building. [28]

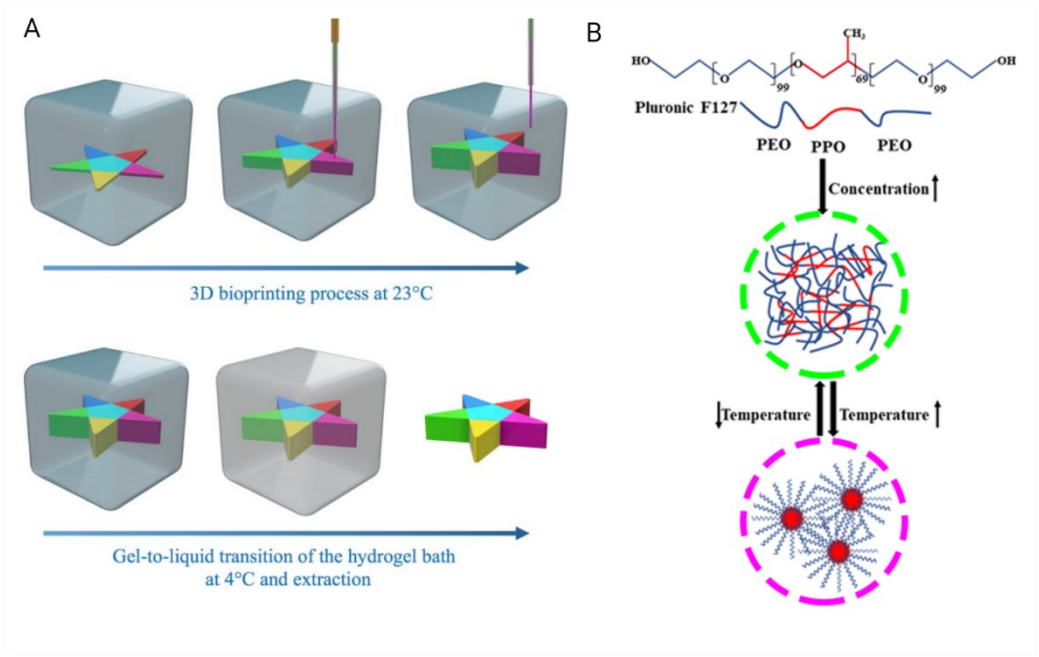

Figure 19: Pluronic F127 FRESH bioprinting procedure. In (A) is reported the concept behind Pluronic F127 FRESH bioprinting. The process occurs at room temperature, indicated as 23°C. [51] In (B) is reported the chemical structure of Pluronic F127, along with the principle of thermosensitivity.. [28]

2.3.5 Mechanical properties characterization

Tissues and ECMs are difficult to recapitulate, not only due to their compositions, but also due to their complex biomechanics. Indeed, they are not simply linear elastic materials, but they also exhibit viscoelasticity, mechanical plasticity and nonlinear elasticity. It had been shown that although ECM elasticity, or stiffness, affects fundamental cellular processes, other key features are involved in regulation of these mechanisms, like ECM's viscoelasticity. A viscoelastic material exhibits a time-dependent mechanical response to a stimulus and dissipates a fraction of the deformation energy. More precisely, when the material is mechanically perturbed, it instantaneously shows an elastic response, followed by a time-dependent mechanical response and energy loss. [53] Rotational rheology tests are usually conducted to analyse the material's behaviour under shear stress. These tests not only can provide valuable information on the material structure and mechanical behaviour but can also be used to predict the material's response during the bioprinting process. Indeed viscosity, elastic modulus or viscoelasticity influence material's stiffness, flow through the nozzle and the structural integrity after bioprinting. [54] In extrusion bioprinting the bioink passes through a nozzle before being extruded, thus it should possess enough fluidity for extrusion and consequently shape-maintaining once deposited on the printing bed. This is possible due to viscoelastic properties of the bioink. Fluidity is influenced both by viscosity and yield stress. Viscosity represents the resistance exerted by the liquid to flow (Figure 20A). Generally, in polymer-based bioinks, it decreases as applied shear forces increases, resulting in a phenomenon known as "shear-thinning". This behaviour is explained by the polymer-based nature of most of the tested bioinks, as under shear forces, their constituting molecules become extended and aligned to each other, decreasing therefore their molecular entanglement (Figure 20C). Yield stress is the threshold value, above which the viscosity starts to decrease (Figure 20B). Both are fundamental in extrusion bioprinting, as lower yield stress and good shear-thinning properties enable the use of low extrusion pressures, reducing cells damages. However, in order to maintain the deposited shape, high yield stress is usually required. Molecular weight and solid concentration can be used to tune fluidity properties. Shape maintenance is related also to other viscoelastic

properties, like storage modulus and thixotropy (Figure 20D). Ideally, a storage modulus higher than the loss modulus and shorter thixotropy is helpful for shape maintenance. As mentioned above, usually bioinks present viscoelasticity, as they possess both viscous and elasticity properties respectively related to solid-like and liquid-like aspects of the material. [29] The elastic or storage modulus (G') is representative of the elastic component of the material, and it's directly proportional to the material's storage energy in one deformation cycle. On the other hand, the viscous or loss modulus (G'') represents the viscous behaviour of the material, with direct proportionality to the material's dissipated energy in one deformation cycle. As the elastic modulus (G') is representative to the elastic component and the loss modulus (G'') represents the viscous behaviour of the material, the predominance of one over the other, informs us about the material state. Taking hydrogel as the example, when G' is higher than G'', the elastic component is predominant, and the material is therefore in a solid state. On the contrary, if G'' is higher than G', the material expresses predominantly a viscous behaviour, resulting in a fluid-like state. [54] To study the possible sol-gel transition, or gelation, of the investigated material, oscillation test is usually performed to measure its components. Gelation can occur either as a function of some crosslinking events (like light, for instance in GelMA) or due to change in temperature (like collagen). The "gelation point", reported in (Figure 20E), is defined as the point in which G' increases above G''. During the extrusion process, G''>G' is favourable, as the bioink behaves like a liquid, [55] while for shape maintenance, it's preferred to be above the gelation point. [29] To investigate gelation kinetics, usually preliminary analysis is required, to set an appropriate strain value to perform the test. This value should lay within the linear viscoelastic region (LVR), the region in which Hooke's law is appliable as G' and G'' remain constant, is determined through a shear strain sweep at constant frequency. [55] Thixotropy could be evaluated through thixotropic analysis. Newtonian fluids are characterized by a constant ratio of shear stress to shear rate. When the ratio isn't constant, fluids are said to be non-Newtonian, in other words, their apparent viscosity varies with the shear rate and/or with their flow history. Generally, the elements in a fluid tend to align themselves with the flow direction, changing its apparent viscosity. There are two scenarios that are

therefore recognizable: a “shear thinning” fluid, when the alignment develops almost instantaneously for a given shear rate, and a “thixotropic” fluid, when alignment requires some time to be developed. [56] Simplifying, thixotropy could be said to be a special case of shear thinning, where the material behaves like a solid under low shear conditions, but quickly changes into a liquid once a critical shear strain is applied. This property is fundamental for bioprinting since it allows the material to flow through the nozzle at lower pressures. Lower levels of applied pressure are also beneficial when cells are embedded inside the bioink: this reduces the stress on the cells thus improving viability. Finally, the ink should recover the solid-like properties after extrusion to assure the printing fidelity and allow a structural stability of the bioprinted structure. [57].

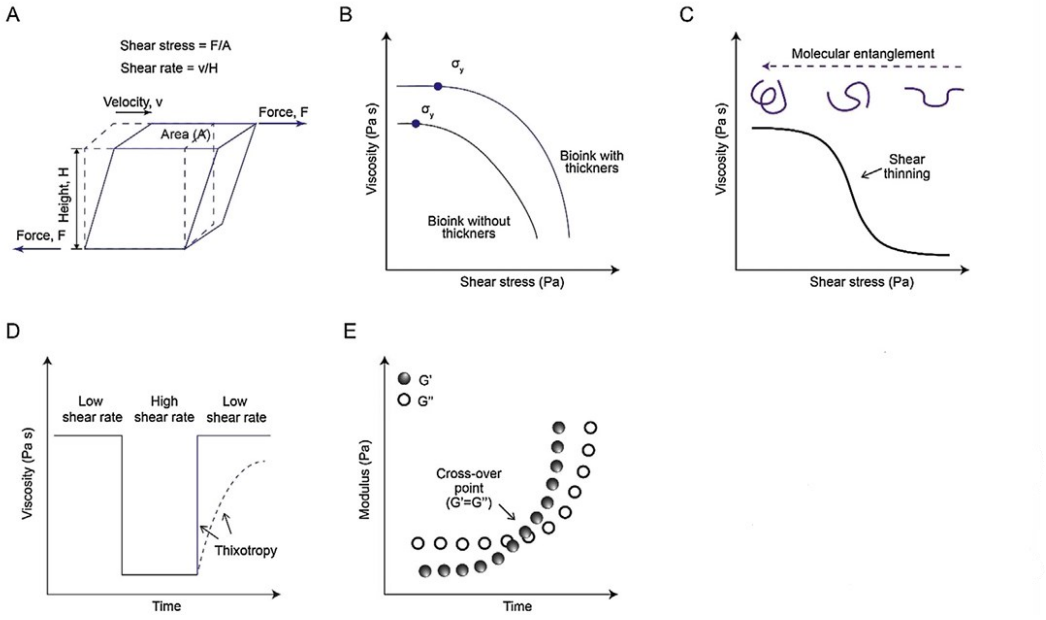

Figure 20: Rheological properties of bioinks evaluation. (A) represents a block of liquid under shear force, (B) yield stress, σ_y, with and without thickeners, (C) shear thinning related to molecular entanglements and shear stress, (D) thixhotropy phenomenon, (E) scheme of a crosslinking process, measured by the storage and loss moduli, respectively indicated as G’and G”. [29]

Printability evaluation

Printability of the investigated material often requires both quantitative and semiquantitative evaluation. Printability in extrusion bioprinting comprises both the “smooth” extrudability and shape fidelity of the filament formation. Shape fidelity relates to the shape retention of the printed filament, while print accuracy relates to

the printed construct resemblance to the original CAD geometry. Many tests exist to determine printability of the material, here we briefly analyzed the principal ones. The layer stacking test is usually performed in multilayer printing, as the hydrogel is expected to form self-supporting 3D structure, without fusion between stacked layers. Usually it's evaluated creating a "plus" sign, of two crossing lines, if they remain stacked atop one another the test is passed. (Figure 21A) In our experiments we evaluated printing accuracy (Figure 21C) by measuring the width (W) of the printed filament, comparing it to the designed value, calculating printing accuracy as:

$$Printing\ Accuracy\ [\%] = \left[1 - \frac{\left|W_{printed} - W_{designed}\right|}{W_{designed}}\right] x\ 100$$

Although we haven't used this test, filament collapse test is commonly used for printability evaluation. It evaluates the mid-span deflection of a suspended filament, to determine when does its collapse. The evaluating platform usually consists of 7 pillars of varying distance between each other's, and the filament is printed on top of them. The collapse factor is calculated considering the decrease of the theoretical area caused by the deflected filament (Figure 21B). [55] Furthermore, rheometric properties highly influence printability, as reported in (Figure 21D), in which loss modulus and storage modulus, and their respective ratio indicated as tan δ are reported as influencing factors. [58] Preliminary to each print, in our experiments we also performed a filament characterization test. Pressure is slowly increase until the filament begins to be extruded steadily. If liquid droplets are formed during the extrusion, the material does not pass the test, otherwise, if a thin filament of more than 5 mm is formed, able to be hang from the dispensing nozzle, the test is passed. [55]

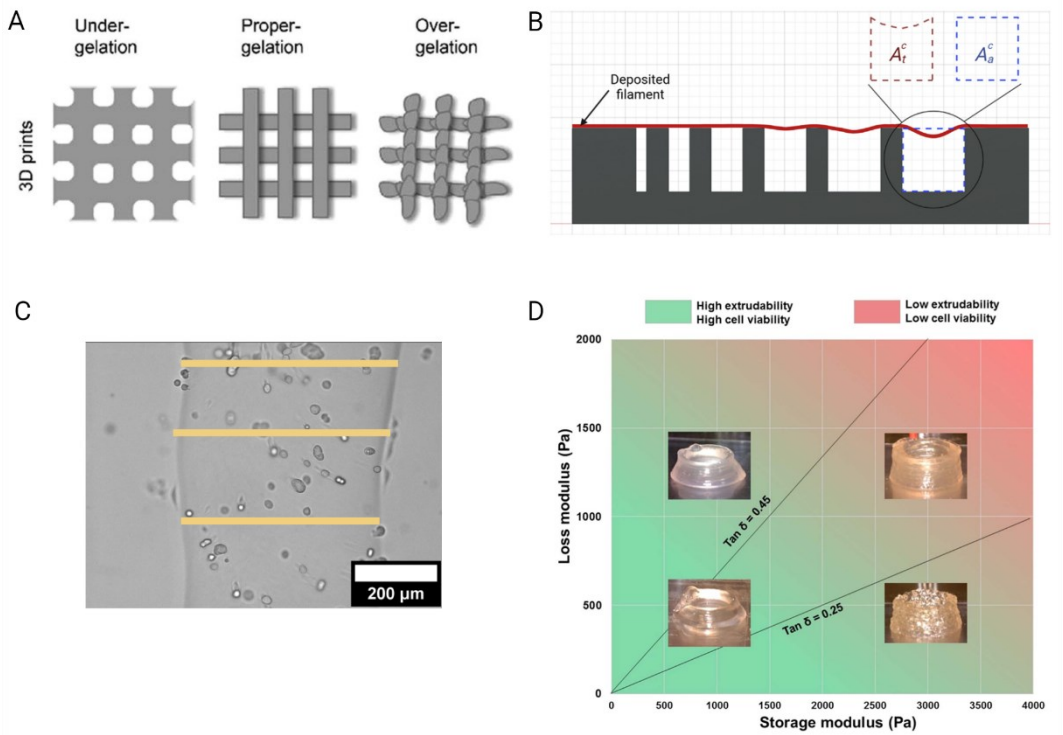

Figure 21: Printability evaluation in bioinks and biomaterials. In (A) are reported 3 conditions in which printability is altered, by testing crossing lines. [29] In (B) is reported the filament collapse test. A_t^c indicates the theoretical area, while A_a^c the actual area. [55] In (C) we showed how we measured our filaments widths, using ImageJ software, later comparing it to the designed structure. In (D) are reported the loss and storage moduli effects on printability of a hollow cylinder. [58]

Chapter III
Materials and Methods

This chapter is divided into paragraphs reporting the materials and methods used during this work of thesis. It opens with reagents and protocols used in cells culture, along with the used cells lines. Consecutively we described the biological methods to study the interactions between cells and environment. Later, we focused on bioprinting, introducing software and hardware, to finally move to bioinks and support baths preparation and protocol. The fourth paragraph regards the rheological evaluations we applied on the study of collagen's hydrogel, while the last paragraph briefly explained the imaging analysis.

3.1 Cells culture

The reagents used in cells culture are mainly trypsin and cell medium. Gibco™ Trypsin-EDTA originates from a mixture of proteases derived from porcine pancreas, and is widely used for cell dissociation. Trypsin concentration depends on the experimental application and cells treated. In our experiments, we normally used 0.005 % trypsin for all the cell lines, except for 4T1-GFP cells, which required a higher concentration of 0.025 % ; Cell media were prepared specifically for each cell line, all deriving from the Minimum Essential Medium (MEM) from Gibco. We used either MEM or DMEM-F12 (Dulbecco's Eagle Medium F12, which is MEM with additional components and increased concentration of both amino acids and vitamins) added both with 10% Fetal Bovine Serum (FBS), 1% Pen Strep (a solution composed of 2 antibiotics: Penicillin and Streptomycin), 1% glucose (Glu). MEM cell medium was used for non-cancerous cells (WI-38, MAF), while DMEM-F12 was used for cancerous cells (A549, 4T1-GFP). When incubated, cells are maintained in normal conditions, at 37°C, in a humidified atmosphere 5% CO_2. For WI-38 cells culture, collagen rat tail I (Corning®) at 0.05 mg/ml was used to initially thin-coat the flask.

Cells were acquired from CCTV, WI-38 are human fetal lung fibroblast cells; MAF cells are mouse adult fibroblasts derived from the skin which are visible under

fluorescence imaging; A549 are cells derived from a human lung adenocarcinoma; 4T1-GFP is a cell-line derived from a mammary carcinoma of a mouse, visible under fluorescence imaging.

3.2 Biological methods

3.2.1 Cells suspension in bioinks

Cells are added to the desired hydrogel from a cell suspension, the method varies depending on the bioink's viscosity. Keeping sterile conditions by working under a biological hood. Cells are detached from the culturing vessels incubating them with a pre-warmed trypsin solution and keep the culturing vessel in the incubator for 5 or 15 minutes depending on the cell line. Trypsin is then inactivated with four times the volume of complete culture medium and cell suspension is transferred in a falcon tube and gently centrifuged 1500 rpm for 4 minutes. Supernatant is discarded and an amount of culture medium, depending on the application, is added to resuspend the cells. Once the cells suspension is formed, this could be applied to three different applications:

- Dry cells suspension: the desired volume of cells is centrifuged, and the supernatant is removed. Gel is added directly on the cells' pellet, and it's gently mixed before being transfer to the printing cartridge. This method is used especially with liquid gels, such as collagen rat tail and Matrigel.
- 10 + 1 cells suspension: it' s the protocol of Cellink for its bioinks (such as GelMA and GelMA C) [59]. Cells are centrifuged and resuspended to reach a 10X concentration compared to the final bioink cell concentration before being mixed with the bioink through two connected syringes as reported in Figure 22. The suspension ratio 10+1, meaning that for 1 ml of bioink, the desired number of cells is resuspend in 100 µl.

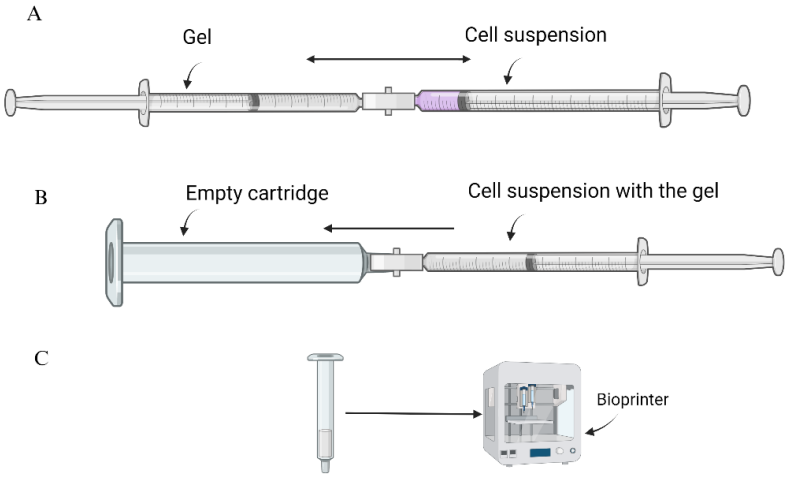

Figure 22: Mixing of gel and cells suspension using Cellink protocol [59]. *Gel is mixed with cells suspension (A) and then it's transferred to an empty cartridge (B), mounting it to the bioprinter. (C)*

- Cells culture: cells suspension is added into a new flask with fresh medium, to continue the cell line. If WI-38 cells are used, the new flask is previously coated with a thin layer of collagen.

3.2.2 Cells counting

We used an automated cell counter (Countess 3, Thermo Fisher Scientific), following the steps as described in its manual [60]. To establish the number of cells in a suspension, firstly we mix a solution of 0.4% Trypan Blue (Thermo Fisher) solution with the cells suspension in a 1:1 ratio. 10 µl of the staining solution was pipetted into both Countess chamber slides, to ensure a reduction in variability in the measurement. The amount of cells present is automatically given in cells/ml.

3.2.3 Live&Dead staining

Live&Dead staining (Thermo Fisher) enable to distinguish between dead and live cells. Calcein AM is a non-fluorescent membrane permeable dye which is enzymatically converted into green fluorescent calcein compound by viable cells. Ethidium homodimer-1 (EthD-1) is a fluorescent nucleic acid dye that enters only in non-viable with damaged cell membrane. It then increases its fluorescence's intensity when bounded to nucleic acids, resulting therefore visible under fluorescence imaging (excitation/emission ~ 495 nm / ~ 635 nm) [61]. The staining solution is prepared with the composition described in **Table 2**.

Table 2: Composition of Live&Dead staining solution

Reagent	**%V/V**
PBS1X	97.5
EthD-1	0.5
Calcein AM	2

The exhausted medium is removed from the printed constructs, and the staining solution is added. As it is light-sensitive, samples were covered with aluminium. Live&Dead staining take place in 30 minutes for cancerous cells, but it could take up to 60 minutes, for WI-38 cells. In some applications it's useful to counterstain the cellular nuclei using Hoechst solution. Hoechst solution (ThermoFisher) is prepared in stock solution of MilliQ water with a concentration of 10 mg/ml and stored at 4°C (excitation/emission ~ 361 nm/ ~ 486 nm). Hoechst solution is added in 1:1000 to the staining solution's volume for each analysed Petri dish and incubated for 15 minutes. [62] Every sample is then washed with PBS1X (EuroClone) once, before imaging analysis. PBS1X is 10X D-PBS (Dulbecco's phosphate buffered saline solution with calcium, w/o Magnesium) diluted in MilliQ, a purified water with no remaining organic and ionic contaminants.

3.2.4 Glass cover functionalization

Before printing, depending on the application, slides may be treated to enable a different interaction between support material and bioink. Plasma treatment was used to activate the surface of glass slides, enabling a better adhesion between bioink and glass, incrementing its hydrophilicity: petri dishes or glass coverslips, were inserted into the plasma cleaner and vacuumed for 2 minutes before applying plasma for 2 more minutes, at high intensity.

For UV crosslinked material (GelMA and GelMA C) a methacrylation of the glass substrate is performed to improve glass-structure adhesion. Firstly, the functionalization's solution was prepared under chemical hood, which composition is reported in **Table 3** .

Table 3: Composition of functionalization's solution

Reagent	**%V/V**
Pure Ethanol	93
Glacial Acetic acid	5
TMSPM	2

Glass slides were activated through flame treatment using a Bunsen burner and then, the functionalization's solution was added till the whole activated surfaces were covered. After 15 minutes, glass slides were washed three times with acetone. Once washed, they were placed on a clean paper towel, with the treated surface facing upwards.

3.3 Bioprinting materials and protocols

We used two bioprinting techniques: in air and FRESH. Each technique has its own protocols and materials, while bioinks can be used for both applications, support baths are related to FRESH bioprinting only. Bioprinting software and hardware are common in both methods.

3.3.1 Bioprinting softwares and hardwares

The bioprinters that were used were Cellink BioX and Cellink Biox 6, with respectively 3 and 6 tool headers. Both are extrusion bioprinters, have temperature-controlled tool headers and printbeds. Both bioprinters are also integrated with UV modules. Particularly, we used the module with wavelength of 405 nm, as considered less harmful to cells, intensities were measured for Cellink BioX and are reported below in **Table 4.**

Table 4: UV's parameters related to Cellink BioX

Distance from UV LED source (cm)	Intensity (mW/cm^2)
4	42.6
5	28.4
6	19.7

The bioprinting software include: Autodesk Fusion to create the construct's design; PrusaSlicer to enable the slicing and construct's characteristics (such as infill's geometry, layer's thickness, …); Repetier Host to manually edit the .gcode, enabling more personalized printheads' movements.

3.3.2 Bioinks preparation

Different materials were tested as bioinks. When treated with cells, we worked in a sterile environment, under a biological hood. Normally, after preparation, bioinks were transferred to 3 ml printing cartridges, if using photo-sensible bioinks, such as GelMA and GelMA C, they were carefully covered with aluminium and/or transferred into UV-protected 3 ml cartridges.

3.3.2.1 GelMA Cellink

GelMA is provided directly in cartridges of 3 ml, with LAP at concentration 0,25% w/v. It's stored at 4°C and it appears solid in these conditions. GelMA is prepared following the manufacturer's printing protocol [63]. Firstly, GelMA cartridge was incubated at 37°C for approximately 30 minutes. We set in advance the temperature of the printhead to 25°C. If required, cells were added as described in section 3.2.1. GelMA cartridge is mounted in the pre-heated temperature-controlled tool for 10-15 minutes, before starting printing. GelMA is a highly temperature-sensitive bioink and if it goes below 24°C it needs to be re-heated at 37°C for 5 minutes to reset. The instability of this bioink requires a tuning of the temperature during printing to maintain the proper bioink viscosity. In our experiments, the temperature ranges from 26°C to 27,5°C and printbed's temperature was set to 15°C. GelMA is UV-sensitive, therefore, to fully crosslink the construct after printing, UV was applied layer by layer. Exposure and intensity were tested as printing parameters, in terms of printability and cell viability. After crosslinking, printed constructs were firstly added with PBS1X, and then incubated at 37°C.

3.3.2.2 GelMA C Cellink

GelMA C is provided directly in cartridges of 3 ml, with LAP at concentration 0,25% w/v. GelMA C is stored at 4°C and it appears solid in these conditions. We followed the manufacturer's printing protocol, [64] similar to the one reported for

GelMA's bioink. GelMA C cartridge was incubated at 37°C for approximately 60 minutes. GelMA C cartridge was then connected through a luer lock with an empty syringe and by slowly pushing the cartridge's piston and simultaneously pulling the syringe's plunger, gel was homogenized. If air bubbles are present in GelMA C bioink, it needs to be centrifuged for 30 seconds at 600g. Printhead temperature was set to 24°C. If required, cells were added as described in section 3.2.1. GelMA C cartridge was then placed in the pre-heated temperature-controlled tool for 10-15minutes. Note that, GelMA C is a highly temperature-sensitive bioink and if it goes below 23°C it needs to be re-heated at 37°C for 5 minutes to reset. As already reported for GelMA bioink, the instability of this bioink requires a tuning of the temperature during printing to maintain the proper bioink viscosity. In our experiments, the temperature ranges from 23.5°C to 24°C and printbed's temperature was set to 15°C. GelMA is UV-sensitive, therefore, to fully crosslink the construct after printing, UV was applied. Exposure and intensity were tested as printing parameters, in terms of printability and cell viability. After crosslinking, add PBS1X or cell medium and incubate the printed construct at 37°C.

3.3.2.3 Collagen rat tail

Collagen requires two steps to be used as a bioink as it's initially stored in acetic acid, in a liquid state, with a concentration range of 3-4 mg/ml. It is first neutralized to a pH of 7.4 and, afterwards, it's usually kept at 4°C to undergo pre-fibrillation, before being transferred to the printing cartridge. The pre-fibrillation's time was a parameter investigated in our experiments.

Collagen neutralization

Rat tail collagen type I was acquired from Corning ® and it's initially stored in acetic acid with a low pH at 4°C. To induce collagen fibrillation, it needs to be neutralized, reaching a physiological pH between 6 and 7. Collagen is also highly sensitive to temperature, therefore when handling it, it's fundamental to work on ice. Keeping sterile conditions, by working under biological hood, collagen needs to be diluted to obtain the desired concentration, using the following proportion:

$$C_{Collagen,initial} * V_{Collagen,initial} = C_{Collagen,final} * V_{Gel,final}$$

Where *C* represents concentration and *V* represents the volume. The amount of PBS 10X is one tenth the gel's final volume, to ensure a physiological level of salts and the maintenance of pH value. NaOH 1M is added to fine tuning the pH of the solution to 7.4, but its volume varies from lot to lot. It is recommended to calculate it in advance neutralizing a sample of collagen from the analysed lot using a pHmeter or litmus paper. Finally, calculate the amount of MilliQ water, to reach the dfinal volume of gel, exploiting the formula below:

$$V_{MilliQ} = V_{Gel,final} - V_{Collagen,final} - V_{PBS10x} - V_{NaOH}$$

On ice, pipet PBS10X in an Eppendorf and add collagen by gently mixing. Add 1M NaOH to the solution and continue mixing trying to avoid air bubbles formation. Lastly add MilliQ water and homogenise the solution with a micropipette.

Collagen in bioprinting

After being neutralized, collagen is usually refrigerated at 4°C for 60 minutes to allow a stabilizing pre-fibrillation, although it's a parameter we will analyse throughout our experiments. If cells are required for the experiment, they are added before gel's transfer into the cartridge. If needed, fluorescent polystyrene nanoparticles (Fluorobeads, Polysciences, with a diameter of 500 nm) can be added in a 1:20000 dilution, to enable fluorescence imaging. Collagen was transferred into a syringe through a luer lock as explained in Figure 23.

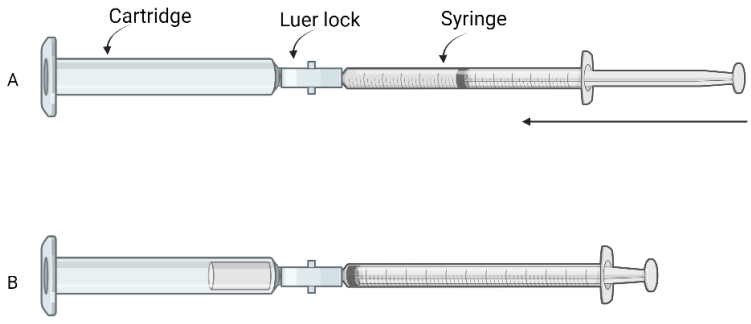

Figure 23: The syringe is attached to the cartridge (A), to transfer its content to it, by pushing the syringe's plunger (B)

Printhead's temperature was set to be around 7°C, to avoid partial fibrillation hence heterogeneities in the cartridge before printing. When printing in air, printbed's

temperature was kept at 37°C, to initiate fibrillation. In FRESH experiments the bed temperature is determined by the support bath. After printing, constructs are incubated at 37°C for ~ 60 minutes, checking every 10-15 minutes to prevent the sample from drying. Add then PBS1X or cell medium and incubate it again at 37°C.

3.3.2.4 Matrigel

Corning ® Matrigel® Growth Factor Reduced (GFR), was used for our experiments. It is maintained at 4°C to avoid premature gelling and minimizing air bubble formation when transferred. We followed the printing protocol proposed by Paola De Stefano et al. ([42]), considering its better printing management. Considering the high temperature sensitivity of the material, we worked in ice and using refrigerated nozzles, syringes, and forceps. If required, cells were added as described in section 3.2.1. Then with a syringe, Matrigel was transferred to a printing cartridge and incubated at 37°C for 15minutes, to obtain its complete gelation. The cartridge was then mounted on the pre-heated printhead to be printed. We used a printhead temperature of 25°C and a printbed of 15°C.

3.3.3 Support baths preparation

In FRESH printing, ink is extruded inside another gel which serves as a container. After printing it's dissolved, to recover the construct. Three support baths were tested, with Carbopol 980 NF and Lifesupport™ stored initially as powders, and Pluronic F127 stored as pastilles.

3.3.3.1 Carbopol 980 NF

We used Carbopol 980 NF, Lubrizol, using a dispersing procedure known as direct method, following the protocol described by the manufacturer. PBS1X was added in a beaker and put under magnetic stirring. While stirring, through a coarse sieve (alternatively, a stainless steel 20 mesh screen) Carbopol 980NF powder was added, avoiding the formation of lumps. The gel resulted acid therefore it was neutralized by a gradual addition of NaOH 1M. Once neutralized, we centrifuged the gel at 1500 rpm at 25°C for 4 minutes to remove air bubbles. Petri dishes were filled with Carbopol's gel, ready for FRESH printing. [65] To liquefy the support bath, the construct is washed with a saline solution composed of 0.9% w/v NaCl dissolved

in MilliQ, to preserve a cellular-friendly environment, till complete removal of Carbopol's bath.

3.3.3.2 LifeSupport™

We used the manufacturer's protocol, FLUIDFORM. It is recommended to keep the gel at a temperature lower than 23°C, therefore pre-refrigerated PBS1X is used. Initially, 1 g aliquot of LifeSupport™ is mixed with 40 ml of PBS1X. To homogenize the solution, it was vortexed and shaken vigorously for 1 minute to enable powder's resuspension. The suspension was left on ice for 15 minutes and then shaken for 10 seconds. We proceeded with the first centrifuge with 5 minutes at 2000g at 20°C, leaving the compacted LifeSupport™ to the bottom. Supernatant was removed, and the gel's containing tube was gently tapped against the edge of a table for 15 times, before shaking it longitudinally for 10 seconds. A second centrifuge step is performed for 5 minutes at 2000 g at 20°C, and the supernatant is removed. Gel's viscosity should be checked before printing, as if gel easily flows when inclined, it needs to be resuspended in cold media and prepared again, following the steps from the first centrifuge, increasing then the second one of 200g. If viscosity is adequate, the gel is scooped into a Petri dish using a spatula, to homogenize its surface and start printing. In our experiments, we used a printbed's temperature of 20°C, to balance Lifesupport™ stability and collagen's fibrillation. After printing, incubate the construct at 37°C for at least 30 minutes, to ensure the releasement of the construct. [66]

3.3.3.3 Pluronic F127

Pluronic F127 is a thermosensitive synthetic copolymer, which results liquid at 4°C and undergoes a liquid to solid transition at higher temperatures, depending on its concentration. To prepare the gel, Pluronic F127 was diluted with PBS1X at 30%w/v and heated up at 75°C for 60 minutes. Then it was left in ice under stirring till its complete dissolution in PBS1X (around 24 hours waiting). At this point, Pluronic solution is liquid, and it's transferred in Petri dishes and later incubated at 37°C till complete gelling occurs (around 10 minutes). To remove Pluronic's support bath after printing, Petri dishes are put in ice for 20 minutes, enabling the liquefaction of Pluronic's gel. The constructs are washed three times with PBS1X,

waiting a 5 minute interval between each of those. If using cells, substitute PBS1X with cell medium.

3.4 Rheometrical characterization

For our evaluations we utilized the rheometer Kinexus Prime Lab+. To analyse collagen's rheometric properties, a plate-plate geometry with a diameter of 40 mm, and a gap of 0.5 mm is used. A solvent trap was used to prevent the sample from drying. Bioinks' rheology is used to investigate a wide range of properties, such as shear thinning, yield stress and recovery after applied yield stress, altogether determining their printability. [67] Tests were performed changing lower plate's temperatures at 7°C, 25°C and 37°C, considering the impact of this parameter in collagen's fibrillation. Three different tests were made: gelling, thixotropy and gelling post-printing.

3.4.1 Gelling

This test is used to analyse the gelling of the material, when using neutralized collagen, it is related to its fibrillation, the test ends when its elastic and viscous components, respectively G' and G'', reach a plateau and are more stable in time. This test was performed using a single time sweep at frequency of 0.5 Hz and 0.75% shear strain, with a sampling time of 10 seconds.

To observe if collagen at 7°C was able to gel once printed, we performed a second gelling test after thixotropy test, with the same parameters of the first one, except for the lower plate temperature increased at 37°C.

3.4.2 Thixotropy

Thixotropy was evaluated following the procedure conducted by Cui et al. ([68]). Before proceeding with the thixotropy test, the Linear viscoelastic region (LVR) is determined by measuring the behaviour of the sample at 25°C, as considered the most representative among the other conditions tested. An amplitude sweep was performed at constant frequency of 1 Hz, with a shear strain ranging from 0.01% to 5%, stopped before increasing of G'' and decreasing of G' occur, determining the LVR. Three intervals were defined differed by their induced shear strain.

1. A single frequency timed analysis with a frequency of 1 Hz and low 0.5% shear strain, inside the LVR (Linear viscoelastic region), with a sampling time of 2 seconds for 30 seconds in total, to mimic a low shear strain.
2. A single frequency timed analysis with a frequency of 1Hz, with a sampling time of 2 seconds for 30 seconds, with a higher shear strain, beyond the LVR, depending on the temperature under testing (100%, 50% and 100% for 7°C, 25°C and 37°C respectively), mimicking the extrusion process.
3. A single frequency timed analysis with a frequency of 1 Hz and with the same shear strain of the first interval, with a sample time of 1 second. The samples were then allowed to reach equilibrium.

3.5 Imaging

The confocal microscope we used was Leica Stellaris 8. In confocal microscopy, images are acquired focusing on a single plane and depending on the acquisition, different plane can be stacked together to create a single image, composed by their projections. Moreover, through reflective mode, we were able to analyse collagen fibers. Brightfield and epifluorescence imaging were performed with Leica DM IL LED microscope. The software we used for image elaboration was FIJI.

Chapter IV
Results

The aim of this work of thesis was to create a multimaterial and multicellular complex structure that can be used as a model for TME. Similarly to the work proposed by Heinrich et al., [69] we wanted to recreate the TME compartmentalization, to study the interactions between the cancer cells and the surrounding ECM. In many solid tumours is present a core of cancerous cells surrounded by the stromal tissue, which helps in tumour progression and migration through ECM remodelling. [9] In order to replicate these complex mechanisms, we aim to develop a multilayered structure, in which its outer shell simulates the stromal tissue, while the core represents the cancerous cells. As basement membrane we used Matrigel, in which its printing procedure has been developed and implemented in literature [42]. Matrigel allows cancer cells to proliferate and interact with the texted stromal material. [1] Firstly, we used GelMA as stromal bioink, as it's a commonly used bioink, highly biocompatible and tuneable. [36] Although it was a commercial bioink, we optimized it for our application, by exploring UV parameters, evaluating both printability and cells viability. GelMA was later replaced with commercial GelMA with nanofibrillated cellulose, later indicated as GelMA C, representing a more stable and efficient bioink, compared to the previous one. Its UV parameters were optimized, and we developed our multilayered structure, with GelMA C and fibroblasts representing the stromal tissue and Matrigel with tumoral cells the basement membrane.

However, GelMA is not naturally present in our bodies, therefore, to achieve more resemblance to the *in vivo* conditions, we evaluated printability of pure collagen. Indeed, collagen is normally present in our bodies, constituting the major protein component of ECM. [40] Furthermore, in TME it plays a fundamental role in ECM remodelling and overall cancer's progression. [9] We decided to use rat tail derived collagen type I, at low concentrations to ensure a suitable fiber network for embedded cells to promote their growth. [41] We studied its fiber alignment under confocal microscope, their rearrangement is involved in cancer's development [14].

However low-concentrated collagen presents low-printability, which limits the development of complex structure. To overcome this limitation, we explored FRESH bioprinting, analysing different support baths material, to improve collagen's printability, with the future perspectives of developing more complex structures.

4.1 GelMA bioprinting

We wanted to recreate the complexity of the TME. To do so, we decided to use GelMA from CELLINK, which come as a commercial bioink. As mentioned earlier, GelMA is a valid choice to recreate ECM *in vitro*, as it is highly biocompatible, has tuneable mechanical strength and it generally, presents good printability. Furthermore, as it derives from collagen, it is a suitable material to mimic the stroma of the ECM and it already contains RGD sequences which promote cell attachments. [17]

4.1.1 Printability and UV parameters evaluation

We first tested the UV crosslinking behaviour of the commercial GelMA and how the UV exposure impacts on GelMA's mechanical. The aim of these initial analysis was to find the optimal photocrosslinking parameters (intensity and exposure time) to obtain good mechanical stability. To allow UV photopolymerization of the methacrylate moieties, a photoinitiator was added to the GelMA solution. Several photoinitiators have been reported in literature for applications with live cells such as IRGACURE 2959 and LAP. Among those, we decided to use Lithium phenyl-2,4,6-trimethylbenzoylphosphinate (LAP) due to its high cytocompatibility, high water solubility and the ability to initiate the polymerization with both 405 nm and 365 nm wavelengths. We decided to use 405 nm wavelength as it less cytotoxic if compared to 365nm radiation. [70] A simple testing geometry consisting of three lines has been printed keeping a fixed nozzle velocity of 3 mm/s. The structure is reported in Figure 24.

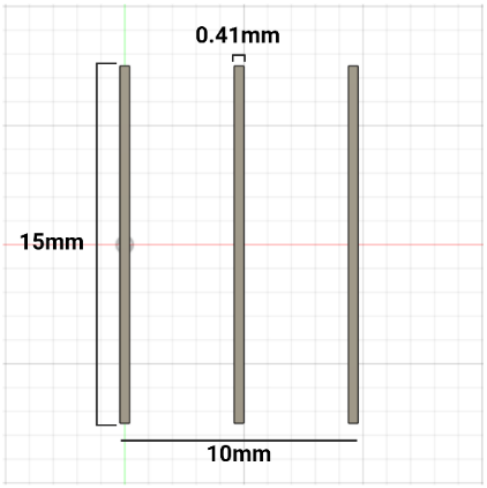

Figure 24: GelMA structure for UV parameters determination.

For all the experiments with GelMA, the fixed printing parameters are reported in the **Table 5** below.

Table 5: Fixed printing parameters for GelMA

Nozzle's diameter	**Printbed's temperature**	**Wavelength**	**Nozzle's temperature**
0.41 mm	15°C	405 nm	26-27.5°C

The bioprinting of GelMA ink showed a significant variation of its physical characteristics over the fabrication time. Initially we had difficulties to extrude the biomaterial from the dispensing nozzle, therefore temperature was increased to 37°C for 5 minutes, before proceeding with the printing temperature reported in **Table 5**. In Figure 25 are reported the first GelMA's prints. We could see that the first reported print is underextruded, although the pressure is higher compared with the other prints, suggesting an increased stiffness of the bioink. The subsequent print is reported after almost 10 minutes, which showed improvements in printing accuracy and a lowered extruding pressure requirement. Although we lowered the pressure, the consequent filament was slightly overextruded, and the printing worsened with the last construct, showing missing fragments and material's heterogenous distribution. We concluded that the material presents instabilities during printing procedure, encountering both underextrusion and overextrusion conditions within a timeframe of ~ 15 minutes.

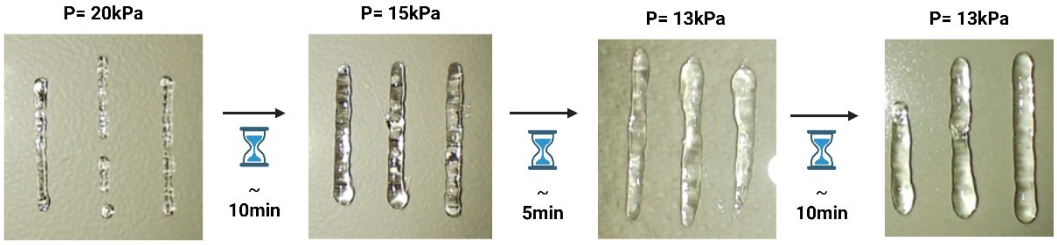

Figure 25: Mechanical properties changed throughout the printing process. Photos were taken immediately after printing, before crosslinking.

To evaluate the crosslinking of the GelMA bioink, UV intensity was tuned changing the distance from the printbed, and different UV exposure times were tested . Higher intensities and longer exposure times, increase the biomaterial's crosslinking degree and stiffness improving the shape fidelity of the structure, however this also lowers its cytocompatibility. Therefore, we decided to test short times and low intensities. We tried three different intensities, 19.7 mW/cm^2, 28.4 mW/cm^2 and 42.6 mW/cm^2, corresponding respectively to 6 cm, 5 cm and 4 cm distance from the bioprinter's UV source. Optimal exposure time was investigated by trying 4 different time intervals, precisely 10s, 20s, 40s, and 60s (Figure 26). To qualitatively evaluate the structural stability of the fabricated structure we used a straightforward test that is reported in Figure 27 and it's here briefly described. After PBS1X addition, for each condition we gently scooped out the filaments from the printing bed. The filaments were then uplifted using two forceps, outcoming 3 distinct situations: the filament couldn't be uplifted, as it was too difficult to be scooped out, showing insufficient photocrosslinking; the filament could be uplifted but presented ruptures in the process, showing incomplete photocrosslinking; the filament could correctly be uplifted, showing both shape maintenance and integrity along the structure, showing complete photocrosslinking conditions.

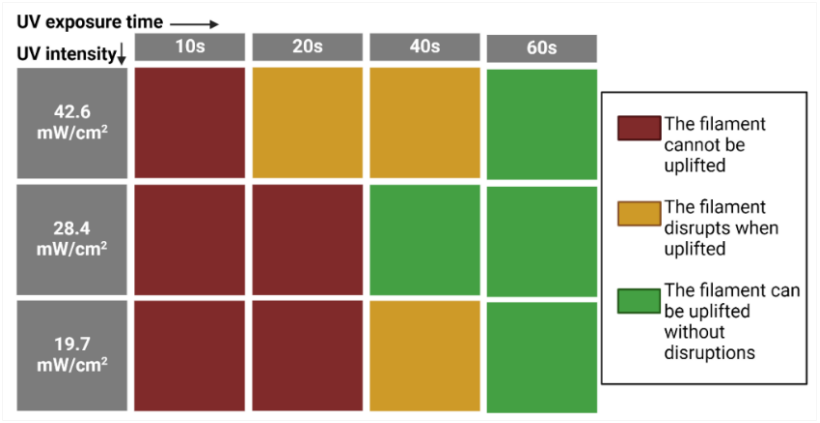

Figure 26: UV parameters influence on GelMA crosslinking.

As reported in green in Figure 26, the best results were achieved at 60s of exposure time. We also saw good results at 40s with intensity of 28.4mW/cm^2. We hypothesized that worse photocrosslinking results at 40s with intensity of 42.6mW/cm^2 were mainly due to instabilities of GelMA's material during extrusion, as increased intensity is related to increased photocrosslinking. Of notice, after crosslinking, no GelMA construct dissolved when PBS1X was added..

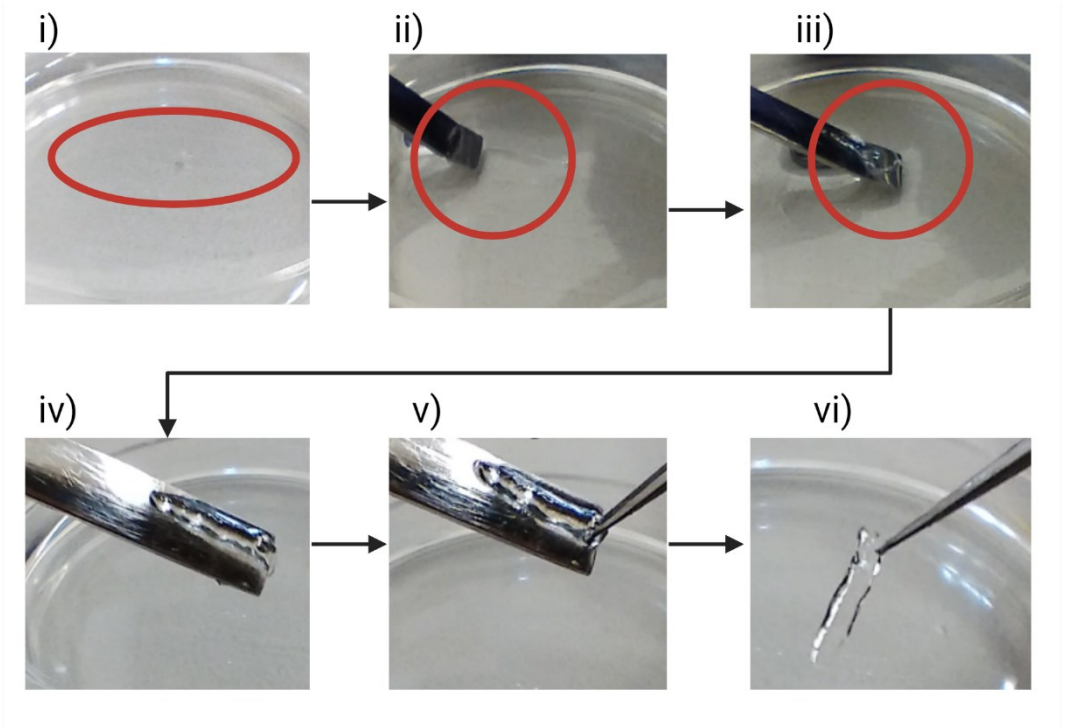

Figure 27: Mechanical test on the printed and crosslinked filament. The filament is gently scooped out from the Petri and consequently uplifted with forceps. In this case (UV intensity: 28.4mW/cm^2, exposure time: 60s), the filament resulted stiff and able to maintain its shape throughout the process.

4.1.2 Cells viability

We initially evaluated tumoral cells viability, using A549 cells in concentration of $2x10^6$ cells/ml. Velocity was set to 3 mm/s and pressures ranged from 16 kPa to 20 kPa during bioprinting. Similarly, three lines of 0.41 mm width were printed, with a shorter length of 10 mm, distanced 2.1 mm from each other's. The intensity of UV was set to 42.6 mW/cm^2. Filaments showed rheological alterations throughout times, measured as changes to filament's width, as well as over-extrusion (Figure 28). On the other hand, cells viability showed promising results, especially for UV exposure times lower than 2 minutes (Figure 29), while for longer times, it drastically decreased.

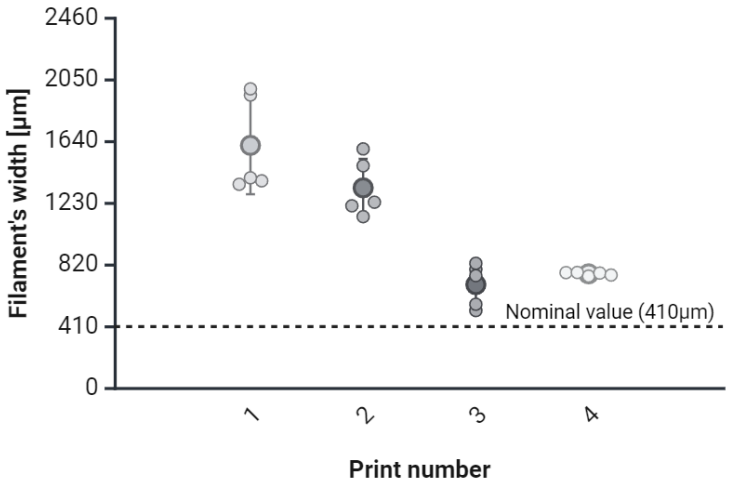

Figure 28: Filament's width variances during the printing process.

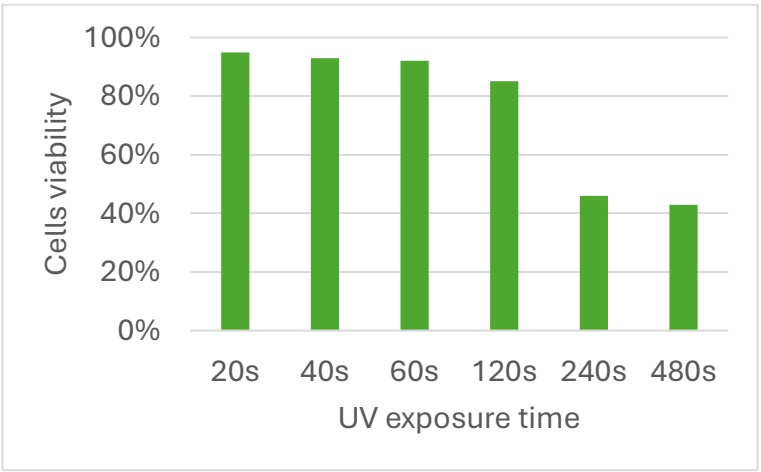

Figure 29: A549 cells viability in GelMA, with UV intensity of 42.6 mW/cm^2.

4.1.3 Structural analysis

We wanted to recreate *in vitro* a simplified model to simulate the TME present *in vivo*. To do so, we aimed to reproduce a complex structure with a peripheral material simulating the stromal tissue with embedded normal fibroblasts, while the inner material simulates the basement membrane with tumoral cells. To correctly implement the theorized structure, we firstly evaluated GelMA printability on multiple layers, starting with a simple square grid consisting of 3 layers, reported in Figure 30a-b. We used UV intensities of 28.4 mW/cm^2 and 42.6 mW/cm^2, with 60s of exposure time per layer, as determined previously (Figure 26) as optimal photocrosslinking parameters. During the bioprinting process, not only GelMA changed its mechanical properties, but it also partially crosslinked at the tip of the printing nozzle. Therefore, the use of a needle was required after every layer to unclog the nozzle. This results in a limitation not only to future cells viability, but also for the structural integrity of the printed construct. Nonetheless the structure resulted correctly printed, with filaments distinguishable among each other's and overall structural integrity after PBS1X addition. The construct's integrity was also tested by scooping and uplifting the structure, (Figure 30b) similarly to the test reported in Figure 27. After these promising results, we tried to recreate a hollow cube, to test mechanical stability under an increased number of layers. The structure reported in (Figure 30c) serves us to preliminarily evaluate the behaviour of GelMA in the absence of cells, to further develop a more complex structure with cancerous cells in the core (replaced now by empty space) surrounded by representing stromal tissue (GelMA) with embedded fibroblasts. The tested structure consisted of 5 rectangular layers, with a pyramidal roof to ensure, together with first layer's solid infill, a closed construct. Each layer received 40 seconds of UV radiation with intensity of 42.6 mW/cm^2 which we expected to be enough to achieve complete crosslinking and low cells mortality, with a total exposure time of 200 seconds. Before starting the print, we improved GelMA's printability, by limiting nozzle's clogging related defects by adding a wipe tower close to the designed structure. These auxiliary structures consists of a line of the material printed in a layer-by-layer fashion, close to the designed structure. This helps to monitor both the

extruding pressure and nozzle's clogging, preventing deformities in the printed filaments.

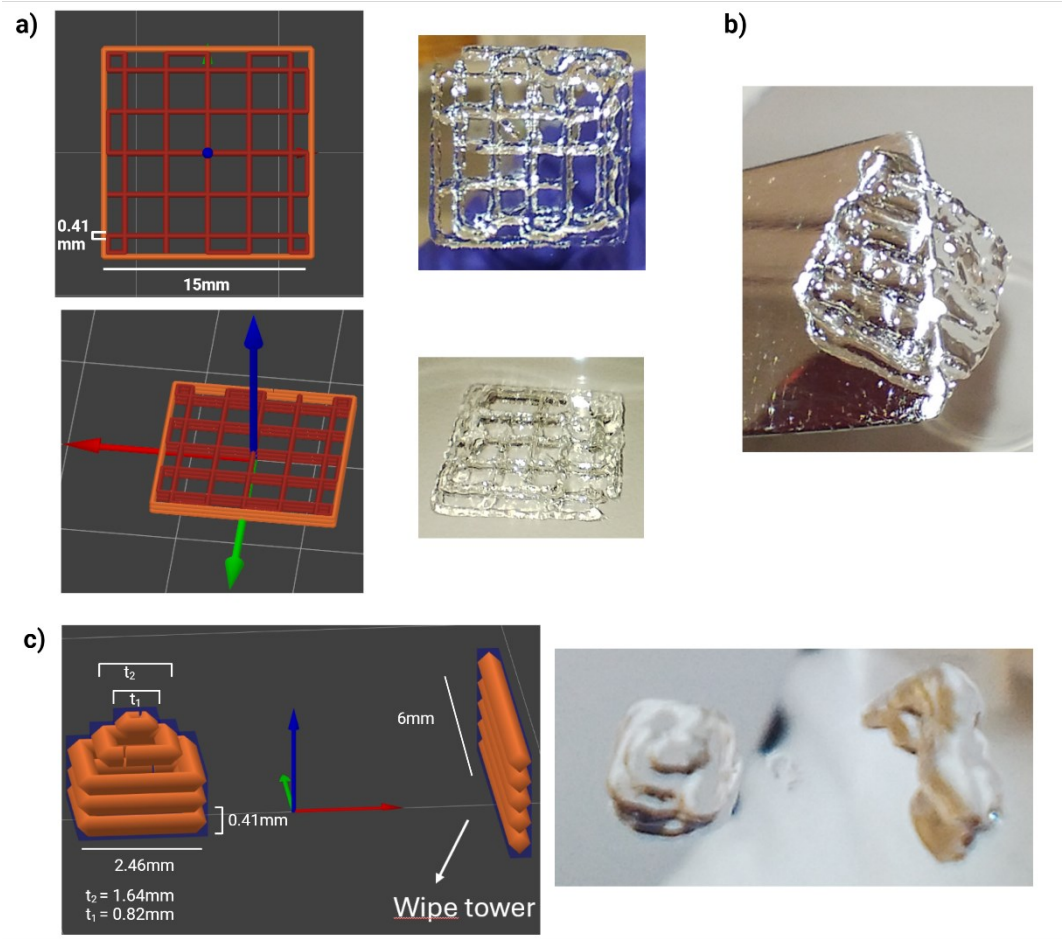

Figure 30: Multilayer printing of GelMA. In (a) is reported on the left the designed structure and on the right the printed one. It consisted of a square of 15x15x1.23 mm (3 layers) with a 25% grid infill. Velocity was set to 3 mm/s and pressure is between 20 kPa and 35 kPa. In (b) is reported similarly on the left the designed structure and on the right the printed one, with the structure consisting of 5-layer cube, with its wipe tower. Velocity is reduced to 2 mm/s and pressure between 20 kPa and 25 kPa.

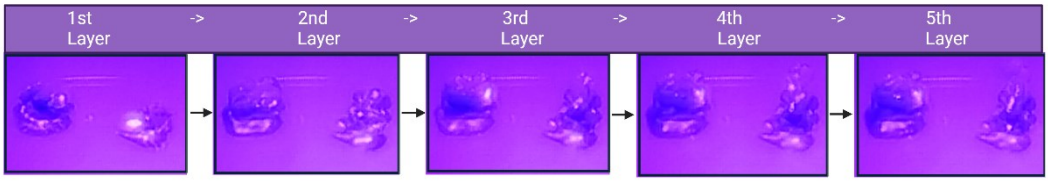

Figure 31: Hollow cubical print of GelMA. The photos were taken during the process, while the printed layer was being UV radiated (resulting in a purple/violet background). Photos were taken approximately 60s from one another.

During the printing, GelMA presents mechanical instabilities reported both as heterogenous printed filaments (Figure 31) and varying pressure throughout the process (from 20 to 25 kPa). Although our construct was able to maintain structural stability, it showed a poor resolution, possibly retaining a reduced internal volume. As we intended to print a second material inside the empty space, these results are not satisfactory. Indeed, increasing complexity to the structure, by using multimaterials embedded with different cell types, could have risked an undesired mix of the bioinks, failing to recreate the designed structure, hence the TME model. We thought that by overcoming material's instabilities, it would have been possible to improve structure's resemblance and overall experiment's significancy. We therefore decided to use a more stable bioink, GelMA with nanofibrillated cellulose, GelMA C.

4.1.4 GelMA C

Similarly to GelMA, printability and UV parameters were evaluated as well as cells viability of both cancerous and normal cells. We then carried on with structural analysis and concluded with the print of a multimaterial and multicellular construct, which exemplified the TME. Throughout our experiments, some printing parameters remained fixed and are reported in the **Table 6** below.

Table 6: Fixed printing parameters for GelMA C

Nozzle's diameter	**Printbed's temperature**	**Wavelength**	**Nozzle's temperature**
0.41 mm	15°C	405 nm	23-24°C

4.1.4.1 Printability and UV parameters evaluation

We evaluated printability of GelMA C, setting a velocity of 2 mm/s. Interestingly, at the beginning of the bioprinting process, GelMA C presented low stiffness and liquid-like extruded filaments. However, the bioink rapidly stabilized, and homogenous filaments were printed with pressures ranging from 17 kPa to 23kPa. No construct dissolved in PBS1X after the crosslinking, and all of them were detachable from the printbed's surface afterwards. Generally, GelMA C showed

good crosslinking also at shorter exposure time. The same GelMA's mechanical test reported in Figure 27 was used and results are reported below in Figure 32.

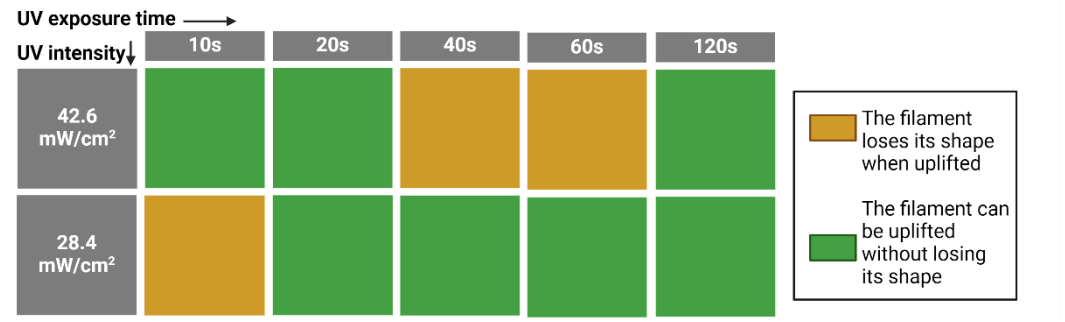

Figure 32: UV parameters evaluation for GelMA C crosslinking.

To determine the stability of GelMA C, we performed a simple test in which we extruded a single line structure of 20 mm, at 2 mm/s, photocrosslinking each filament at the same conditions (intensity of 28.4 mW/cm^2, exposure time of 60s). Prior to the printing, we left GelMA C's cartridge at 24°C for 15 minutes, to stabilize and then we proceeded with the first print. From our experiment (Figure 33) we showed that the material remained stable across time, both after short (3 minutes) and long (15 minutes) time interval between consecutive prints. Furthermore, extruding pressure remained unchanged (at 11 kPa) during the whole experiment. The first and the last construct, showed little differences between each other's although they were printed 33 minutes apart from one another.

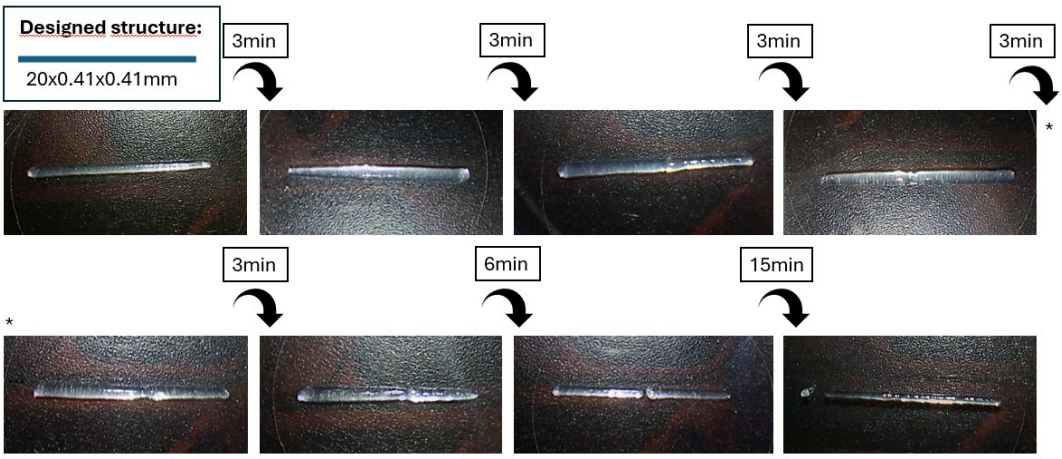

Figure 33: Consecutive prints of GelMA C.

4.1.4.2 Cells viability

As lowered UV doses were used, we evaluated both tumoral and normal cells viability. We set the intensity to 28.4 mW/cm^2, as it showed good results in crosslinking, and induces lower harm to embedded cells. We used WI-38 fibroblasts as normal cells, while 4T1-GFP cells were used as cancer cells. WI-38 showed low cells viability even at 20s, with a decreasing trend till 2 minutes of exposure, in which no live cells were detected (Figure 34a). Considering a multicellular print, one medium needs to be used, which should enable both cell types survival and proliferation. As cancerous cells medium is richer in terms of components, compared to MEM, we chose it. We compared the WI-38 cells viability with exposure time of 20 seconds in both media, and no significant differences were reported (Figure 34b). Lastly, we monitored the tumoral cells viability, which was higher than WI-38's, and generally above than 85% for up to 2 minutes of exposure (Figure 34c).

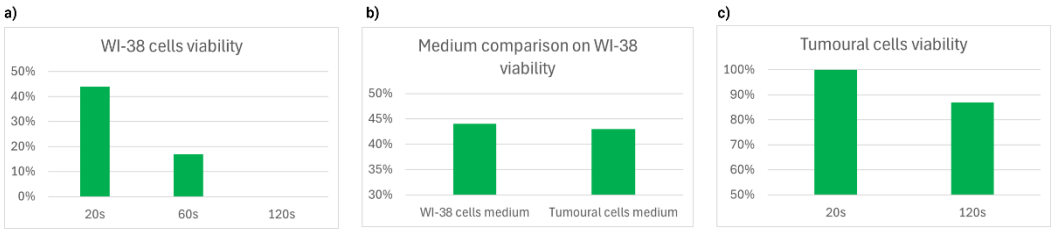

Figure 34: Cells viability under UV radiation. In (a) is reported WI-38 cells viability; in (b) WI-38 cells viability compared between the two cell culture media; in (c) 4T1-GFP cells viability.

Although in further experiments we used A549 instead of 4T1-GFP cells, we expect to have similar results, as comparable outcomes were obtained in with GelMA's cells viability.

4.1.4.3 Structural analysis

Considered the increased stability and cells viability under UV radiation, we decided to print the same structure previously described for GelMA: a closed hollow cubical structure (Figure 35). Printing parameters are reported in the **Table 7** below.

Table 7: Parameters for GelMA C multilayer printing

UV intensity	UV exposure time per layer	Pressure range	Velocity
28.4 mW/cm^2	20 seconds	22-26 kPa	1 mm/s

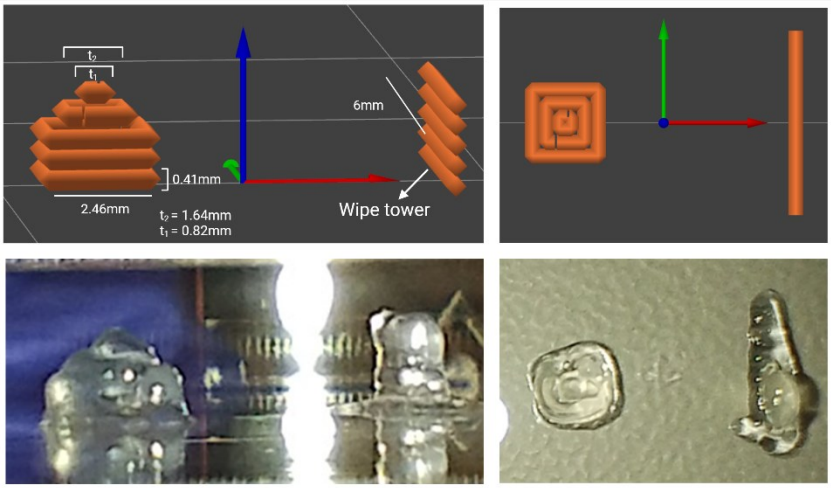

Figure 35: Closed hollow cubical structure printed with GelMA C. Upwards is reported the designed structure, while downwards the printed construct.

Although slightly improved from GelMA's construct, GelMA C's construct revealed low-resolution, probably related to the absence of material inside the cubical structure and overall construct's size. To overcome these limitations, we increased structure's size, and we added a solid infill with a different composition. The designed structure and its printed outcome are reported in Figure 36. The whole construct consisted of 10 layers of 0.41 mm, with the parameters reported in **Table 7**, with a total exposure time of 200 seconds. Preliminarily, we used GelMA C for both the inner and outer part of the structure, although they differed in composition by the presence of cells. The core cube was printed with tumoral cells (A549, concentration of 2x10^6 cells/ml) embedded, while the outer shell consisted of cell-free GelMA C. As expected, pressures changed in the two materials, shell's pressures ranged from 15 kPa to 20 kPa, while core's pressures ranged from 9 kPa to 11 kPa. We expected this result, as cells alter hydrogel's rheologic property like viscosity, generally decreasing proportionally to cellular concentration, [24] which explained the decreased extruding pressure during the printing process. Gel with embedded cells appeared more stable in terms of mechanical properties, and both gels showed good printability.

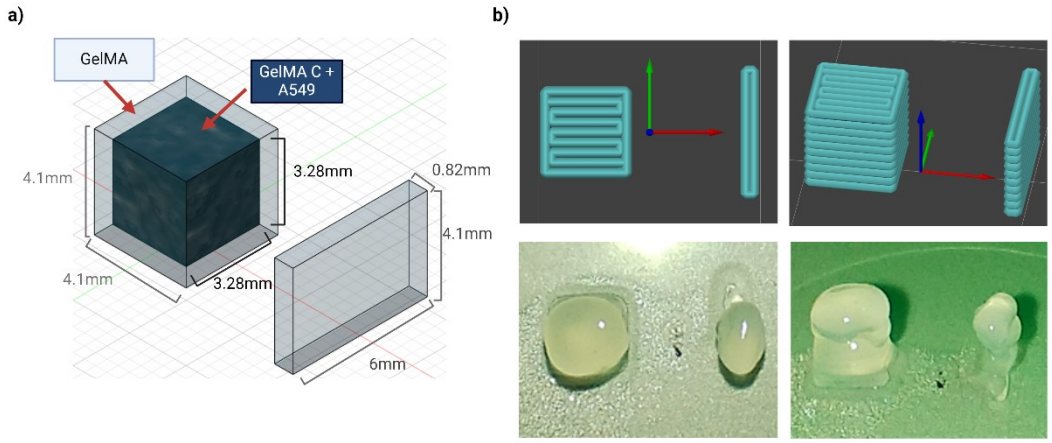

Figure 36: Printing of a filled cubical structure, with GelMA C on the outside, and GelMA C with embedded cells on the inside. In (a) are reported the data regarding the designed structure, while in (b) we reported the comparison between the designed (up) and the printed structure (down).

Unlucky, the printed structure resulted distorted on top, as the last layer (consisting of pure GelMA) was over extruded. However, as the other layers appeared correctly deposited, with good resemblance to the designed structure, we decided to move forward toward a more complex but more relevant structure fabricated with two different bioinks, Matrigel and GelMA C, embedded respectively with tumoral and normal cells.

4.1.4.4 Recreation of a TME with GelMA C and Matrigel

To recreate the multicellular environment of the tumour microenvironment, we designed the structure reported in Figure 37, in which the outer shell consists of GelMA C with fibroblasts (WI-38), while the core consists of Matrigel with tumoral cells (A549). GelMA C with fibroblasts represented the stromal tissue, while Matrigel served as the basement membrane for tumoral cells. Matrigel was mixed with fluorescent polystyrene nanoparticles, to better discriminate Matrigel from gelMA C through the fluorescent signal. The velocity was set for both materials, at 1 mm/s, while printbed temperature was set to 15°C. During the printing, every layer of the construct was UV irradiated for 20s at 28.4 mW/cm^2, for a total exposure time of 200 seconds. The printing parameters are reported in **Table 8**.

Table 8: Multimaterial and multicellular printing parameters

	Nozzle's temperature	Pressures range	Cells concentration	Cells type
Matrigel (Core)	25°C	15-16 kPa	$2x10^6$ Cells/ml	A549
GelMA C (Shell)	24°C	18-28 kPa	$4x10^5$ Cells/ml	WI-38

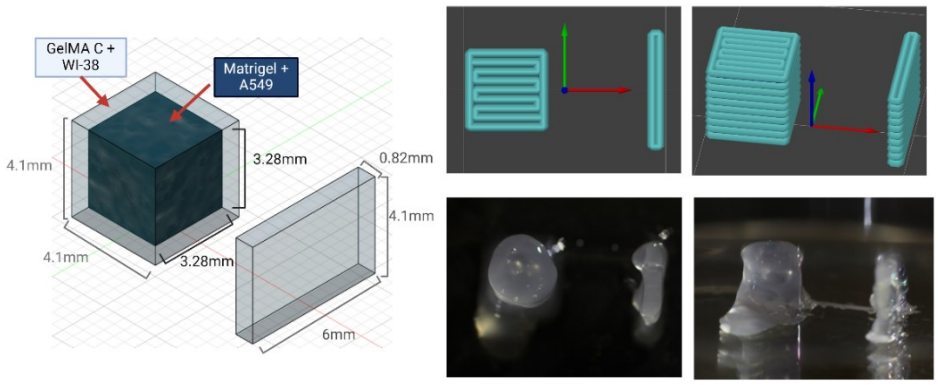

Figure 37: Multicellular and multimaterial printing. On the left is reported the structure with its dimensions,ma while on the right the comparison between the designed (up) and printed structure (down).

We printed 10 layers of 0.41 mm (nozzle's diameter) thickness each, with a resulting 200s of exposure time. Although resolution was not optimal, we achieved a stable structure modelling a simplified TME. After the printing, we let the Matrigel complete the gelling for 60 minutes in the incubator and then we added the cell culture medium. The structure was constantly monitored for 5 days (Figure 38).

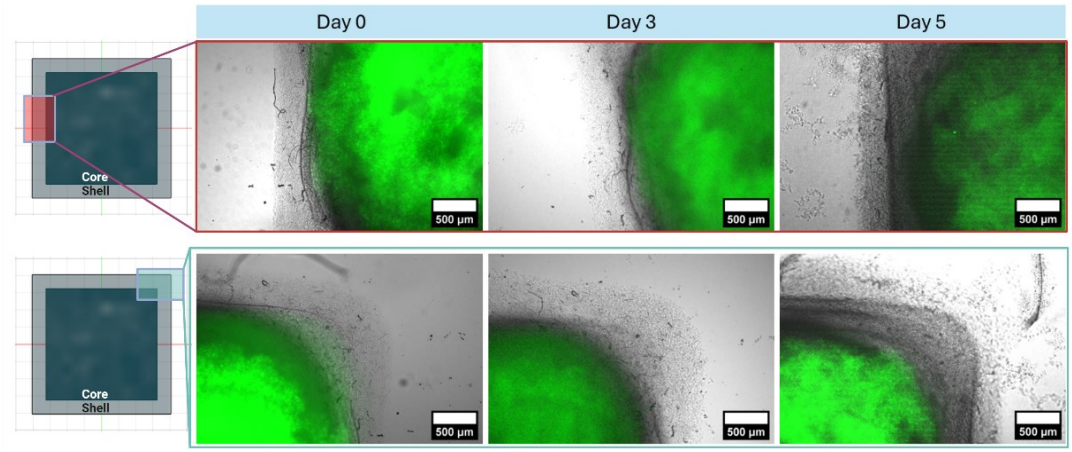

Figure 38: Multicellular and multimaterial cube print analysis throughout 5 days. On the left is reported the construct from above, and the visualized image on the right. Photos are reported as composite of two channels, one green (Matrigel + A549) and the other one gray (GelMA C + WI-38).

We noticed that after 3 days there seemed to be a contraction of the Matrigel, which is even more highlighted at the 5th day. A plausible reason is the increasing number of cancerous cells induce a remodeling of the Matrigel matrix inducing the contraction. However, our evaluations resulted inaccurate due to the thickness of the structure, which hindered our microscopy imaging. Cancerous cells migration and activity couldn't be evaluated due to this limitation. Therefore, we decide to printed a simpler figure, consisting of two co-planar layers: the outer one consisting of GelMA C with WI-38 and the inner one consisting of Matrigel with A549, reported in Figure 39. As for the UV crosslinking, we chose 20s with intensity of 28.4 mW/cm^2 while the other printing parameters are reported in **Table 8**.

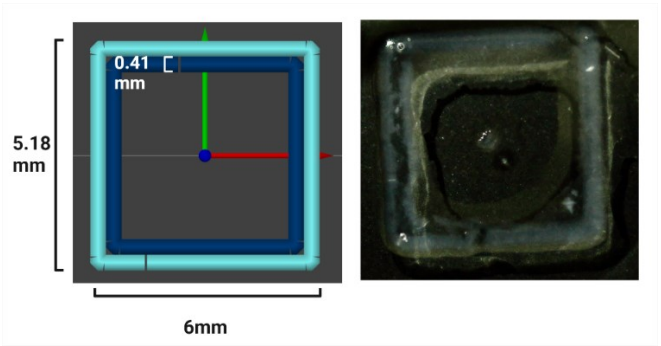

Figure 39: Multicellular and multimaterial frame print. In dark blue is reported Matrigel with A549, in light blue GelMA C with WI-38. On the left is reported the designed structure, while on the right the printed construct.

We examined the structure for 5 days and we noticed that Matrigel tended to be contracted by the cancerous cells (Figure 40a) as we already observed on the previous cube print (Figure 38). After 5 days, we observed a delamination of Matrigel from GelMA C's filament. Cancerous cells remodelled the basement membrane, indicating their strong interactions with the material (Figure 40). However, we haven't observed a migration of cancerous cells towards the stromal tissue. We hypothesized that cancerous cells preferred Matrigel's environment as it highly promoted their growth. GelMA C, on the contrary, could have discouraged cancer migration, due to its high stiffness. The unsuitability of the GelMA matrix for the proliferation and migration of the embedded cells was also showed by the morphology of the fibroblasts. Indeed, the few cells present in the GelMA matrix showed a round-shaped morphology, typical of cells that cannot interact with their surrounding or that are blocked by the matrix which results non remodellable. Moreover, fibroblasts were less than expected, which can be caused, possibly, by high mortality or adverse interactions with GelMA C. This low number of cells also hindered cells-cells interactions evaluations.

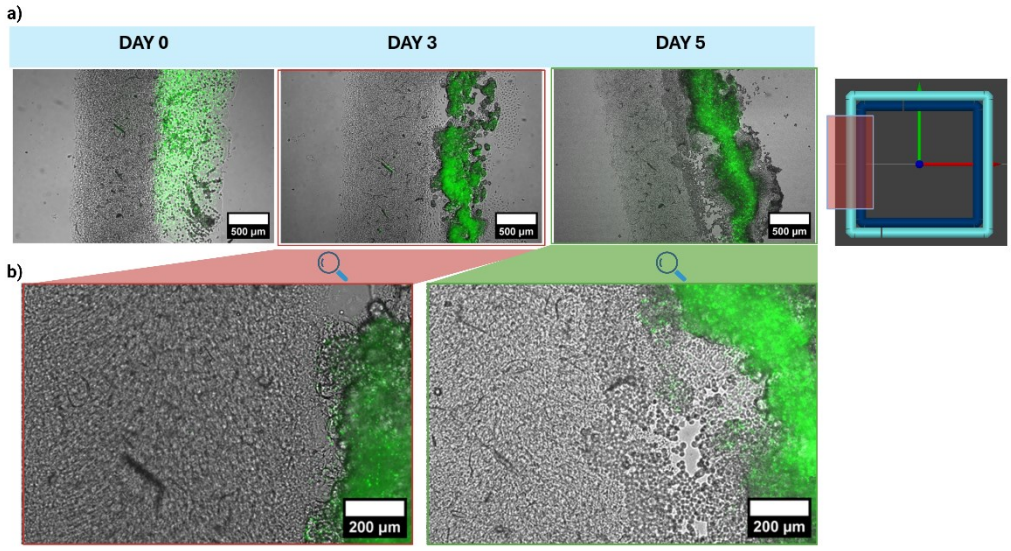

Figure 40: Multicellular and multimaterial frame print analysis throughout 5 days. Photos are reported as composite of two channels, one green (Matrigel + A549) and the other one gray (GelMA C + WI-38). In (a) are reported the same construct's area, form day 0 to day 5, while on the right is reported the designed structure. In (b) is reported the zoomed image of day 3 and day 5.

4.1.4.5 Final considerations and future perspectives

We managed to reproduce a complex structure of 10 layers, resembling the interaction between stromal tissue (GelMA C and fibroblasts) and cancerous core (Matrigel and cancer cells). We observed its development for 5 days, and we showed a contraction in its core. However, we were limited with the imaging analysis, due to the construct's size. To overcome this limitation, we reproduced approached the problem in a simpler way, with a single-layer structure with an external stromal and internal tumoral tissue representation, using the same bioinks of the previous experiment. Similarly, we showed increasing contraction in Matrigel's layer throughout the 5 days of observation, without evidence of cancerous migration towards the stromal tissue (GelMA C with fibroblasts). We hypothesized that this was related to GelMA C's excessive stiffness, which discouraged tumour migration and encouraged the cancerous growth in Matrigel environment. Moreover WI-38 cells were very sparse and difficult to be seen, either due to initial insufficient concentration, UV radiation induced mortality or incompatibility with GelMA C material. This resulted in low interactions between cells resulting in poor ECM remodelling of the resembled stromal tissue. Future work could focus on the biomaterial's composition, which could be customized, to have control on GelMA and CNF composition, which directly affect mechanical properties and bioactivity of the bioink. Moreover, further optimization can be performed in photocrosslinking since it alters the stiffness of the material, affecting both its mechanical properties and cellular viability. This could be easily tuned by changing UV parameters, regulating either exposure time or intensity. Finally, cells concentration could be optimized to achieve better cells-cells communication.

4.2 Collagen bioprinting

Although GelMA represents a valid choice to recreate the ECM with a good printability, it is not present in native tissues. Hence, we wanted to use a material that better resemble the native ECM present in tissues. Collagen, indeed, contrarily to GelMA, enabled us to mimic the fibrillar structure of the ECM, which has a fundamental role in TME development. [12] With bioprinting it is furthermore possible to control fibers features like alignment, elongation and thickness.

Collagen has been used widely as bioink, because not only it's the main structural protein in ECM, but it also presents high affinity for adherent cells. Its biomedical uses ranges from tissue modelling to drug testing, including clinical practice, due to its low immunogenicity and good biocompatibility. [41]. Among the various collagens, we decided to use collagen type I, as considered the most abundant type of collagen in ECM [40] and an important factor for cancer diagnostics [12]. Our collagen derived from rat tail tendons, further purified and stored in low pH conditions. We decided to use a low concentration collagen, 3 mg/ml, to obtained structures with appropriate mechanical properties avoiding high density of the matrix that could impact on the cell's viability. We firstly, evaluated collagen's rheology at different temperature and analysed its printability. Further, we conducted a thoroughly analysis on printability, with and without embedded cells. Analysis on fibers alignment was also conducted, as considered to be an important hallmark in cancer's diagnostics. [12] Finally, we tested new strategies to improve collagen's printability, focusing on FRESH bioprinting. This method gives support to soft and liquid-like bioinks, such as low-concentrated collagen, till they reach stability. [27] Different support baths have been tested and compared, to evaluate the best candidate for collagen's bioprinting.

4.2.1 Rheological characterization

Collagen is highly sensitive to temperature, we therefore wanted to evaluate its the evolution of its mechanical properties in function of this parameter. Three conditions were tested to evaluate collagen's behaviour, low (7°C), ambient (25°C) and high (37°C) temperature after collagen neutralization. Firstly, we evaluated its gelling properties. Specifically, we performed a single frequency shear stress controlled oscillatory measurement to evaluate the time required by the material to stabilize its structure. Results are reported in Figure 41 below.

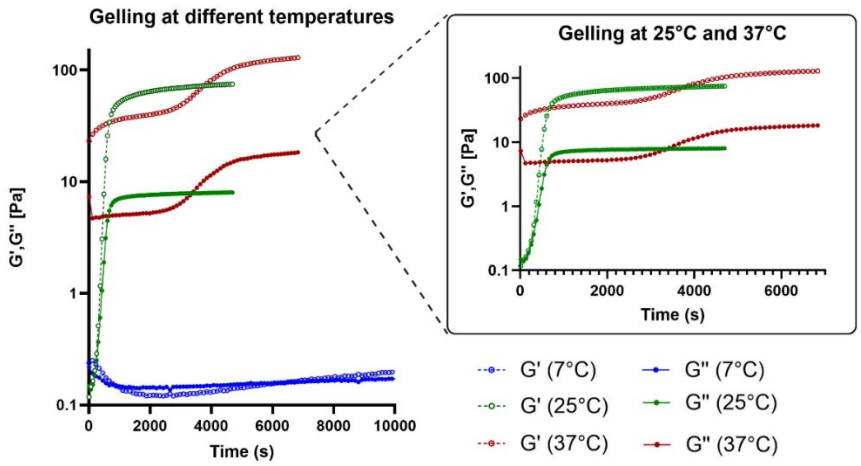

Figure 41: Gelling test of collagen at different temperatures.

The highest value of G' and G'' are reached at 25°C and 37°C, both showing complete gelling process of collagen (G'> G''). At 7°C, on the contrary, no significant variation of the moduli up to 3 hours showing that lowering the temperature was sufficient to hinder the gelation (**Table 10**). Upon neutralisation of collagen, a gelation process allows the formation of a fibrous network. Gelation temperature, amongst other parameters, primarily impacts on the morphology of this network. [71] Holder et. al ([71]) showed that by manipulating gelation conditions it is possible to control certain mechanical properties of collagen, which directly influence cells behaviour. Upon neutralisation, collagen forms a branched fiber network, which morphology and characteristics depend also on the gelation conditions. Gelation at sub-physiological temperature (20°C), generates large pore spaces and dense fiber bundling in collagen's fiber network, while at physiological temperature (37°) pores show a decrease in size and less fiber bundling. At 25°C and 37°C, the time required to set the instrument, hindered the gelation point, the time in which the transition from liquid to gel occurs. However, we know that gelation time drastically shorten as temperature increase, arising difficulties in the measurement. [71]

Secondly, we tested the thixotropic properties of collagen, following the procedure suggested by Cui et al. ([68]) by dividing the tests in 3 sub-sections, simulating low-shear strain, high shear strain and again low shear strain. This test emulates the stress experienced by the hydrogel during the printing process: firstly, low shear

strain is induced as gel stays in the cartridge prior to extrusion; then it experiences high shear strain, as gel is dispensed through the nozzle through applied pressure; and lastly low-shear strain occurs, as the biomaterial is finally deposited on the printing bed. In Figure 42 are reported the graphs, and in **Table 9** are reported the parameters measured, namely G' and G'' at the initial low-stress regime (G_0' and G_0'') and G' and G'' after the high shear strain regime (G_1' and G_1''), as well as the percentual decrease for each component.

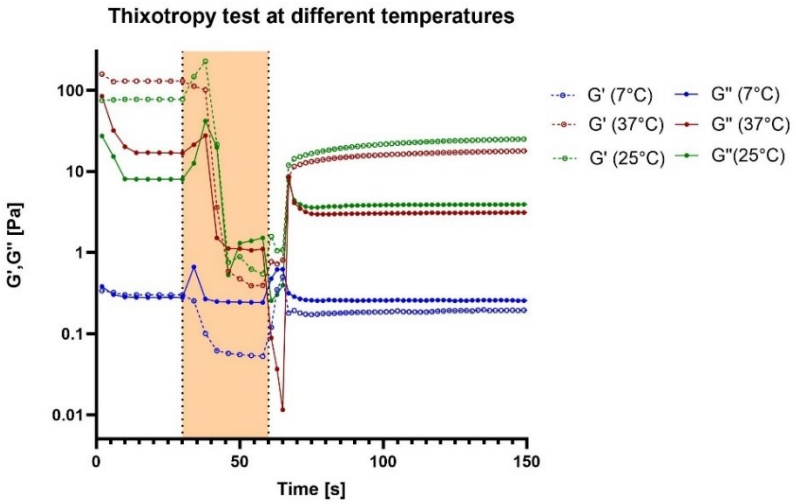

Figure 42: Thixotropy testing at different temperatures. The high shear strain region is highlighted in light orange. Tests were conducted after the equilibrium conditions were reached, therefore at 200 min, 80 min and 120 min respectively for 7°C, 25°C and 37°C.

Table 9: Measured parameters of thixotropic testing at different temperatures

Temperature °C / **Parameter**	**7°C**	**25°C**	**37°C**
G_0' [Pa]	0.3	77.5	130
G_1' [Pa]	0.21	30.8	20.7
Percentage decrease of G'	30%	60%	84%
G_0'' [Pa]	0.28	8	17.1
G_1''[Pa]	0.26	4	3.2
Percentage decrease of G''	7%	50%	81%

Thixotropy could be simplified as a special case of shear thinning, [57] which is a fundamental property for bioprinting. As said before, by increasing the temperature, collagen molecules self-assembly into fibrillar hydrogels, forming a fibrillar network held together by weak interactions, such as electrostatic and hydrophobic bonds. Viscoelasticity is related to the unbinding of these weak interactions under stress, which cause the fiber slippage. [72] At 25°C and 37°C, the induced high shear strain, drastically decreased both G' and G'' (50-84%). At 7°C nothing could be said as the moduli are both too small and close to each other's. [72] In all the cases collagen showed shear thinning behaviour, recovering partially its decrease in loss and storage moduli. We finally wanted to investigate if, once printed at 7°C, collagen was able to increase its mechanical strength and transit from a liquid to a gel-state once temperature was increased to physiological values of 37°C. We therefore, simulated this fibrillation post-print, by testing collagen incubated at 7°C after thixotropy tests, with a second gelling test, this time at 37°C, emulating the incubator's temperature (Figure 43).

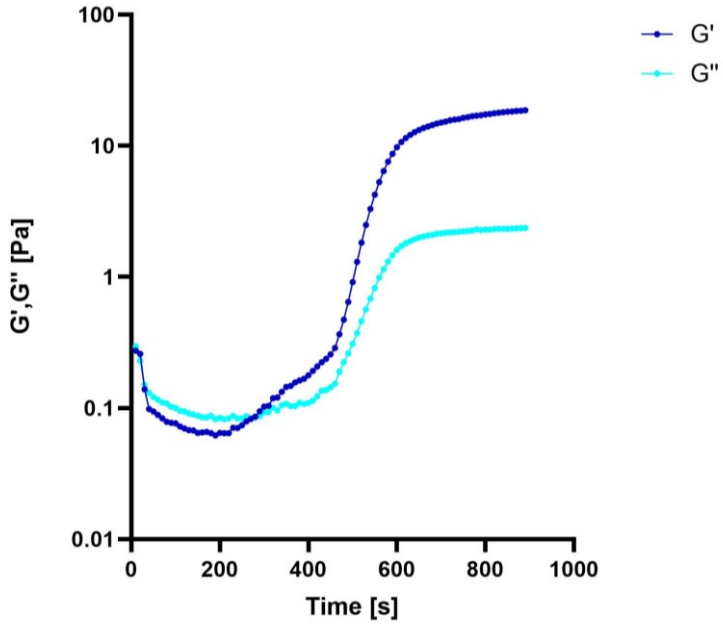

Figure 43: Stabilization post-printing analysis.

The gelation point, characterized by the crossover of the G' and G'' curves, was reached in less than 5 minutes, indicating that, after bioprinting of collagen at low temperatures, it could later complete the transition from liquid to gel, which would

give the printed structure increased mechanical strength. In **Table 10**, we reported the components of collagen after gelling tests (GT) at the investigated temperatures. Interestingly, these values were approximately one fourth the moduli reported after gelling tests at 25°C as can be seen from **Table 9**).

Table 10: Elastic and viscous components after gelling tests (GT) at different temperatures

	After 1st GT at 7°C	**After 2nd GT at 7°C**	**After GT at 25°C**	**After GT at 37°C**
G' [Pa]	0.22	18.7	74.5	127.9
G"[Pa]	0.18	2.4	8.0	18.3

We showed that collagen gelation temperature highly impacts on the rheology of the material, as described also in literature. [71] Indeed, temperature influenced on fiber network's organization, which we observed as a decrease in the recovery of the elastic and viscous component after thixotropy test at 25°C and 37°C. During printing we want the material to experience low alteration in rheologic properties, although it experiences variation in induced shear strain. For these reasons we decided to use 7°C as nozzle's temperature for our further experiments. Furthermore, we investigated the effect of the low the period of gelation at low temperature, pre-fibrillation, to control fibers formation, in order to optimize the bioprinting process.

4.2.2 Printability without cells

To evaluate the collagen printability, we firstly started without cells, as it's known how cells tend to impact hydrogels rheometric properties. Cells influence not only the bioprinting's process, but also may cause long-term changes in the bioprinted construct's characteristics, as cells could promote material remodelling interacting with the matrix. [24] The fixed printing parameters are reported in **Table 11** below.

Table 11: Printing fixed parameters

Collagen's concentration	Printbed's temperature	Nozzle/Needle's diameter	Printhead's temperature	Printing surface
3mg/ml	37°C	0.41mm	7°C	Non-treated glass coverlips

Collagen was neutralized prior to the bioprinting, and its concentration was kept constant at 3 mg/ml. Printbed's temperature was chosen to be equal to the collagen's physiological temperature, to enable the gelling once deposited required to maintain the shape of the designed structure. However, further fibrillation is required to complete collagen's gelation. The nozzle/needle diameter was kept constant at 0.41 mm, considered to be a good trade-off between resolution and low-shear stress induced while printing. Printhead's temperature was kept at 7°C to ensure low self-assembly of collagen before being printed, enabling further control on fibers alignment. Non-treated glass coverslips were considered optimal compared to other surfaces like Fluorodish and treated glass coverslips (either by ethanol washes or plasma-functionalization), as they caused alterations in collagen's deposition, either due to excessive hydrophilicity or irregular printing plane (Figure 45). Other factors were changed throughout the analysis, including pressure and velocity, and pre-fibrillation time. Pre-fibrillation time represents the period in which neutralized collagen is kept at 4°C before being printed, it serves to stabilize the material's properties. After being printed, collagen's constructs were incubated at 37°C for 60 minutes to ensure collagen's fibrillation. After 30-60 minutes from the print, depending on the amount of deposited material, constructs were added with PBS1X to prevent dehydration. The printed structure is reported in Figure 44. This simple structure allows the study of filament's thickness, resolution and reproducibility. The structure's width and height are equal to the needle/conical nozzle' diameter.

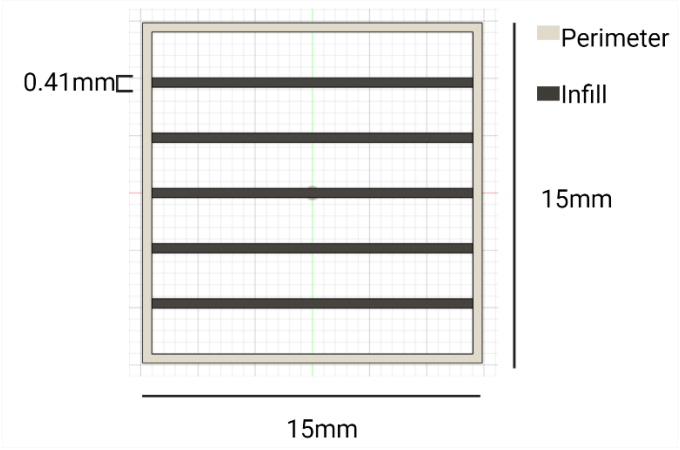

Figure 44: Printed structure 15x15x0.41 mm.

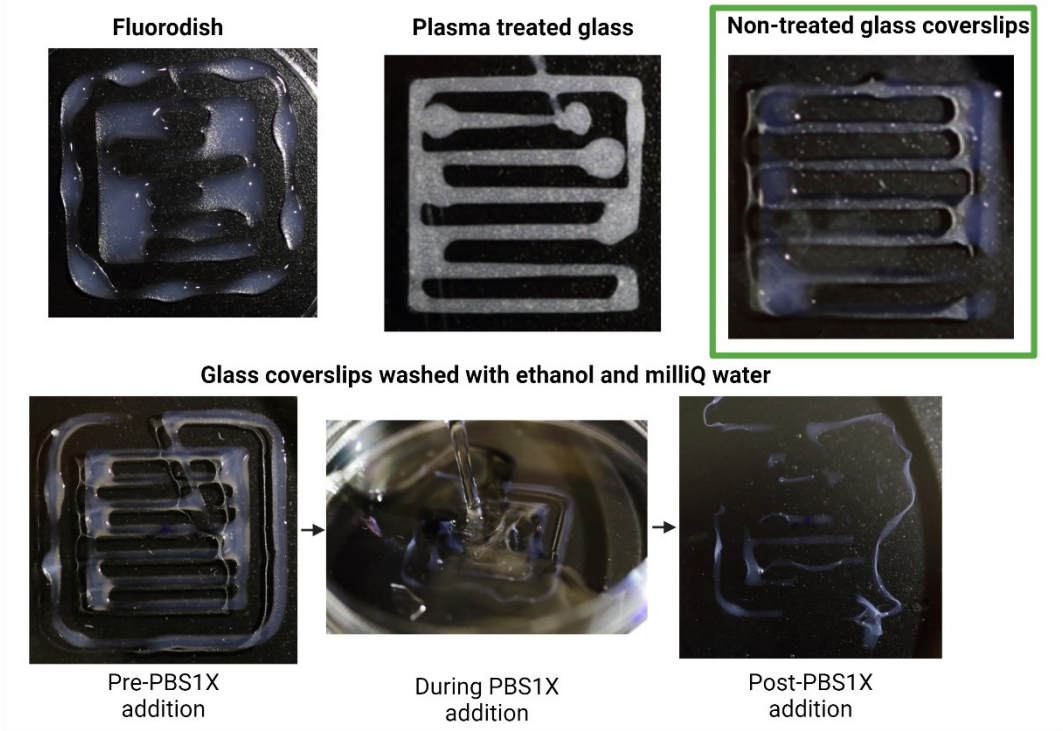

Figure 45: Printing surface effects on collagen's printability. The designed structure is reported in Figure 44.

4.2.2.1 Influence of pressure and velocity

Initially, we studied the effects of extruding pressure and velocity, using a needle of 410µm. The tests were conducted with 1h of collagen's pre-fibrillation at 4°C. Printability was qualitatively determined considering material's resemblance to the designed structure and detachment after 1X PBS addition, as described in **Table 12**. To study these factors, we tried different combinations of pressures and velocities, which are reported in Figure 46.

Table 12: Printability parameters to evaluate collagen's hydrogel

Not printable	The printed structure shows a poor resemblance to the original design. And/or it showed increased detachment after PBS1X addition.
Low-printability	The printed structure shows better resemblance to the original design, but the material presents distribution's irregularities. And/or it showed detached structure's portions after PBS1X addition.
Good printability	The printed structure shows good resemblance to the original design. And/or it showed no detachment after PBS1X addition

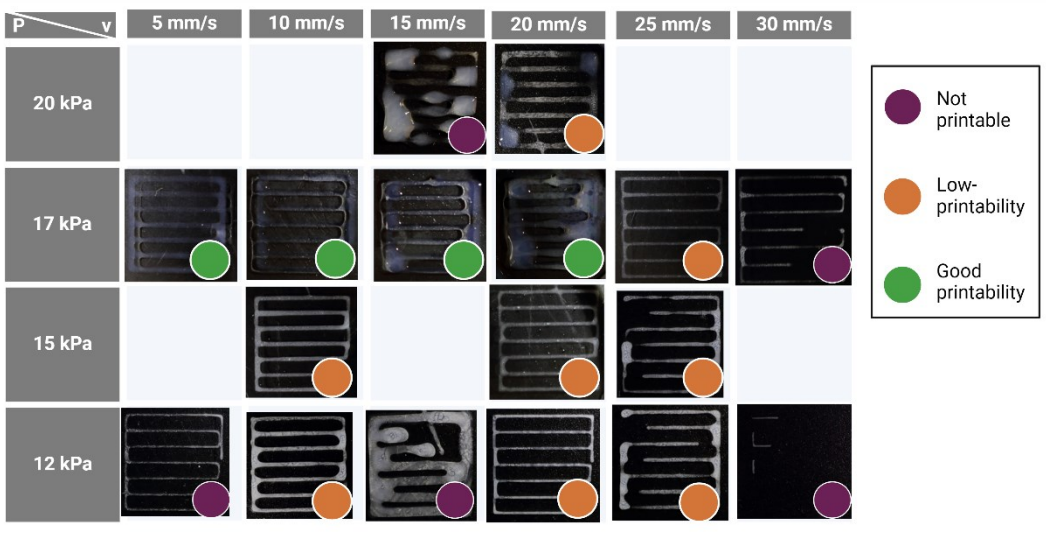

Figure 46: Evaluation of the influence of pressure and velocity on collagen's printability.

No construct detached after PBS1X addition, although many conditions showed good resemblance to the designed structure. From the tested conditions we concluded that optimal pressures lie close to 17 kPa, with a velocity ranging from 5 mm/s to 20 mm/s, although structure's resolution seemed to lower at higher velocities. For further experiments, we replaced the dispensing needle with a nozzle, to both reduce the induced shear strain, which could be damaging to cells, and to allow more control in material's deposition.

4.2.2.2 Influence of pre-fibrillation time in collagen's printability

We wanted to investigate the role of pre-fibrillation in collagen's printability. Indeed, Huang et al ([72]) showed how pre-fibrillation at 4°C, affects self-assembly of collagen, as well as viscoelasticity. More organized and interconnected fibers networks occurred with extended pre-fibrillation, along with increased fibers' length and width. We focused on analysing the differences in collagen's printability, using the parameters defined in **Table 12**, considering also filament's width variance in the same printed construct. Interestingly, filament's thickness didn't vary significantly among the three tested conditions, lying averagely between 950 µm and 1050 µm, but it changed in terms of inner variance depending on pressure and velocity (Figure 47).

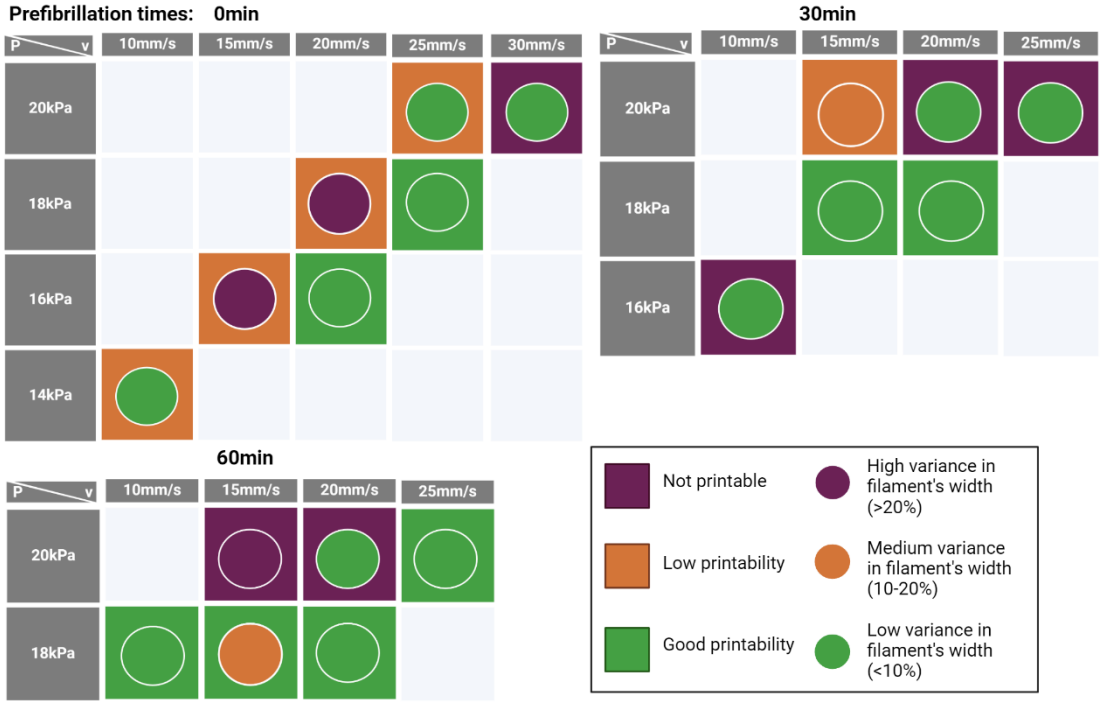

Figure 47: Pre-fibrillation time's influence on collagen's printability at 7°C.

Printability with pre-fibrillation of 60 minutes with conical nozzle (in Figure 47) showed not only comparable results with the printings obtained with the needle (in Figure 46), but it also showed good results at higher velocities. Filament's width inner variance alone is not able to fully describe printability, but it's an interesting parameter to keep in consideration for more complex structure development. We demonstrated that pre-fibrillation has an impact on hydrogel's printability. Indeed,

longer pre-fibrillation times (e.g. 60 minutes) improve printability widening the range of printing speed maintaining a low pressure. Moreover, in 4.2.2.3, pre-fibrillation with 0 minutes will be compared with the one obtained at 60 minutes pre-fibrillation, showing shorter and less aligned fibers.

4.2.2.3 Pre-fibrillation influence on collagen fibers network

Pre-fibrillation is known to show different results in terms of fibers width, elongation and overall fibers network [72]. We previously reported the effects of pre-fibrillation on collagen's printability, with better results obtained with a period of 60 minutes, which we know is dependent on the different hydrogel's fiber network. To confirm that, we formulated neutralized collagen, dispensed it through a micropipette on a glass plate, and tested 2 conditions of pre-fibrillation, respectively 1h at 4°C, 1h at 16°C and compared them to sample with no pre-fibrillation. Afterwards, they were incubated at 37°C for 1h and consequently imaged under the confocal microscope. The procedure is visually described in Figure 48.

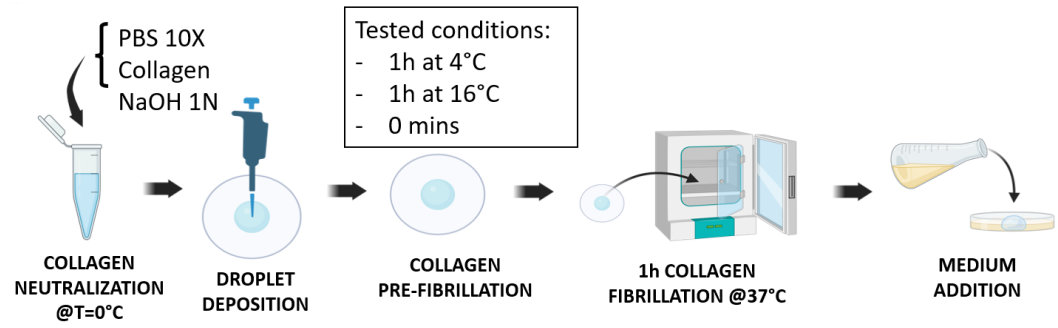

Figure 48: Procedure to investigate the pre-fibrillation effects on fiber-network's structure in collagen's hydrogel.

Temperature of pre-fibrillation highly impacts on collagen's mechanical properties. As we reported Figure 49a, after pre-fibrillation at 7°C collagen is still in a liquid-like phase, similarly to what we achieved in rheological evaluations (784.2.1). At 16°C, we observed a white gel, with a more defined shape. After fibrillation at 37°C for 60 minutes, collagen's pre-fibrillated at 7°C appeared white, similarly to the one pre-fibrillated at higher temperatures (Figure 49b).

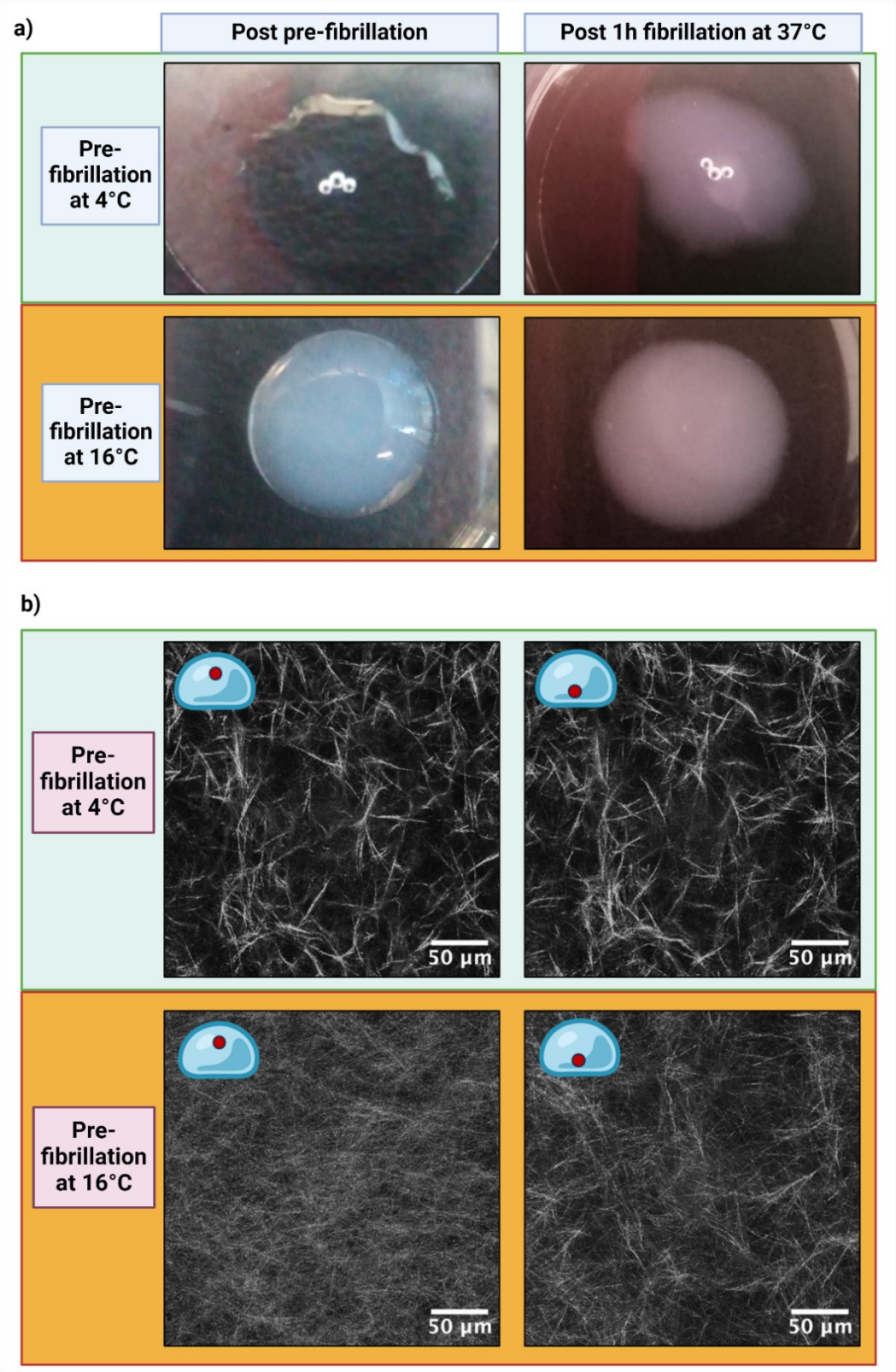

Figure 49: Influence of pre-fibrillation's temperature on collagen's fiber-network. In (a) is reported the qualitative difference between post pre-fibrillation and post-fibrillation conditions. In (b) are reported the differences in fiber network after fibrillation at 37°C under reflective mode imaging. Red point indicates the area of the bulk (light-blue) analyzed.

We observed thicker, longer fibers and overall, a more organized fiber-network with pre-fibrillation at 4°C compared to the results obtained at 16°C. Furthermore, at 4°C we highlighted a more homogenous fibers' distribution compared to 16°C, in which fibers were more organized at the bottom and less at the top. As showed by Huang et al ([72]), pre-fibrillation's duration, impacts on fibers organization, shape and overall hydrogel's mechanical properties. We explored two extreme conditions: first with 60 minutes of pre-fibrillation at 4°C and secondly, without pre-fibrillation. Similarly to Figure 49a , collagen without pre-fibrillation resulted opaque and gelled after 60 minutes of incubation at 37°C. On the other hand, fibers network presented many differences with its pre-fibrillated counterpart (Figure 50).

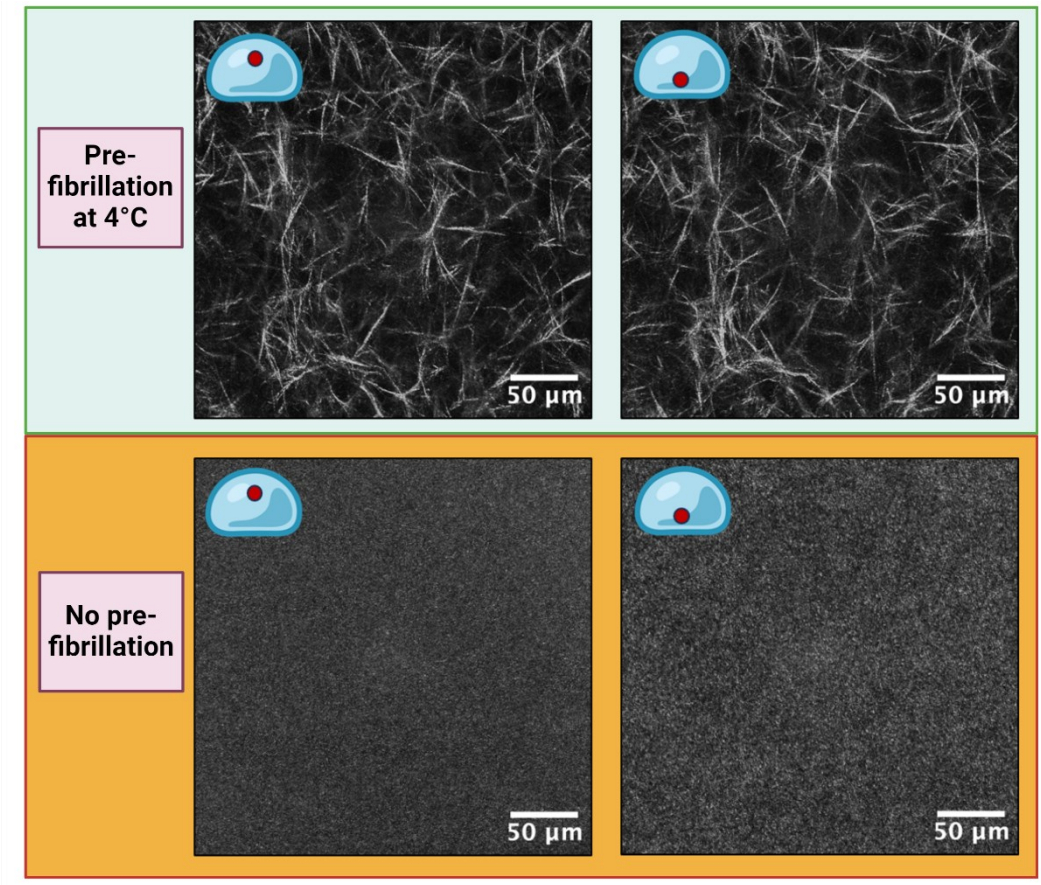

Figure 50: Effects of pre-fibrillation's presence in collagen's fibers network.

Without pre-fibrillation, collagen showed sparse short collagen's fibers, with a slight increased density at the bottom, showing heterogeneity in the investigated hydrogel. Our results regarding pre-fibrillation's influence on collagen's fibrous network is consistent with the ones reported in literature [72]. We showed that

fibrillar network influences rheological properties and furthermore, that it could be controlled by temperature and pre-fibrillation duration.

4.2.3 Printability with cells

Collagen's bioink proved to be printable, although many factors should be considered. With cells embedded in the bioinks, further optimization needs to be performed, as cells alter hydrogel's mechanical properties. [24] For our investigations, we used MAF cells, varying between 1 - 3 x 10^6 cells/ml. We monitored how fibers alignment change, comparing different factors, including pre-fibrillation time and temperature. Although our analysis is mainly qualitative, we reported interesting results, which could be a start to enlighten new aspects on bioprinting of collagen at low concentrations.

4.2.3.1 Printing and cell mediated collagen fibers alignment

As mentioned before, different factors influence on collagen's fibers rearrangement. We extensively explored the role of pre-fibrillation in 4.2.2.3 involved in collagen's fibrillar structure, and explained the differences shown in its rheological properties in 4.2.1. We firstly studied how the printing procedure impacts on the organization and fiber morphology of pre-fibrillated collagen. We observed the differences between printed and non-printed collagen (dispensed through a micropipette, as described in Figure 48). Both hydrogels were pre-fibrillated at 4°C for 60 minutes, then incubated at 37°C for 1h to complete gelation, before imaging, with results reported in Figure 51. Printed collagen presented an heterogenous fiber-network, with fibers showing both different elongation and thickness size between each other's. Furthermore, when compared with micropipetted collagen, printed collagen presented both a higher density of fibers and averagely decreased fibers' size.

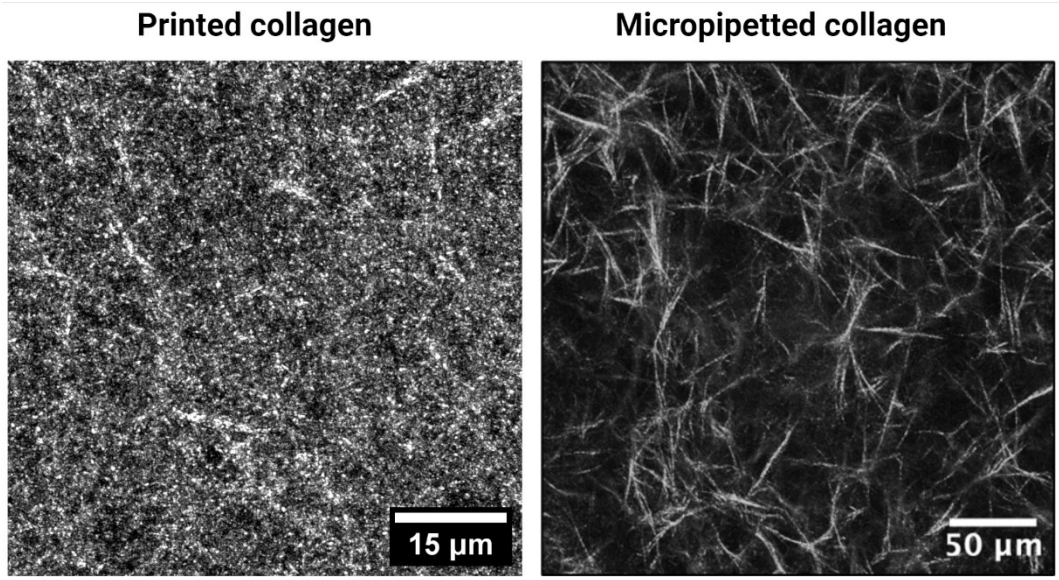

Figure 51: Influence of collagen dispensing method on its fibrillar structure

However, we know that cells alter hydrogel's rheological properties, both during bioprinting and afterwards as they interact with the hydrogel, remodelling it to perform their biological functions (like migration, proliferation, …). [24] We therefore, analysed collagen's embedded with fibroblasts (MAF), in different conditions, reported as A, B and C also in Figure 52. Collagen was printed with different parameters, which are summarized in (**Table 13**). The experiments were both conducted with a nozzle temperature varying between 7-10°C, and extruding pressures were considered not harmful for cells, as being lower than 40 kPa. [41] Pre-fibrillation highly impacted on collagen's fibers dimensions, as non-pre-fibrillated collagen (A) resulted shorter compared to pre-fibrillated one (B), similarly to our previous findings.

Table 13: Collagen's bioprinting parameters

	Pre-fibrillation at 4°C	**MAF cells concentration**
Sample A	None	$2x10^6$ cells/ml
Sample B	60 minutes	$1x10^6$ cells/ml
Sample C	60 minutes	0 cells/ml

Interestingly, as reported in Figure 52, collagen seems to promote cells elongation (Figure 52a), and on the other hand, cells seemed to improve fibers alignment (Figure 52b).

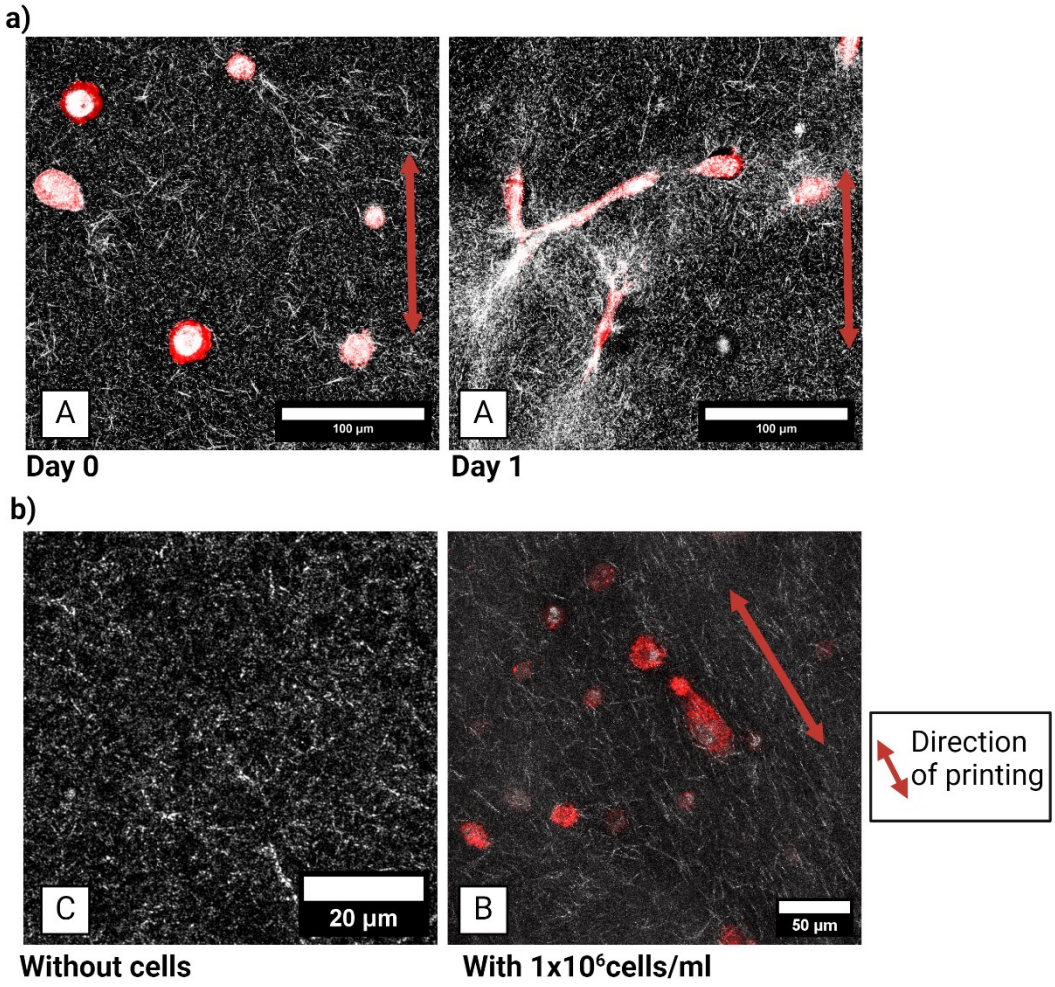

Figure 52: Cells mediated effects on collagen's fibers network. MAF cells are reported in red, while collagen fibers in gray. In (a) are reported cells effects after 24h, in (b) the effects of cells on collagen's fiber network. A, B and C referred to collagen's bioprinting conditions, reported in Table 13.

Indeed, immediately after the print, cells appeared with a rounded shape, while after 24 hours cells resulted more elongated, indicated as Day 0 and Day 1 respectively. Furthermore, fibroblasts modified their surroundings, observed as an increased alignment of collagen fibers around them. In Figure 52b, we reported the effects of the presence of cells on fibers' network. Collagen printed without cells appeared without observable fibers alignment, showing moreover, decreased fibers

dimensions. Therefore, cells remodel hydrogels fibers network from the beginning, giving it a more complex fibrillar organization.

Therefore, even though bioprinting process alters the fibrillar structure of collagen, we observed that cells improved both fibers organization (Figure 52a) and alignment (Figure 52b) by interacting with the microenvironment and remodelling the surrounding collagen. [72]

4.2.3.2 Modeling the TME with collagen and Matrigel

Considering collagen promising results, we tried to replicate the experiments obtained with GelMA C, aiming to recreate the TME. However, pure collagen at 3mg/ml is not suitable for a multilayer structure print, as immediately after printing it's in a liquid-like state and requires time to complete the gelation thus impeding the stacking of the subsequent layers. We therefore decided to print a single layer to have the opportunity to investigate the interaction between tumor cells and fibroblast in a setting that better replicate the in-vivo situation if compared to GelMA. The structure was formed by an outer frame consisting of collagen with fibroblasts (WI-38), resembling the stromal tissue, and an inner square of Matrigel, used as the basement membrane, with tumoral cells (4T1-GFP), all together resembling the cancerous core. The designed structure is reported in Figure 53, along with the printed construct. Printbed temperature was set to 37°C, with a velocity of 2 mm/s, in **Table 14** are reported the other printing parameters.

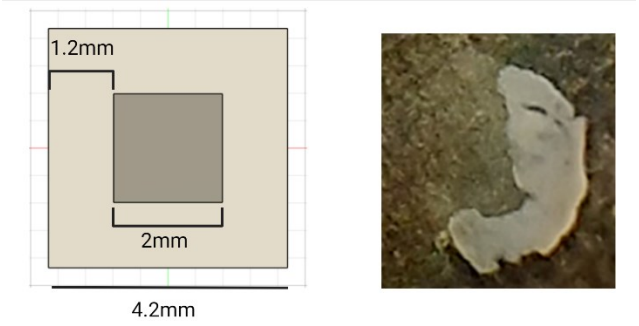

Figure 53: Multicellular and multimaterial single layer print. On the left is reported the designed structure, in which dark gray represents Matrigel with 4T1-GFP, and light gray collagen with WI-38. On the right is reported the printed construct after fibrillation at 37°C. Pre-fibrillation time is 60 minutes, and post-fibrillation time is 60 minutes.

Table 14: Printing parameters of collagen's multimaterial structure

	Nozzle's temperature	Pressures	Cells concentration	Cells type
Matrigel (Core)	25°C	16kPa	$3x10^6$ Cells/ml	4T1
Collagen (Shell)	7-8°C	8kPa	$1.5x10^6$ Cells/ml	WI-38

The fibroblasts concentration was noticeably increased (compared to GelMA C experiments, where it was below $5x10^5$ cells/ml), to allow more cellular interactions and communication. However, the printed construct almost immediately detached from the printbed (Figure 53). Nonetheless, we were able to analyse cells behaviour throughout 6 days, results are reported in Figure 54. We clearly saw the proliferation of the tumoral cells in collagen. After the print (day 0) collagen and Matrigel, with their distinctive cell types, were distinguishable from each other's, while after 24h (day 1) tumoral cells migration became evident. Collagen shell is also darker compared to the day before, suggesting a remodelling of the matrix done by fibroblasts. From day 4 we saw how cancerous cells successfully spread all over the construct and contraction rapidly increased. Interestingly, the contraction involved both the stromal (collagen with fibroblasts) and the cancerous core (Matrigel and 4T1-GFP).

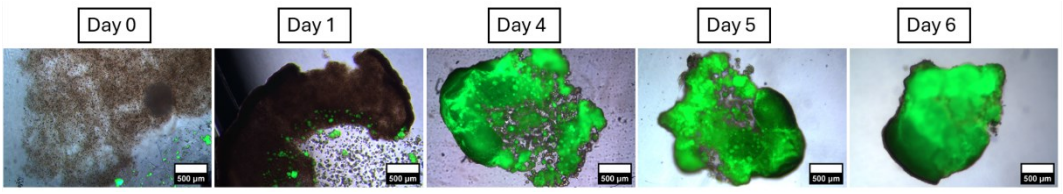

Figure 54: Multicellular and multimaterial single layer print analysis throughout 6 days. Photos are reported as an overlay of a bright field image and a green fluorescent image (4T1-GFP in Matrigel). In (a) are reported the images of the construct from day 0 to day 6, while in (b) are reported the border magnified of day 5 and day 6.

The low resolution of the printed construct makes the experiment difficult to reproduce and furthermore, showed low control on collagen's printability. Resolution could have been affected both by the liquid-like behaviour of collagen,

and by the reduced structure' size. To overcome these limitations, the structure's size could easily be increased, to allow more controlled nozzle's movements. To improve the low viscosity collagen's printability, we move toward FRESH bioprinting, considered in literature [27] to be an effective solution as it provides support to the extruded hydrogel till gelation occurs.

4.2.4 Limitations and future perspectives

Although collagen showed promising results, its printability is hindered by the time required for it to become a gel. As it's deposited as a liquid-like material, only simple shapes could be printed, not allowing multiple layer deposition. However, TME is a complex structure, therefore, to study it, further improvements should be made. We investigated other strategies searching in literature, trying to use additives to increase viscosity and overall mechanical properties in collagen's hydrogel. We found that Pluronic F127 [73], and riboflavin [74], [75] showed promising results when used as additives, but we couldn't be able to observe any significant improvements in printability results. However, as collagen's highly involved in TME and it's normally present in ECM, we decided to focus on methods to improve pure collagen's printability, rather than additives to combine it within. Improving its mechanical properties, will give us better results in terms of resemblance to TME. Collagen offers indeed, control on the fibrillar structure and allows good stromal tissue representations, with increased cellular rearrange of the surrounding material, as well as tumour's invasion modelling. We therefore, moved towards a different bioprinting technique: the FRESH bioprinting method.

4.2.5 FRESH bioprinting

FRESH is an embedded printing approach, generally used to improve soft biomaterials printability, which often results low due to their rheological properties. This technique overcome these limitations, by giving physical support on the extruded bioink, enabled it to reach structure stability, either by gelation or crosslinking mechanisms. [27] Recently, gelatin, Carbopol and Pluronic F127 gained interest in 3D bioprinting field, as they enabled increased printability to soft hydrogels considered to be "unprintable". These materials indeed, are able to act as supporting suspension and can be gently removed with cell compatible procedures.

FRESH supporting bath removal could occur either via chemical or physical principles the latter being more compatible with embedded cells. [28] We therefore investigated physically removable sacrificial biomaterials, which are also commonly used in bioprinting scenario: Pluronic F127, Carbopol and Lifesupport (a gelatin-based biomaterial). All of them are reported as biocompatible [28] and used in collagen bioprinting. [46] We tested these three different support baths to optimize the deposition of collagen filaments.

In FRESH bioprinting, nozzles are replaced by needles, as they ensure more control on hydrogel's deposition, as less support bath's material is moved during the extrusion process. As in needles a region of high shear is present throughout the whole dispensing structure, while with nozzles, the highest shear stress is present only on their outlet, we increased the dispenser diameter from 410 μm to 840 μm, to allow a reduced shear stress. [76] As we used collagen as bioink, we used the optimized parameters achieved previously and described in the previous paragraphs. Therefore, we maintained cartridge's temperature keeping it close to 7°C to prevent undesirable fibrillation and to enable better printability, as observed also in rheological evaluations. Collagen's pre-fibrillation was performed at 4°C for 60 minutes, as it showed a more organized fibrillar structure, as well as better printability compared to the other conditions tested. Immediately after being printed, collagen was incubated at 37°C for 60 minutes. For our evaluations we decided to extrude collagen mixed with cells, as they alter the rheological properties of the hydrogel. [24] We used 4T1-GFP cells during our analysis, as they resulted fluorescent and easily detectable inside the support bath. The printed filaments were printed 1-1.5 mm from the bottom, to allow complete immersion of the extruded bioink in the support bath, as well as to avoid cells adhesion to the container. **Table 15** summarizes the printing parameters.

Table 15: Fixed FRESH bioprinting parameters

Needle's diameter	Collagen's pre-fibrillation	Needle's temperature	Distance from the capsule's bottom	Cells type
840µm	60 minutes	7-10°C	1-1.5mm	4T1-GFP (Cancerous)

We designed a simple structure (Figure 55) composed of three lines to test the ability of the support baths to sustain the deposition of collagen's filaments.

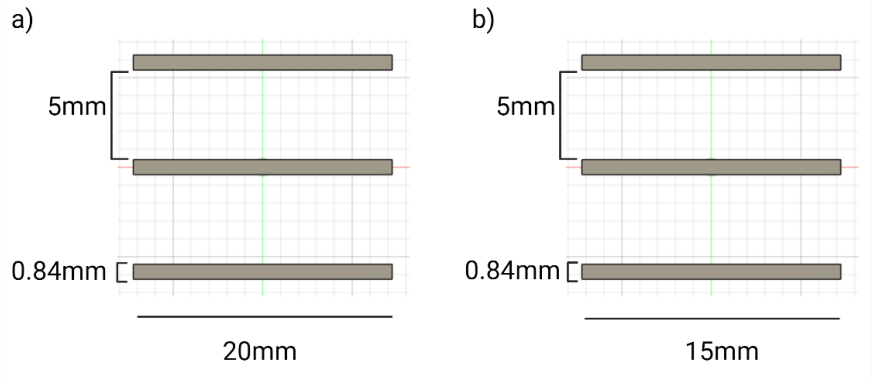

Figure 55: Designed structure for FRESH bioprinting. (a) For Carbopol and (b) for Lifesupport and Pluronic F127. In all the tested support baths, the structure's height was equal to the needle's width of 0.84mm.

4.2.5.1 Carbopol

As Carbopol is not a thermo-sensitive material, we kept a printing bed temperature of 37°C, to facilitate a more rapid gelation of collagen once extruded, similarly to previous experiments *in air* (not in FRESH). Carbopol was then removed with multiple washes with 0.9 % w/v NaCl solution, till its complete dissolution. It was then replaced by medium. Carbopol's rheology is highly influenced by its concentration therefore we prepared 2 different concentrations, 0.8% w/v and 1.2% w/v to investigate the impact of the polymer concentration in collagen's printability. As reported in (Figure 56), Carbopol's concentration is directly proportional to its viscosity.

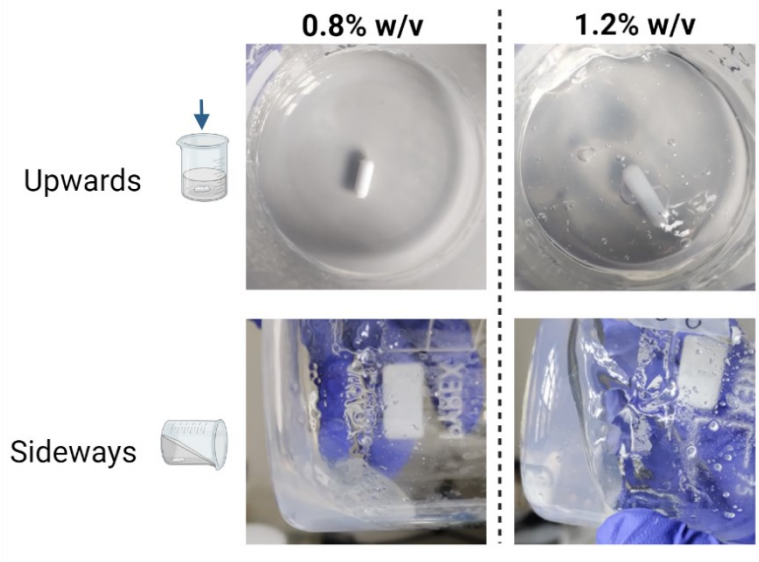

Figure 56: Carbopol gels at different concentration. Gels are reported with the magnetic stirrer used throughout the synthesis process.

We decided to start with the lowest concentration tested, 0.8% w/v. We tested it using collagen embedded with $2x10^6$ cells/ml varying the extrusion pressure and the printing speed. Results reported in Figure 57 show the effects of pressure and speed on the filament's deposition. In all the tested conditions we observed major limitations that hinders the production of a collagen filament with a homogeneous thickness and a proper shape fidelity. As reported in Figure 57b, the filaments exhibited lower width compared to the nominal value of 840 µm. Moreover, the printed filaments are also highly inhomogeneous with strong variance in filament's width. This low print fidelity of the collagen filaments seemed to be related to an insufficient viscosity of the support material. Indeed, collagen and cells were not confined as they should have been, diffusing outside the designed path (Figure 57a).

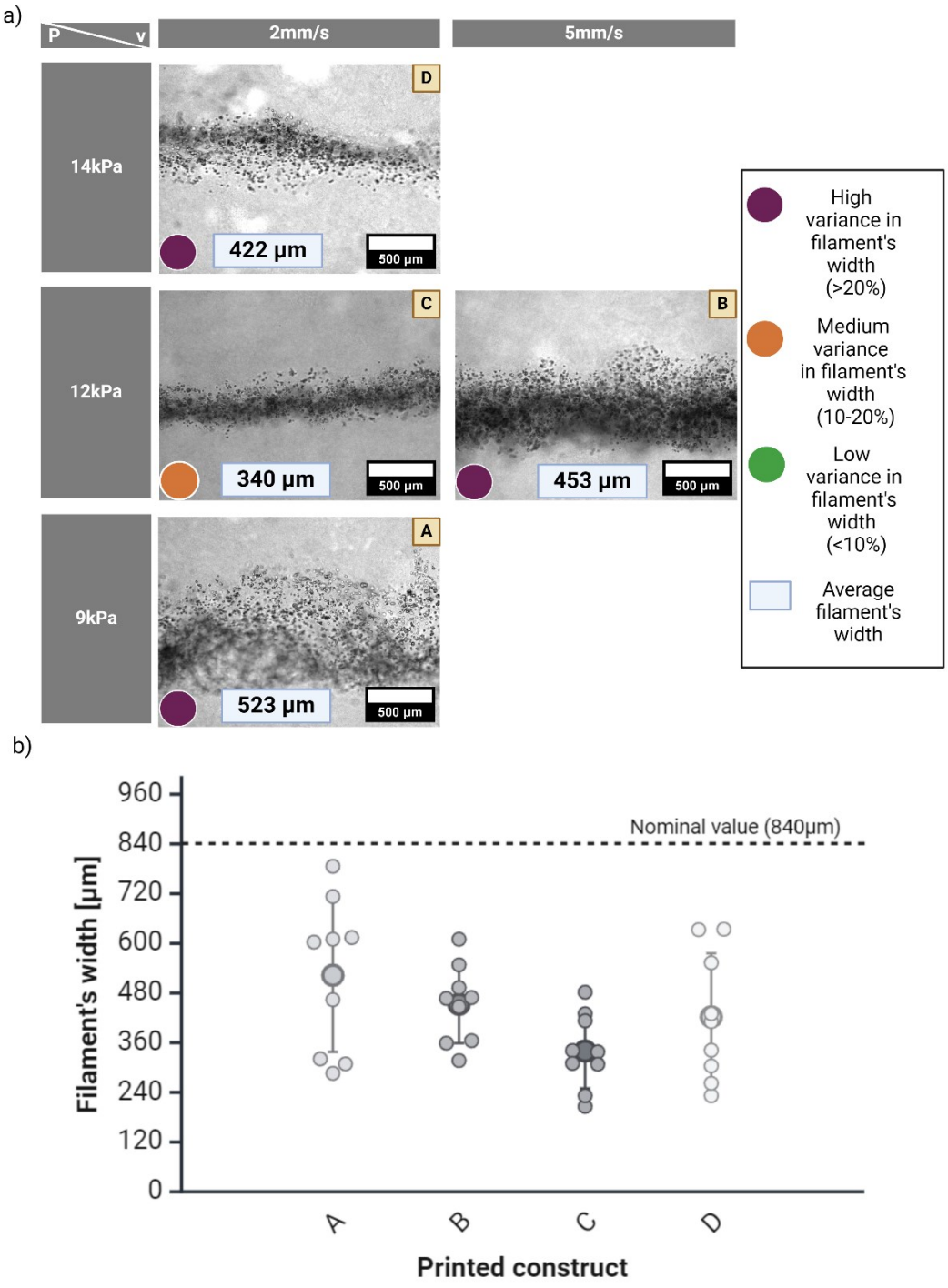

Figure 57: FRESH bioprinting of collagen with embedded cells in Carbopol 0.8%. In (a) are visually reported the results. In (b) the same results are reported graphically.

We thought that this lack of a defined and stable interface between collagen and Carbopol, could have been improved by increasing the support bath's concentration, which would consequently increase gel's viscosity. Finally, after

complete fibrillation, support bath was removed with several washes. This procedure led to a fragmentation of the printed filaments highlighting a lack of mechanical stability and structural properties of the printed collagen. To overcome the observed limitations, we tried to use Carbopol with higher concentration, at 1.2% w/v. However, high concentration Carbopol bath exhibited excessive stiffness unable to achieve proper collagen's deposition. Printed filaments appeared highly irregular, thinner and showed overall a decreased printability (Figure 58).

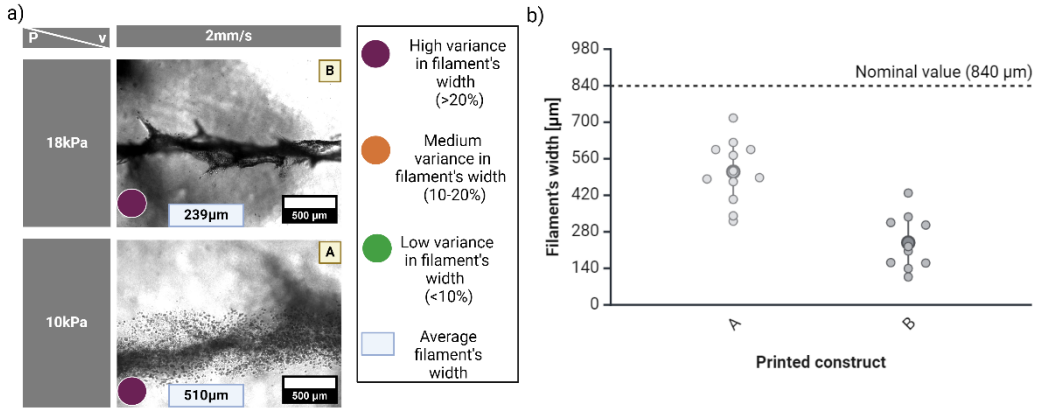

Figure 58: FRESH bioprinting of collagen with embedded cells in Carbopol 1.2%. In (a) are visually reported the results of Carbopol 1,2%. In (b) the same results are reported graphically.

As different washes are involved to remove Carbopol bath, collagen's filaments were easily damaged, resulting in fragments after support bath's removal. This could be related to altered collagen structure, as reported by Wen Shi ([46]) Carbopol bath could absorb water easily, damaging collagen's structure. This, combined with low filament's width and high variance inside the same constructs, led us to exclude Carbopol from further experiments.

4.2.5.2 Lifesupport

Lifesupport is the trade name of a gelatin based microparticles gel. [44] We used it to extrude collagen mixed with a cellular concentration of $3x10^6$ cells/ml and we printed 2 constructs consisting of three filaments each. Gelatin's support bath appeared yellowish and its low transparency resulted as a limitation in the monitoring of the collagen's extrusion, in which the extruded filaments are difficult to be observed. Moreover, similarly to Carbopol's experiments, reported in the previous paragraph, gelatin's bath couldn't maintain a steady interface between

collagen and support material, resulting in dispersed collagen and cells outside the designed path (Figure 59a). Moreover, pressures were changed during the printing process from 17 kPa to 20 kPa, as the filaments struggled to be evenly extruded, while velocity was kept constant at 2 mm/s. Indeed, even though constructs were printed with the same conditions they differed greatly in terms of filament's width as reported in Figure 59b. Both showed over-extruded collagen, observed as increased filament's width, with more pronounced results with construct B in comparison to construct A. Relative to the heating bed temperature, it was kept at 20°C to prevent precocious gel-to-sol transition of the gelatin bath and to allow collagen to start the gelling process after being extruded. At 20°C indeed, it had been shown also by Holder et al. ([71]), that collagen is able to gel, although with a slower process compared to gelation at physiological temperature (37°C). This partial gelation was instrumental to counteract one of the main drawbacks of the gelatin bath: the quick dissolution at 37°C that hinders the achievement of its mechanical stability. [46] Indeed, even though we waited 60 minutes for the retrieval of the printed collagen to ensure complete collagen's fibrillation, gelatin already underwent to the gel-sol transition after 30 minutes. We also observed that the support bath's removal fragmented the printed filaments, and this is a paramount limitation as it prevents further development of complex structures. We then analyzed the constructs after 24 h observing a contraction in filament's width as well as an increased in cells assembly along the extruded filament. This is related to cells-collagen interactions, which showed positive results as they were able to rearrange it to promote their growth and migration.

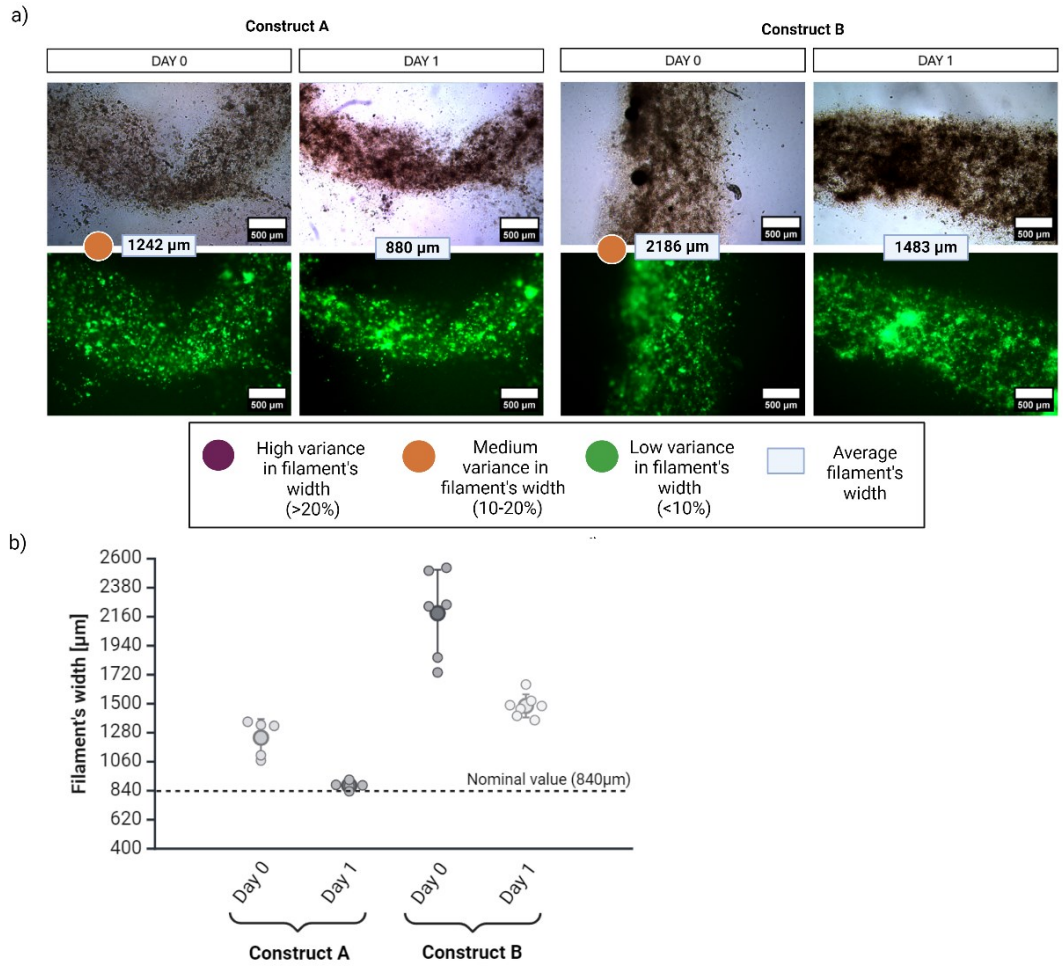

Figure 59: Collagen FRESH bioprinting in Lifesupport with 4T1-GFP cells. In (a) are visually reported the printed constructs after 24 hours, both (A and B) were printed at the same conditions. In (b) are graphically reported the filament's width for both constructs

In conclusion, although cells maintain high viability and proliferation inside the printed collagen, Lifesupport showed overall problems with printability, both during the printing process and afterwards. Indeed, at the same conditions, collagen showed great differences in terms of extruded filament's width, and during bath's removal collagen's filaments were fragmented, with complete loss of resemblance to the original structure. We decided therefore to move to another support material.

4.2.5.3 Pluronic F127

This material is a copolymer of PEO/PPO/PEO. It's a thermosensitive material, which turns liquid under a certain temperature, which, although altered by its concentration, is generally close to 4°C. At temperatures higher than 10°C it

behaves like a gel. We therefore used a printbed's temperature of 37°C, to better initiate collagen's gelation while being deposited, without altering Pluronic's mechanical properties. After being printed, collagen was incubated at 37°C for 60 minutes, afterwards, Pluronic F127 was removed by dropping the temperature at 4°C, till complete liquefaction occurs, and thoroughly washed with PBS. Collagen with embedded cells in concentration of $2x10^6$ cells/ml has been used, to determine cells migration and cells behaviour.

Compared to the other considered FRESH techniques, it showed better results in terms of printability (Figure 60a), with overall homogenous filaments deposition. Indeed, it showed less variation in filament's width, and higher printing fidelity (Figure 60a-b). Furthermore, Pluronic showed versatility in terms of pressures and velocities and no fragmentations occurred after bath's removal, highlighting a stronger network formation and increased mechanical properties of the filaments.

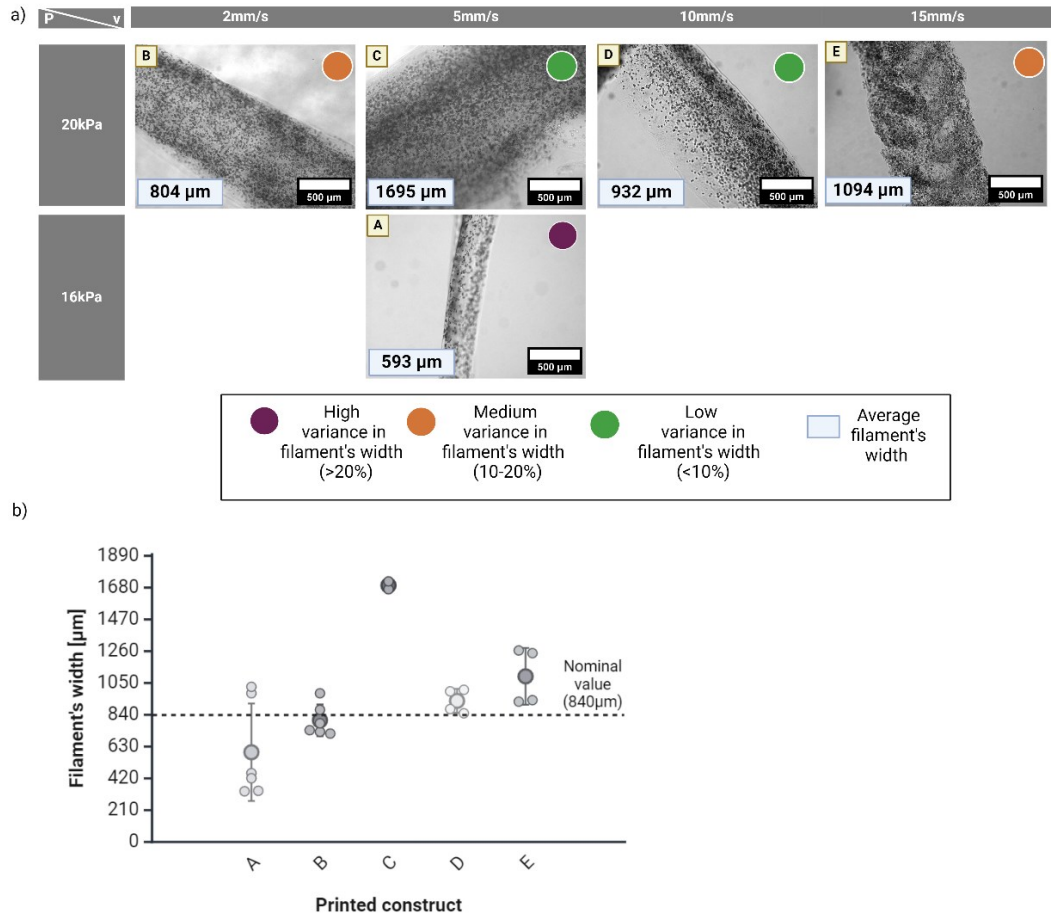

Figure 60: FRESH printability of collagen with embedded cells in Pluronic F127.

Considering the promising results, we evaluated the fibers alignment through a confocal imaging under reflective mode (Figure 61). Fibers tended to align along with the direction of printing and showed increased length compared to collagen printed in air. Furthermore, in FRESH bioprinted collagen, fibers appeared thicker, although sparser, while cells seemed to be homogenously distributed in both conditions.

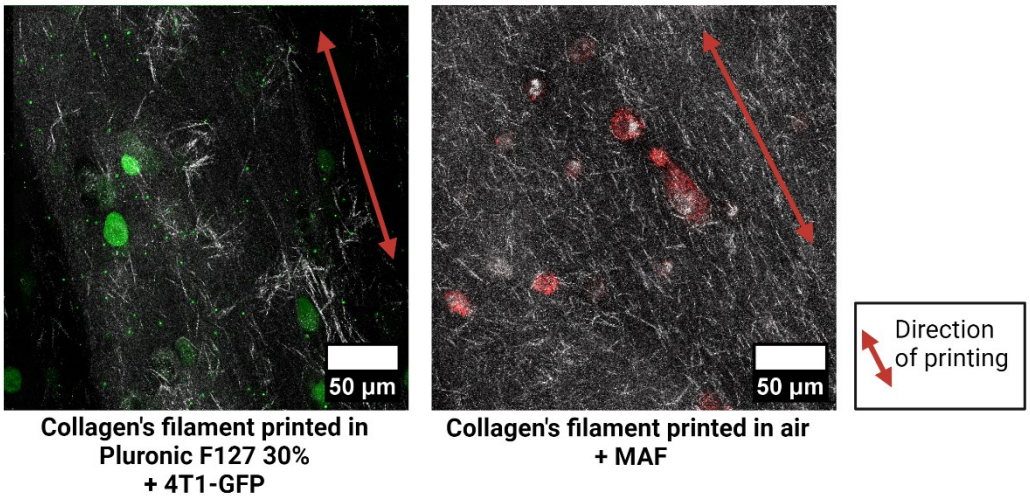

Figure 61: Comparison between collagen printed FRESH in Pluronic (left) and collagen printed in air (right). 4T1 cells are reported in green, along with Fluorobeads (smaller dots), MAF cells are red and collagen fibers in gray. Both cells concentration is $2x10^6$ cells/ml.

4.2.5.4 Comparisons and future perspectives

Compared to Carbopol and Lifesupport, Pluronic showed improved printability and cells confinement in the printed filament. Furthermore, no fragmentation had been seen while removing the support bath. This enabled us to proceed with the fibers analysis, which showed a bias along the printing direction. More tests should be run to monitor the effects of tumoral cells on collagen's fibers, to see the expected collagen's remodelling. [12] Moreover, future tests will include also the development of complex structures with multiple layers and multiple materials, essential to simulate the TME. In Figure 62 are reported representative images of results obtained with the three-supporting baths as a comparison.

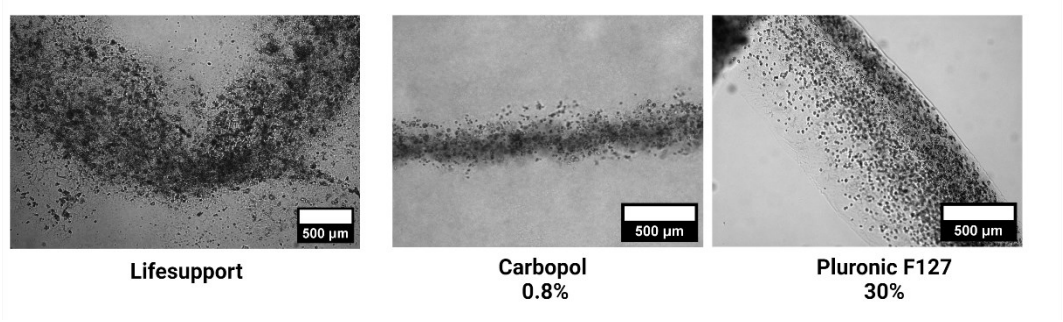

Figure 62: Comparison between the different support baths tested.

Conclusion

The aim of this work of thesis was the development of a 3D model to mimick the tumour microenvironment using 3D bioprinting. 3D extrusion bioprinting allow to replicate the complexity of the tumour microenvironment overcoming the limitations of the well-studied, yet limited, 2D models. Two different material approaches were investigated, one through semi-synthetic biomaterials, GelMA and GelMA with nanofibrillated cellulose (GelMA C), and one through a natural bioink that better resemble the in-vivo condition, collagen. Both the materials were tested in terms of printability and mechanical properties, as well as cytocompatibility.

We first investigate the use of GelMA, a widely used biomaterial for 3D printing, analyzing its printability, in terms of printing fidelity, photocrosslinkability and related cells viability. Our results, however, showed structural instabilities during the bioprinting process and a significant sensitivity to subtle temperature variations that limited the printability of the designed structures. We therefore tested the use of GelMA C, being able to develop a 3D structure to model of TME consisting of an inner cube, the core, made of Matrigel and tumoral cells (A549), resembling the cancerous basement membrane and an outer stromal tissue, formed of GelMA C and fibroblasts (WI-38). GelMA C exhibited better print ability enabling the fabrication of a stable 10 layer structure showing a good compartmentalization of the cancerous core and the stromal-mimicking outer shell. A long term analysis of the printed structure, however, shown the drawbacks of this approach: we observed the contraction of the Matrigel core due to proliferating cancerous cell interaction with material and a weak bonding between Matrigel and GelMA leading to a delaminating of the two compartments. The same results were observed when we fabricated a single layer structure with the same inner and outer compositions to allow a better imaging of the cell-cell cell-material and material-material interactions. Moreover, no evidence of cancerous cells migration from the Matrigel core to the GelMA C shell was observed. Furthermore, low fibroblast concentration was observed due to initial low-concentration or high mortality derived from UV radiation or incompatibility with the embedding material. This limited the

observation of the ECM remodelling of the stromal compartment, as well as cancerous and non-cancerous cellular interactions.

We then investigated the use of collagen I, the main protein component of ECM, to better replicate the *in vivo* condition. We used low-concentration collagen (3 mg/ml) to allow cell proliferation and high viability of the embedded cells. We first tested the printing procedure of collagen in air. We successfully controlled collagen fibers structure, optimizing the pre-fibrillation conditions, to allow the formation of thick collagen bundles. We also investigated the alignment the fibers along the direction of printing to model the hallmark structure of the in vivo microenvironment, and we proved the efficiency in cells spreading and collagen remodel. With collagen, we were able to recreate the interface between cancerous and normal stromal cells, by printing a single layer structure consisting of an inner square of Matrigel and cancerous cells (4T1-GFP) surrounded by a shell of collagen and fibroblasts (WI-38). We showed a good initial compartmentalization of normal and cancerous tissue, which further developed in the cell-mediated remodelling the microenvironment. Indeed, not only tumoral cells proliferated from Matrigel to collagen, but they also contracted the material and visibly remodel the microenvironment. Long term analysis up to 6 days after printing, exhibited fibroblasts segregation on the outer shell, forming an irregular and non-continuous border with the external environment. However, collagen's low printability hindered more complex structures development, as well as better resolution. To overcome these limitations, we explored the printing of this low viscosity collagen bioink with the FRESH method. We optimized the support bath's material to improve collagen's stability and printing's resolution. We tested Lifesupport, Carbopol and Pluronic as support baths. Among all the tested materials, Pluronic showed better results in terms of printability showing more versatility in terms of pressures and velocities, along with low variance between filaments' widths and overall more resemblance to the designed construct. We further investigated the fibers alignment through reflection confocal microscopy. Collagen's fibers resulted well aligned with the printing's direction, and furthermore, showed increased size in fibers thickness and elongation compared to collagen printed in air. Moreover,

we observed extended cell-material interaction with cells proliferating inside the fibrous network.

In conclusion, in this work of thesis, we explored several approaches to reproduce a compartmentalized TME. The reported results showed interesting results both with semi-synthetic and natural biomaterials and can be instrumental for future biologically relevant investigations on cancer onset and development.

Bibliography

[1] I. Parodi, D. Di Lisa, L. Pastorino, S. Scaglione, and M. M. Fato, “3D Bioprinting as a Powerful Technique for Recreating the Tumor Microenvironment,” Jun. 01, 2023, *MDPI*. doi: 10.3390/gels9060482.

[2] G. Bahcecioglu, G. Basara, B. W. Ellis, X. Ren, and P. Zorlutuna, “Breast cancer models: Engineering the tumor microenvironment,” Apr. 01, 2020, *Acta Materialia Inc*. doi: 10.1016/j.actbio.2020.02.006.

[3] H. Samadian *et al.*, “3D bioprinting technology to mimic the tumor microenvironment: tumor-on-a-chip concept,” Dec. 01, 2021, *Elsevier Ltd*. doi: 10.1016/j.mtadv.2021.100160.

[4] C. Frantz, K. M. Stewart, and V. M. Weaver, “The extracellular matrix at a glance,” Dec. 15, 2010. doi: 10.1242/jcs.023820.

[5] B. Yue, “Biology of the extracellular matrix: An overview,” Dec. 10, 2014, *Lippincott Williams and Wilkins*. doi: 10.1097/IJG.0000000000000108.

[6] J. K. Kular, S. Basu, and R. I. Sharma, “The extracellular matrix: Structure, composition, age-related differences, tools for analysis and applications for tissue engineering,” Jan. 17, 2014, *SAGE Publications Ltd*. doi: 10.1177/2041731414557112.

[7] A. Y. Galvez-Contreras, T. Campos-Ordonez, V. Lopez-Virgen, J. Gomez-Plascencia, R. Ramos-Zuniga, and O. Gonzalez-Perez, “Growth factors as clinical biomarkers of prognosis and diagnosis in psychiatric disorders,” Dec. 01, 2016, *Elsevier Ltd*. doi: 10.1016/j.cytogfr.2016.08.004.

[8] S. Pompili, G. Latella, E. Gaudio, R. Sferra, and A. Vetuschi, “The Charming World of the Extracellular Matrix: A Dynamic and Protective Network of the Intestinal Wall,” Apr. 16, 2021, *Frontiers Media S.A.* doi: 10.3389/fmed.2021.610189.

[9] P. Shukla, S. Yeleswarapu, M. A. Heinrich, J. Prakash, and F. Pati, “Mimicking tumor microenvironment by 3D bioprinting: 3D cancer

modeling," Jul. 01, 2022, *Institute of Physics*. doi: 10.1088/1758-5090/ac6d11.

[10] G.-F. Xiong and R. Xu, "Function of cancer cell-derived extracellular matrix in tumor progression," *J Cancer Metastasis Treat*, vol. 2, no. 9, p. 357, Sep. 2016, doi: 10.20517/2394-4722.2016.08.

[11] T. J. Puls, X. Tan, M. Husain, C. F. Whittington, M. L. Fishel, and S. L. Voytik-Harbin, "Development of a Novel 3D Tumor-tissue Invasion Model for High-throughput, High-content Phenotypic Drug Screening," *Sci Rep*, vol. 8, no. 1, Dec. 2018, doi: 10.1038/s41598-018-31138-6.

[12] K. Song, Z. Yu, X. Zu, G. Li, Z. Hu, and Y. Xue, "Collagen Remodeling along Cancer Progression Providing a Novel Opportunity for Cancer Diagnosis and Treatment," Sep. 01, 2022, *MDPI*. doi: 10.3390/ijms231810509.

[13] S. Cannito, E. Novo, and M. Parola, "Therapeutic pro-fibrogenic signaling pathways in fibroblasts," Nov. 01, 2017, *Elsevier B.V.* doi: 10.1016/j.addr.2017.05.017.

[14] S. Z. Despotović *et al.*, "Altered organization of collagen fibers in the uninvolved human colon mucosa 10 cm and 20 cm away from the malignant tumor," *Sci Rep*, vol. 10, no. 1, Dec. 2020, doi: 10.1038/s41598-020-63368-y.

[15] A. S. Piotrowski-Daspit, B. A. Nerger, A. E. Wolf, S. Sundaresan, and C. M. Nelson, "Dynamics of Tissue-Induced Alignment of Fibrous Extracellular Matrix," *Biophys J*, vol. 113, no. 3, pp. 702–713, Aug. 2017, doi: 10.1016/j.bpj.2017.06.046.

[16] R. Sharma *et al.*, "3D bioprinting complex models of cancer," 2023, *Royal Society of Chemistry*. doi: 10.1039/d2bm02060b.

[17] G. Ying, N. Jiang, C. Yu, and Y. S. Zhang, "Three-dimensional bioprinting of gelatin methacryloyl (GelMA)," Dec. 01, 2018, *Springer*. doi: 10.1007/s42242-018-0028-8.

[18] R. Pinos, F. V. Sbrana, and C. Scielzo, “Bioprinting functional tissues: cell types and a focus on cancer modeling,” in *Bioprinting: From Multidisciplinary Design to Emerging Opportunities*, Elsevier, 2022, pp. 247–269. doi: 10.1016/B978-0-323-85430-6.00005-4.

[19] A. F. Bonatti, G. M. Fortunato, C. De Maria, and G. Vozzi, “Bioprinting technologies: an overview,” in *Bioprinting: From Multidisciplinary Design to Emerging Opportunities*, Elsevier, 2022, pp. 19–49. doi: 10.1016/B978-0-323-85430-6.00006-6.

[20] C. Jamieson *et al.*, “A Review of Recent Advances in 3D Bioprinting With an Eye on Future Regenerative Therapies in Veterinary Medicine,” Feb. 16, 2021, *Frontiers Media S.A.* doi: 10.3389/fvets.2020.584193.

[21] B. Yilmaz, A. Al Rashid, Y. A. Mou, Z. Evis, and M. Koç, “Bioprinting: A review of processes, materials and applications,” Aug. 01, 2021, *Elsevier B.V.* doi: 10.1016/j.bprint.2021.e00148.

[22] K. Tappa and U. Jammalamadaka, “Novel biomaterials used in medical 3D printing techniques,” Feb. 07, 2018, *MDPI AG*. doi: 10.3390/jfb9010017.

[23] S. Marconi, G. Alaimo, V. Mauri, E. Negrello, and F. Auricchio, “3D printing technologies and materials in the medical field,” in *Bioprinting: From Multidisciplinary Design to Emerging Opportunities*, Elsevier, 2022, pp. 1–17. doi: 10.1016/B978-0-323-85430-6.00004-2.

[24] K. Hölzl, S. Lin, L. Tytgat, S. Van Vlierberghe, L. Gu, and A. Ovsianikov, “Bioink properties before, during and after 3D bioprinting,” Sep. 23, 2016, *Institute of Physics Publishing*. doi: 10.1088/1758-5090/8/3/032002.

[25] Y. S. Zhang *et al.*, “3D extrusion bioprinting,” Dec. 01, 2021, *Springer Nature*. doi: 10.1038/s43586-021-00073-8.

[26] S. V. Murphy and A. Atala, “3D bioprinting of tissues and organs,” 2014, *Nature Publishing Group*. doi: 10.1038/nbt.2958.

[27] D. J. Shiwarski, A. R. Hudson, J. W. Tashman, and A. W. Feinberg, “Emergence of FRESH 3D printing as a platform for advanced tissue

biofabrication," Mar. 01, 2021, *American Institute of Physics Inc.* doi: 10.1063/5.0032777.

[28] S. Liu, T. Wang, S. Li, and X. Wang, "Application Status of Sacrificial Biomaterials in 3D Bioprinting," Jun. 01, 2022, *MDPI*. doi: 10.3390/polym14112182.

[29] Z. Luo, X. Mu, and Y. S. Zhang, "Biomaterials for bioprinting," in *Bioprinting: From Multidisciplinary Design to Emerging Opportunities*, Elsevier, 2022, pp. 51–86. doi: 10.1016/B978-0-323-85430-6.00001-7.

[30] J. M. Unagolla and A. C. Jayasuriya, "Hydrogel-based 3D bioprinting: A comprehensive review on cell-laden hydrogels, bioink formulations, and future perspectives," Mar. 01, 2020, *Elsevier Ltd*. doi: 10.1016/j.apmt.2019.100479.

[31] J. Yin, M. Yan, Y. Wang, J. Fu, and H. Suo, "3D Bioprinting of Low-Concentration Cell-Laden Gelatin Methacrylate (GelMA) Bioinks with a Two-Step Cross-linking Strategy," *ACS Appl Mater Interfaces*, vol. 10, no. 8, pp. 6849–6857, Feb. 2018, doi: 10.1021/acsami.7b16059.

[32] A. I. Cernencu *et al.*, "3d bioprinting of biosynthetic nanocellulose-filled gelma inks highly reliable for soft tissue-oriented constructs," *Materials*, vol. 14, no. 17, Sep. 2021, doi: 10.3390/ma14174891.

[33] K. Yue, G. Trujillo-de Santiago, M. M. Alvarez, A. Tamayol, N. Annabi, and A. Khademhosseini, "Synthesis, properties, and biomedical applications of gelatin methacryloyl (GelMA) hydrogels," Dec. 01, 2015, *Elsevier Ltd*. doi: 10.1016/j.biomaterials.2015.08.045.

[34] Y. Piao *et al.*, "Biomedical applications of gelatin methacryloyl hydrogels," Jan. 01, 2021, *KeAi Communications Co.* doi: 10.1016/j.engreg.2021.03.002.

[35] J. Yang, H. He, D. Li, Q. Zhang, L. Xu, and C. Ruan, "Advanced strategies in the application of gelatin-based bioink for extrusion bioprinting," Sep. 01, 2023, *Zhejiang University*. doi: 10.1007/s42242-023-00236-4.

[36] I. Pepelanova, K. Kruppa, T. Scheper, and A. Lavrentieva, “Gelatin-methacryloyl (GelMA) hydrogels with defined degree of functionalization as a versatile toolkit for 3D cell culture and extrusion bioprinting,” *Bioengineering*, vol. 5, no. 3, Sep. 2018, doi: 10.3390/bioengineering5030055.

[37] Y. C. Chen *et al.*, “Functional human vascular network generated in photocrosslinkable gelatin methacrylate hydrogels,” *Adv Funct Mater*, vol. 22, no. 10, pp. 2027–2039, May 2012, doi: 10.1002/adfm.201101662.

[38] W. Xu *et al.*, “On Low-Concentration Inks Formulated by Nanocellulose Assisted with Gelatin Methacrylate (GelMA) for 3D Printing toward Wound Healing Application,” *ACS Appl Mater Interfaces*, vol. 11, no. 9, pp. 8838–8848, Mar. 2019, doi: 10.1021/acsami.8b21268.

[39] S. Shin *et al.*, “CNF in gelatin derivatives,” 2017.

[40] I. N. Amirrah, Y. Lokanathan, I. Zulkiflee, M. F. M. R. Wee, A. Motta, and M. B. Fauzi, “A Comprehensive Review on Collagen Type I Development of Biomaterials for Tissue Engineering: From Biosynthesis to Bioscaffold,” Sep. 01, 2022, *MDPI*. doi: 10.3390/biomedicines10092307.

[41] J. Stepanovska, M. Supova, K. Hanzalek, A. Broz, and R. Matejka, “Collagen Bioinks for Bioprinting: A Systematic Review of Hydrogel Properties, Bioprinting Parameters, Protocols, and Bioprinted Structure Characteristics,” *Biomedicines*, vol. 9, no. 9, 2021, doi: 10.3390/biomedicines9091137.

[42] P. De Stefano *et al.*, “Bioprinting of matrigel scaffolds for cancer research,” *Polymers (Basel)*, vol. 13, no. 12, Jun. 2021, doi: 10.3390/polym13122026.

[43] J. E. Snyder *et al.*, “Bioprinting cell-laden matrigel for radioprotection study of liver by pro-drug conversion in a dual-tissue microfluidic chip,” *Biofabrication*, vol. 3, no. 3, Sep. 2011, doi: 10.1088/1758-5082/3/3/034112.

[44] H. Budharaju, D. Sundaramurthi, and S. Sethuraman, “Embedded 3D bioprinting – An emerging strategy to fabricate biomimetic & large

vascularized tissue constructs," Feb. 01, 2024, *KeAi Communications Co.* doi: 10.1016/j.bioactmat.2023.10.012.

[45] E. O. Osidak, V. I. Kozhukhov, M. S. Osidak, and S. P. Domogatsky, "Collagen as bioink for bioprinting: A comprehensive review," Apr. 01, 2020, *Whioce Publishing Pte. Ltd.* doi: 10.18063/IJB.V6I3.270.

[46] W. Shi *et al.*, "Embedded Bioprinting of Breast Tumor Cells and Organoids Using Low-Concentration Collagen-Based Bioinks," *Adv Healthc Mater*, vol. 12, no. 26, Oct. 2023, doi: 10.1002/adhm.202300905.

[47] T. J. Hinton *et al.*, "Three-dimensional printing of complex biological structures by freeform reversible embedding of suspended hydrogels," *Sci Adv*, vol. 1, no. 9, Oct. 2015, doi: 10.1126/sciadv.1500758.

[48] D. Baruffaldi, C. F. Pirri, and F. Frascella, "3D bioprinting of cell-laden carbopol bioinks," *Bioprinting*, vol. 22, Jun. 2021, doi: 10.1016/j.bprint.2021.e00135.

[49] A. Shapira and T. Dvir, "3D Tissue and Organ Printing—Hope and Reality," May 01, 2021, *John Wiley and Sons Inc*. doi: 10.1002/advs.202003751.

[50] C. S. O'Bryan, T. Bhattacharjee, S. L. Marshall, W. Gregory Sawyer, and T. E. Angelini, "Commercially available microgels for 3D bioprinting," *Bioprinting*, vol. 11, p. e00037, 2018, doi: https://doi.org/10.1016/j.bprint.2018.e00037.

[51] M. Rocca, A. Fragasso, W. Liu, M. A. Heinrich, and Y. S. Zhang, "Embedded Multimaterial Extrusion Bioprinting," *SLAS Technol*, vol. 23, no. 2, pp. 154–163, Apr. 2018, doi: 10.1177/2472630317742071.

[52] T. Hu *et al.*, "3D Embedded Printing of Complex Biological Structures with Supporting Bath of Pluronic F-127," *Polymers (Basel)*, vol. 15, no. 17, Sep. 2023, doi: 10.3390/polym15173493.

[53] O. Chaudhuri, J. Cooper-White, P. A. Janmey, D. J. Mooney, and V. B. Shenoy, "Effects of extracellular matrix viscoelasticity on cellular

behaviour," Aug. 27, 2020, *Nature Research*. doi: 10.1038/s41586-020-2612-2.

[54] L. Mendoza-Cerezo, J. M. Rodríguez-Rego, A. Macías-García, A. Callejas-Marín, L. Sánchez-Guardado, and A. C. Marcos-Romero, "Three-Dimensional Bioprinting of GelMA Hydrogels with Culture Medium: Balancing Printability, Rheology and Cell Viability for Tissue Regeneration," *Polymers (Basel)*, vol. 16, no. 10, May 2024, doi: 10.3390/polym16101437.

[55] F. V. Sbrana, C. Scielzo, D. Ribezzi, and S. Farè, "Read-out in bioprinting," in *Bioprinting: From Multidisciplinary Design to Emerging Opportunities*, Elsevier, 2022, pp. 109–135. doi: 10.1016/B978-0-323-85430-6.00003-0.

[56] P. Coussot, "1 - Introduction to the rheology of complex fluids," in *Understanding the Rheology of Concrete*, N. Roussel, Ed., in Woodhead Publishing Series in Civil and Structural Engineering. , Woodhead Publishing, 2012, pp. 3–22. doi: https://doi.org/10.1533/9780857095282.1.3.

[57] C. C. Clark, J. Aleman, L. Mutkus, and A. Skardal, "A mechanically robust thixotropic collagen and hyaluronic acid bioink supplemented with gelatin nanoparticles," *Bioprinting*, vol. 16, Dec. 2019, doi: 10.1016/j.bprint.2019.e00058.

[58] T. Gao *et al.*, "Optimization of gelatin-alginate composite bioink printability using rheological parameters: A systematic approach," *Biofabrication*, vol. 10, no. 3, Jun. 2018, doi: 10.1088/1758-5090/aacdc7.

[59] "Mixing-cells-and-bioink-Protocol_5-Jan-2023-1".

[60] T. Fisher Scientific, "Countess ™ 3 Automated Cell Counter USER GUIDE Catalog Number AMQAX2000," 2021.

[61] "MP 03224 LIVE/DEAD ® Viability/Cytotoxicity Kit Product Information." [Online]. Available: www.omegafilters.com

[62] "Hoechst 33342," 2010. [Online]. Available: www.thermo.com/pierce.

[63] G. Bioink, “BIOPRINTING PROTOCOL Protocol aim.” [Online]. Available: www.cellink.com

[64] “Protocol aim.” [Online]. Available: www.cellink.com

[65] Lubrizol, “PHARMACEUTICAL BULLETIN,” 2011. [Online]. Available: www.pharma.lubrizol.com

[66] “LI FES U PPO RT ™ D I R ECTI O N S FO R U S E SUPPORT BATH FOR FRESH ™ 3D BIOPRINTING Difficulty.” [Online]. Available: www.fluidform3D.com

[67] N. Diamantides, C. Dugopolski, E. Blahut, S. Kennedy, and L. J. Bonassar, “High density cell seeding affects the rheology and printability of collagen bioinks,” *Biofabrication*, vol. 11, no. 4, Aug. 2019, doi: 10.1088/1758-5090/ab3524.

[68] R. Cui *et al.*, “Natural polymer derived hydrogel bioink with enhanced thixotropy improves printability and cellular preservation in 3D bioprinting,” *J Mater Chem B*, vol. 11, no. 17, pp. 3907–3918, Apr. 2023, doi: 10.1039/d2tb02786k.

[69] M. A. Heinrich, R. Bansal, T. Lammers, Y. S. Zhang, R. Michel Schiffelers, and J. Prakash, “3D-Bioprinted Mini-Brain: A Glioblastoma Model to Study Cellular Interactions and Therapeutics,” *Advanced Materials*, vol. 31, no. 14, Apr. 2019, doi: 10.1002/adma.201806590.

[70] M. Klak *et al.*, “Irradiation with 365 nm and 405 nm wavelength shows differences in DNA damage of swine pancreatic islets,” *PLoS One*, vol. 15, no. 6 June, Jun. 2020, doi: 10.1371/journal.pone.0235052.

[71] A. J. Holder, N. Badiei, K. Hawkins, C. Wright, P. R. Williams, and D. J. Curtis, “Control of collagen gel mechanical properties through manipulation of gelation conditions near the sol-gel transition,” *Soft Matter*, vol. 14, no. 4, pp. 574–580, 2018, doi: 10.1039/c7sm01933e.

[72] D. Huang *et al.*, “A P P L I E D S C I E N C E S A N D E N G I N E E R I N G Collagen hydrogel viscoelasticity regulates MSC chondrogenesis in a

ROCK-dependent manner," 2023. [Online]. Available: https://www.science.org

[73] K. K. Moncal, V. Ozbolat, P. Datta, D. N. Heo, and I. T. Ozbolat, "Thermally-controlled extrusion-based bioprinting of collagen," *J Mater Sci Mater Med*, vol. 30, no. 5, May 2019, doi: 10.1007/s10856-019-6258-2.

[74] A. Tirella, T. Liberto, and A. Ahluwalia, "Riboflavin and collagen: New crosslinking methods to tailor the stiffness of hydrogels," *Mater Lett*, vol. 74, pp. 58–61, May 2012, doi: 10.1016/j.matlet.2012.01.036.

[75] N. Diamantides *et al.*, "Correlating rheological properties and printability of collagen bioinks: The effects of riboflavin photocrosslinking and pH," *Biofabrication*, vol. 9, no. 3, Jul. 2017, doi: 10.1088/1758-5090/aa780f.

[76] E. Reina-Romo, S. Mandal, P. Amorim, V. Bloemen, E. Ferraris, and L. Geris, "Towards the Experimentally-Informed In Silico Nozzle Design Optimization for Extrusion-Based Bioprinting of Shear-Thinning Hydrogels," *Front Bioeng Biotechnol*, vol. 9, Aug. 2021, doi: 10.3389/fbioe.2021.701778.